TECH LIBRARY KAFB, NM
0061722

NASA CONTRACTOR REPORT

NASA CR-2877

NASA-CR-2

LOAN COPY: RETURN TO
AFWL TECHNICAL LIBRARY
KIRTLAND AFB, N. M.

COMPUTER CONSIDERATIONS FOR REAL TIME SIMULATION OF A GENERALIZED ROTOR MODEL

R. M. Howe and L. E. Fogarty

Prepared by
THE UNIVERSITY OF MICHIGAN
Ann Arbor, Mich. 48109
for Ames Research Center

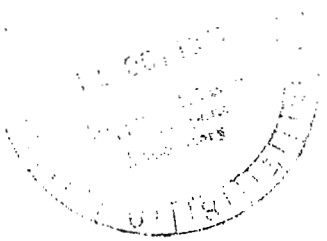

NATIONAL AERONAUTICS AND SPACE ADMINISTRATION • WASHINGTON, D. C. • SEPTEMBER 1977

TECH LIBRARY KAFB, NM

0061722

1. Report No. NASA CR-2877	2. Government Accession No.	3. Recipient's Catalog No.
4. Title and Subtitle Computer Considerations for Real Time Simulation of a Generalized Rotor Model.		5. Report Date September 1977 6. Performing Organization Code
7. Author(s) R. M. Howe and L. E. Fogarty		8. Performing Organization Report No. 10. Work Unit No.
9. Performing Organization Name and Address Department of Aerospace Engineering The University of Michigan Ann Arbor, Michigan 48109		11. Contract or Grant No. NCA2-OR440-601
12. Sponsoring Agency Name and Address National Aeronautics & Space Administration Washington, D.C.		13. Type of Report and Period Covered Final Contractor Report 14. Sponsoring Agency Code

15. Supplementary Notes

16. Abstract

This report summarizes the results of a 12-month study of real-time computer simulation requirements for the Rotor System Research Aircraft (RSRA). The report develops scaled equations suitable for simulation of the rotor system. These equations form the basis for consideration of both digital and hybrid mechanization for real time simulation. For all-digital simulation estimates of the required speed in terms of equivalent operations per second are developed based on the complexity of the equations and the required integration frame rates. For both conventional hybrid simulation and hybrid simulation using time-shared analog elements the amount of required equipment is estimated along with a consideration of the dynamic errors. It is concluded that conventional hybrid mechanization using analog simulation of those rotor equations which involve rotor-spin frequencies (this constitutes the bulk of the equations) requires too much analog equipment. Hybrid simulation using time-sharing techniques for the analog elements appears possible with a reasonable amount of analog equipment. All-digital simulation with affordable general-purpose computers is not possible because of speed limitations, but specially-configured digital computers do have the required speed and constitute the recommended approach.

17. Key Words (Suggested by Author(s))	18. Distribution Statement
Flight simulation Rotors	UNCLASSIFIED-UNLIMITED

19. Security Classif. (of this report)	20. Security Classif. (of this page)	21. No. of Pages	22. Price*
UNCLASSIFIED	UNCLASSIFIED	112	4.50

*For sale by the National Technical Information Service, Springfield, Virginia 22161

SUMMARY

This report summarizes the results of a 12-month study of real-time computer simulation requirements for the Rotor System Research Aircraft (RSRA). The report develops scaled equations suitable for simulation of the rotor system. These equations form the basis for consideration of both digital and hybrid mechanization for real time simulation. For all-digital simulation estimates of the required speed in terms of equivalent operations per second are developed based on the complexity of the equations and the required integration frame rates. For both conventional hybrid simulation and hybrid simulation using time-shared analog elements the amount of required equipment is estimated along with a consideration of the dynamic errors. It is concluded that conventional hybrid mechanization using analog simulation of those rotor equations which involve rotor-spin frequencies (this constitutes the bulk of the equations) requires too much analog equipment. Hybrid simulation using time-sharing techniques for the analog elements appears possible with a reasonable amount of analog equipment. All-digital simulation with affordable general-purpose computers is not possible because of speed limitations, but specially-configured digital computers do have the required speed and constitute the recommended approach.

TABLE OF CONTENTS

1. INTRODUCTION

This report presents the results of a 12-month study of real-time computer simulation requirements for the Rotor System Research Aircraft (RSRA). The original math model to be used as a basis for the study included only the equations for the rotor system and was furnished by the Simulation Sciences Division of the NASA Ames Research Center.[1] These equations were originally developed by Sikorsky Aircraft and have also been used extensively by the NASA Langley Research Center. At both Langley and Ames major difficulties have arisen in trying to simulate the RSRA in real time, largely because of the complexity of the rotor model. This motivated the present study, which originally had the objective of developing a hybrid computer mechanization of the rotor equations in order to permit adequate real-time simulation.

In order to better understand the RSRA equations, and in particular the rotor system equations, the simplifications in the equations and the frequency content in the various state variables, the equations were rederived from first principles (see Appendix A) and rewritten in scaled, dimensionless form (Appendix B). In addition to the rotor-system equations the six-degree-of-freedom rigid aircraft equations have also been included with the exception of the aerodynamic terms. Thus the only aerodynamic forces considered in the model are the aerodynamic forces acting on the rotor blade segments. These forces, however, are predominant and also the complexity associated

---

[1] Mackie, D. Brian and Thomas S. Alderete, "A Real-Time Dual Processor Simulation of the Rotor System Research Aircraft," NASA TN-D-8328, January, 1977.

with calculating them and the resulting blade motion and forces is predominant in the computer simulation of the RSRA. For this reason the RSRA model considered in this report is felt to be reasonable as a basis for comparing different computer mechanizations. The additional computation required for the fuselage, tail, and wing aerodynamic forces should not change substantially the conclusions of the study. This is especially true when one considers that the rotor blade equations in their entirety are not only more complex but also contain much higher frequencies than the aircraft equations.

In the rotor model each blade is represented as a rigid body with two degrees of freedom (lagging and flapping). The model can be altered to allow flexible blades by using normal coordinates for the elastic degrees of freedom, but this would further increase the equation complexity and high-frequency content of the problem. It is probably not necessary for simulation associated with either man-in-the-loop or control-system studies.

In Chapter 2 the scaled equations in Appendix B are used as a basis for a total count of various computational operations. This count, in turn, allows requirement estimates for various types of computer mechanization of the equations. Chapter 3 discusses the requirements for all-digital mechanization, Chapter 4 for conventional hybrid mechanization and Chapter 5 for hybrid mechanization using a time-shared analog system for computing blade forces. Finally, Chapter 6 provides summary recommendations as a result of the study.

2. COMPUTATIONAL OPERATIONS REQUIRED TO IMPLEMENT THE RSRA MODEL

2.1 Basic Model

The math model for the RSRA is developed in Appendix A. Figure 2.1 in Section A.2 in the appendix shows a block diagram of the equations in vector form. The six-degree-of-freedom rigid aircraft equations are shown in block 1 of the figure. The equations for the two degrees of freedom (lagging and flapping) for each of the rotor blades are shown in blocks 9 and 12. Blocks 2 through 8 represent the equations for transforming the angular and translational velocity and acceleration components of the aircraft to velocity and acceleration components along each rotor blade. Block 10 represents the computation of aerodynamic forces (lift and drag) on each blade segment and block 11 represents the calculation of the resulting moments on each blade, as needed for solving the blade equations of motion. Finally, blocks 13 through 15 represent the conversion of individual blade forces to overall force and moment components acting on the rigid aircraft.

In Appendix A the scalar equations in each of the 15 blocks in Figure 2.1 are developed in the 15 respective subsections of A.2. In Appendix B these equations are rewritten in dimensionless form as needed for analog/hybrid or fixed-point digital solution. It is the equations of Appendix B which are used as the basis for determining real-time computer requirements. Certain modifications, such as subtracting off the principal centrifugal acceleration term in computing blade accelerations, are made in the equations in Appendix B to improve scaling and avoid taking small differences of large quantities. These modifications appear necessary in order to use the RSRA rotor model

in analog or 16-bit fixed-point digital simulation. They are probably not needed for floating-point or 24 bit fixed-point digital computation. The complexity added to the equations with these modifications (the equations are still exact) is minimal.

The equations in Appendix B do not have any terms dropped for simplification purposes. This could be done in a number of cases (e.g., dropping terms involving the product of sines of two small angles) but the resulting simplifications in the equations would not be very substantial. In general the equations are similar to the ARC equations[1] except in the approach for computing $\dot{\delta}_j$ and $\dot{\beta}_j$, the time-rate-of-change of the lagging and flapping angles, respectively, for the j^{th} blade. In the ARC equations $\ddot{\delta}_j$ and $\ddot{\beta}_j$ are computed by approximate equations of motion, from which $\dot{\delta}_j$, δ_j, $\dot{\beta}_j$, and β_j are computed assuming a periodic fourier series form for the solution. In Appendices A and B the exact blade equations are integrated to compute blade angular velocity components, which are then subtracted from rotating shaft-axis angular velocity components to compute $\dot{\delta}_j$ and $\dot{\beta}_j$ respectively. These in turn are integrated to obtain δ_j and β_j. The equation complexity is comparable with the ARC equations. Actual computer simulation will be needed to determine which method gives better results.

Table 2.1 summarizes the operations count involved in each of the computational blocks. The operations shown are needed to compute the right-hand side of all equations, including those with first time derivitives on the

[1] Mackie and Alderete, NASA-TN- D-8328, op. cit.

left side. Thus the additional operations needed to implement the numerical integration formulas are not included in the count. This is because those operations are simple and quite small in number compared with the operations required to complete each pass through the calculation of all the state-variable derivitives, which is what Table 2.1 does represent. The table shows the count based on N rotor blades with s segments per blade. Where the equations must be solved for each blade, the operations count is multiplied by N; where the equations must be solved for each segment of each blade, the operations count is multiplied by Ns.

It should be noted that there are some alternate ways of mechanizing some of the equation terms. For example, in Eq. (12.1) the term $(1 - \cos \beta_j)$ is counted as a one-variable function, whereas it might be acceptable to compute the term approximately as $0.5 \beta_j^2$. Similarly, the term $(1 - \cos \delta_j \cos \beta_j)$ in Eq. (13.2) is counted as a two-variable function, whereas it might be accurate enough to compute it approximately as $(\delta_j^2 + \beta_j^2)/2$. Also, in Eq. (10.14), Appendix A, the equation for segment angle of attack, $\alpha_{TRANS_{jk}}$, is counted as a two-variable function, whereas it can alternatively be mechanized as a combination of boolean and algebraic computations[1].

In the count of multiple/divides in Table 2.1 a separate column is shown for digital and analog mechanization. This is because multiplications of variables by constants require multiply operations in digital computation, whereas they can be implemented using coefficient devices in analog computation.

---

[1] Mackie and Alderete, NASA-TN D-8328, op. cit.

Table 2.1 Summary of Operations Count for Solving the RSRA Equations for N Blades, s Segments per Blade

Block #, Fig 2.1, Ap.A	Eq. # in Ap. B	# Mult/Div's Digital	# Mult/Div's Analog	# Adds	# Trig Fncts	#1 Var Fnct's	#2 Var Fnct's	# Sq. Roots
1.	(1.7-1.9)	14	8	9	4			
	(1.12-1.14)	9	3	3				
	(1.16-1.18)	6	6	3				
	(1.19-1.21)	21	21	10	2			
2.	(2.2-2.4)	8	0	5				
	(2.5-2.7)	4N	4N	2N	2N*			
	(2.8-2.9)	7N	7N	3N	4N			
3.	(3.1-3.3)	8	0	5				
	(3.4-3.5)	2N	2N	N				
4.	(4.3-4.5)	6	0	3				
	(4.6-4.8)	11	0	8				
5.	(5.3-5.5)	15	6	12				
	(5.7-5.9)	8	0	5				
6.	(6.1-6.3)	7N	4N	5N				
7.	(7.1-7.3)	4N	4N	2N				
	(7.4-7.6)	12N	6N	9N				
8.	(8.1-8.3)	10N	10N	5N				
	(8.6-8.8)	6Ns	0	3Ns				
9.	(9.1-9.3)	12N	10N	7N				
	(9.5-9.6)	9N	3N	6N				
10.	(10.7-10.9)	11Ns	10Ns	3Ns				
	(10.3,4,ApA)	4Ns	4Ns	Ns				Ns
	(10.5)	Ns	Ns	Ns				Ns
	(10.23,ApA)	6N	N	N(5+s)	2N			
	(10.12,ApA)	6Ns	6Ns	2Ns	2Ns			
	(10.15,ApA)	2Ns	Ns	Ns				Ns
	(10.14,16,17, ApA)						3Ns	
11.	(11.1-11.2)	N(3+2s)	0	N(2+2s)		N		
12.	(12.1-12.2)	4N	2N	3N		N		
13.	(13.1-13.3)	18N	8N	7N			N	
	(13.6-13.8)	3N	0	3Ns				
14.	(14.1-14.3)	10N	10N	7N				
	(14.4-14.6)	6N	6N	4N				
	(14.8-14.10)	N	0	3(N-1)				
	(14.11-14.13)	8	0	5				
15.	(15.2-15.3)	3N	N	2N				
	(15.5-15.7)	2N	2N	0				
	(15.8-15.10)	3N	0	3(N-1)				
	(15.11-15.13)	8	0	5				
	(15.15-15.17)	9	0	6				
Total Operations Count		131 + 126N + 32Ns	44 + 80N + 22Ns	73 + 75N + 18Ns	6 + 8N + 2Ns	2N	N + 3Ns	3Ns

At the end of Table 2.1 is shown a total count for each of the operation categories. Where a count in multiplied by N, the number of operations depends on the number of rotor blades, N. It also means that those equations involve the rotating blade frequency Ω_s, typically the order of 30 radians per second, and N can range up to 6. Where a count is multiplied by Ns the number of operations depends not only on the blade count N, but also the number of segments s taken per blade. A typical value for s is 5, so that Ns might be 6 x 5 = 30. Hence those operations multiplied by Ns can become very numerous indeed. They also clearly involve the rotor frequency Ω_s.

The total operations count for each column in Table 2.1 is used in the next three sections to estimate the requirements for real time digital and hybrid simulation. It should be noted that the equations in Appendices A and B and hence Table 2.1 do not include the aerodynamic forces due to aircraft fuselage, wing and tail, nor do they include rotor downwash effects. It is believed that this omission does not affect substantially the conclusions in the next three sections.

3. ALL-DIGITAL SIMULATION

3.1 Choice of Integration Method

The choice of numerical integration method for implementing an all-digital simulation of the RSRA is important in establishing the required integration frame rates and the corresponding estimate of digital operations per second based on Table 2.1. For non real-time helicopter simulation, studies have shown that the 4th-order Runge-Kutta method is a good choice[2]. Although RK-4 gives good accuracy for fairly large integration step size and also has good stability characteristics, it does require four passes through the equations (four derivative evaluations) per integration step. It also requires input data points one-half and one step ahead of the current point in time for evaluation of the required derivatives. This is a problem in real time simulation with external inputs unless extrapolation algorithms are used on the inputs.

If dynamic accuracies of the order of one percent are adequate for RSRA flight simulation, which we believe they are, then 2nd-order Runge Kutta (RK-2) may be preferable over fourth order (RK-4). It still suffers from the real-time data input problem noted above, however.

The data input problem is eliminated by using a multistep predictor algorithm such as Adams-Bashforth. Such numerical integration algorithms have the added advantage of requiring only one derivative evaluation per

2. Davis, J.M., R.L. Bennett, and B.L. Blankenship, "Rotorcraft Flight Simulation with Aeroelastic Rotor and Improve Aerodynamic Representation", USAAMRDL-TR-74-10A, Fort Eustis, Va., June, 1974.

integration step, the other derivatives needed for the algorithm having been already evaluated in previous steps. Also, for dynamic accuracy in the area of one percent, 2nd order Adams-Bashforth may be a good compromise and has indeed been widely used in digital flight simulation.

In lieu of actually trying various integration schemes on the full RSRA equations, the most effect analysis technique is to consider linearized equations about some trim or steady-state condition. In this case the overall linearized set of equations will have n characteristic roots, i. e, the system transfer function will have n poles. With the use of a partial fraction expansion the system can then be decomposed into separate paralleled first and second order linear systems. The errors in transfer functions and/or characteristic roots due to any integration algorithm can be studied by considering the errors in the individual first and second order systems due to each algorithm. Then by superposition the overall dynamic error can be estimated.

For example, with z-transform analysis methods[3] we can show that using RK-2 integration, the damping ratio and fractional frequency errors in simulating an underdamped second-order system are the following:

$$\hat{\xi} - \xi \tilde{=} \left(\frac{1}{2}\xi - \frac{2}{3}\xi^3\right)(aT)^2 - \left(\frac{1}{8} - \xi^2 + \xi^4\right)(aT)^3 \qquad (3.1)$$

$$\frac{\hat{\omega}}{\omega} - 1 \tilde{=} \left(\frac{1}{6} - \frac{2}{3}\xi^2\right)(aT)^2 \ , \ aT << 1 \qquad (3.2)$$

3. Gilbert, E. G., "Dynamic Error Analysis of Digital and Combined Analog-Digital Computer Systems", SIMULATION, Vol. 6, No. 4, April, 1966, pp. 241-257.

Here ξ is the exact damping ratio and $\hat{\xi}$ the damping ratio resulting from use of RK-2. Similarly, ω is the exact root frequency and $\hat{\omega}$ the frequency when using RK-2. T is the integration interval and a the undamped natural frequency of the system. For given accuracy requirements in ξ and ω Eqs. (3.1) and (3.2) can be used to compute aT and hence the number of frames (integration steps) per cycle of the transient oscillation exhibited by the second-order system.

As an illustration, let aT = 0.2. This corresponds to 5 integration steps per radian or 31.4 steps per cycle. Let ξ = 0.1 and assume we use RK-2. Then from Eqs. (3.1) and (3.2) we find that $\hat{\xi} - \xi \tilde{=} 0.001$ (damping ratio is .101 instead of .1) and $\frac{\hat{\omega}}{\omega} - 1 = .0064$ (frequency is 0.64% high).

The counterparts of Eqs. (3.1) and (3.2) are more complex for RK-4. For $\xi = 0$ the formulas are given by[3]

$$\underline{\xi = 0} \qquad \hat{\xi} - \xi = \hat{\xi} \tilde{=} \frac{2}{9} (aT)^5 \tag{3.3}$$

$$\frac{\hat{\omega}}{\omega} - 1 \tilde{=} -\frac{2}{15} (aT)^4 \qquad aT \ll 1 \tag{3.4}$$

For the case considered above for RK-2, namely ξ = .1, numerical solution of the z-transform equations shows that with RK-4 using aT = 0.4 (2.5 integration steps per radian or 15.7 per cycle), $\hat{\xi} - \xi = 0.00059$, $\hat{\omega}/\omega - 1 = -0.0036$ (3.6%). In this case RK-2 and RK-4 give comparable accuracy when the step-size for RK-4 is twice as big, which actually means the same number of passes (derivative evaluations) per integration step. Since RK-4 errors depend on $(aT)^4$ compared with $(aT)^2$ for RK-2,

3. Gilbert, op. cit

higher accuracy simulation requiring smaller step sizes would favor use of RK-4.

For 2nd-order Adams-Bashforth (AB-2) the following formula counterparts to Eqs. (3.1) and (3.2) can be derived:

$$\hat{\xi} - \xi \tilde{=} \xi \left[\frac{43}{32} - \frac{169}{96} \xi^2 \right] (aT)^2 \qquad (3.5)$$

$$\frac{\hat{\omega}}{\omega} - 1 \tilde{=} \frac{\frac{5}{12} - \frac{209}{96} \xi^2 + \frac{169}{96} \xi^4}{1-\xi^2} (aT)^2, \; aT \ll 1 \qquad (3.6)$$

Using AB-2 in simulating a second order system with damping ratio $\xi = 0.1$ and $aT = 0.1$ (62.8 integration steps per cycle) we find from numerical solution of the z-transform equations that $\hat{\xi} - \xi = 0.00101$ and $\hat{\omega}/\omega - 1 = 0.00412$ (0.4%). The damping ratio error is the same as that for RK-2 with $aT = 0.2$ (31.4 steps/cycle) and the frequency error is about 2/3 that of RK-2. Both schemes under these conditions require the same number of passes (derivative evaluations) per integration step. This is because RK-2 requires two passes per step versus one per step for AB-2.

On the basis of the above type of analysis we conclude that for dynamic accuracy of the order of one percent 2nd order Adams-Bashforth with aT somewhere between 0.1 and 0.2 will be satisfactory, i.e., say ~ 50 integration steps per cycle of the highest important problem frequency. One difficulty with Adams-Bashforth is the startup problem, but for an ongoing real-time simulation this shouldn't result in significant errors. 3rd-order Adams-Bashforth should probably also be considered and analyzed.

3.2. Required Integration Frame Rates

If we settle on 2nd-order Adams Bashforth as a proposed integration scheme with 50 steps per cycle of highest problem frequency, then the next consideration in real-time digital simulation is an estimate of the highest problem frequencies in the RSRA. For the rigid aircraft itself 1 hertz is a reasonable estimate. When non-elastic rotor blades are considered, then the maximum rotor speed, roughly 30 radians per second or about 5 hertz, is a dominant high frequency. This suggests a minimum of 5 x 50 = 250 integration steps per second (4 millisecond step size) using AB-2 wherever the rotor-blades are involved in the equations. Incidentally, 50 integration steps per cycle corresponds to one step every 7.2 degrees of azimuthal advance for the rotor, a result not inconsistent with Houck's conclusions[4]. His studies showed that somewhat larger steps can be taken, but he was using a higher-order integration algorithm (RK-4, we believe). There has been some speculation that the integration frame rate should be based on a highest problem frequency equal to the rotor speed times the number of blades. Nevertheless, we will assume a 4 millisecond integration step using 2nd order Adams-Bashforth (one pass per step) to analyze the real-time digital computer requirements.

3.3 Required Digital Operations per Second for the Real-Time RSRA Simulation

Let us assume 6 rotor blades with 5 segments per blade as

4. Houck, J.A., "Computational Aspects of Real-Time Simulation of Rotary-Wing Aircraft", Masters Thesis, George Washington University, May, 1976.

representative of a worst case RSRA simulation. Then N = 6 and s = 5 in Table 2.1, which results in the breakdown of digital operations per pass shown in Table 3.1. Clearly an overwhelming fraction of the total operations are dependent on the blade number, N, and hence involve the rotor spin frequency of 30 rad/sec. Very little would be saved by solving the non-N dependent equations at a lower frame rate.

From Table 3.1 rough estimates of actual frame times required for one pass through the equations and hence one integration step (assuming AB-2) can be made for specific digital computers. The actual number of individual digital operations (load, store, add, multiply, sign-test, etc.) for each of the categories in Table 3.1 can be estimated, assuming a conventional general purpose computer with no pipelining[5]. For example, to compute a function of two variables takes 34 operations (10 adds, 6 multiply/divides, 13 loads, 1 store, and a nominal 4 sign tests). Since the multiply/divide time on many general-purpose computers takes roughly 4 times the time required for the other operations, we use the concept of normalized operations by weighting all multiply/divides by a factor of 4. Using this concept the above two-variable function computation takes 46 normalized operations per pass. Extending this concept to the total count in Table 3.1 yields 23,603 normalized digital operations required per pass through the RSRA equations. Since typical general purpose computers in use

5. Howe, R. M., and J. Paul Landauer, "A Quantitative Method of Speed Comparison between Analog/Hybrid and Digital Computers", IEEE Computer Magazine, Vol. 9, No. 7, July, 1976, pp. 31-36.

Table 3.1 Digital Operations per Derivative Evaluation for N = 6 Blades, s = 5 Segments per Blade

	# M~H /Div's	# Adds	# Trig Fnct's	#1 Var Fnct's	#2 Var Fnct's	# Sq. Roots
Operations Independent of N or s	131	73	6			
Operations dependent on N = 6	756	450	48	12	6	
Operations dependent on Ns= 30	960	540	60		90	90
Grand Total	1847	1063	114	12	96	91

today take an average of 1 to 6 microseconds per operation (large super computers excluded) the frame time would range between 23.6 and 142 milliseconds, far more than our 4 millisecond goal for real-time RSRA simulation. And we haven't included fuselage, wing, and tail aerodynamic forces in our RSRA model, which will add somewhat more time per frame.

Assuming 50,000 normalized digital operations per pass as a rough overall estimate, including overhead, we conclude that a general purpose digital computer capable of 12.5 million operations per second (50,000x 250 hertz) is needed for the real-time RSRA simulation. The alternative is to use a specially configured digital computer with pipelining and some parallelism. Computers in this category with processing speeds in the correct range to solve the RSRA problem are, or soon will be, available at reasonable cost. Higher level compilers (e.g., Fortran IV) are a long way off for such machines, however, so that assembly language programming will be required, at least for some time. If analysis shows that floating-point versions of such machines are fast enough, then clearly that is the preferred alternate. With the scaling techniques used to develop the equations in Appendix B we are also convinced that a 16-bit fixed point digital mechanization can also do the job, if that approach becomes necessary.

4. CONVENTIONAL HYBRID SIMULATION

4.1 Basic Approach

From the previous section it is clear that the speed capabilities of small to medium-size general-purpose digital computers are at least an order of magnitude below the requirements for a real-time RSRA simulation. One possible alternative would be to use conventional all-parallel analog mechanization for the portions of the simulation involving the rotor frequencies (30 hertz) and digital mechanization for the low speed (rigid airframe) simulation. Unfortunately, reference to Table 3.1 shows that roughly 95 percent of the computational load involves the rotor frequencies (all the N or Ns dependent operations). With a conventional hybrid approach this implies a very sizeable analog requirement.

4.2 Hybrid Requirement

Let us assume that a typical analog console includes as many as 64 multipliers. In Table 3.1 the total multiple/divide count was based on digital mechanization. If we go back to Table 2.1 where the number of multiply/divides was also tabulated assuming analog mechanization, we calculate the following multiply/divide count for $N = 6, s = 5$:

$$\#\ \text{multipliers/dividers} = 80 \times 6 + 22 \times 30 = 1140$$

Assuming 64 multipliers per analog console, this implies 18 analog consoles! Also, the 96 two-variable functions represent a formidable task if implemented with analog mechanization. To be sure, these could be generated using an available specially-configured digital computer at a frame rate sufficiently high (e.g., $\sim$ 500 hertz or above) to avoid degrading the hybrid simulation.

But if a specially-configured digital computer is used for the function generation, why not use it for the whole simulation, assuming the speed is adequate? Thus the conventional hybrid approach appears quite unattractive to us.

There is one approach which might be considered. That alternative is to do all the computation except the actual integration on a specially-configured 16-bit digital computer with the integration performed on one analog console. This avoids the problems which would otherwise arise on the 16-bit computer if it were used for the numerical integration as well. I. e., for the slow-varying state variables the incremental change in state from one frame to the next is too small compared with the state variable itself to permit reasonable sealing of the increment with a 16-bit computer. Having more than 16 bits (say 32) representing the integrands solves this problem but requires hardware development. Using analog integration is an immediate way around the problem. For the RSRA with 6 rotor blades there are $6 + 12 = 18$ degrees of freedom, or 36 integrators minimum.

5. TIME-SHARED HYBRID SIMULATION

5.1 Basic Concept

An alternative hybrid mechanization of the RSRA equations involves the use of an analog circuit to compute the aerodynamic forces and moments along each blade and, possibly, to solve the blade equations of motion. The single analog circuit is then time shared amongst the N blades. This approach has been the basis for hybrid mechanization of rotary-wing aircraft simulations in the past using general-purpose analog/hybrid computers, and is the concept used in at least one current special-purpose hybrid design for helicopter simulation.

In this approach the aerodynamic forces on a given rotor blade are computed continuously on the analog computer as a function of distance along the blade, from hinge to tip. An analog integrator with fixed input provides a high-speed sweep voltage representing distance along the blade. The resulting aerodynamic force components at each point along the blade, as voltage outputs of the analog circuit, are integrated with appropriate weighting factors so that at the end of each sweep the total force and moment components acting on the blade are represented by the final integrator outputs. The integrators are then reset to zero and the sweep is repeated with the same analog circuit representing the next blade, etc., until total force and moment components for all N blades have been computed. The process is then repeated cyclically, with the result that a descrete time-series of analog voltages representing force and moment components for each blade is generated. These

can then be used to solve the blade equations of motion, either with analog or digital integration. The result is a considerable reduction in required digital computer load for the overall simulation. By time-sharing a single analog circuit over all blades a substantial saving in analog equipment is achieved.

5.2 Equipment Requirements

First of all, let us assume that the time-shared analog scheme described above is used only for computing overall blade force and moment components. Then the saving in digital operations applies to all the operation counts in Table 2.1 involving s, the blade segment number. Thus the velocity-component calculation along the blades in Eqs. (8.6)-(8.8), all the aerodynamic force components in the equations of block 10, the blade moment computation in block 11, and the force summations in Eqs. (13.6)-(13.8), in short, all the equations in Table 2.1 where the equipment count is multiplied by Ns, are included. Thus 32Ns multiplies, 18Ns adds, 2Ns trig functions, 3Ns two-variable functions, and 3Ns square root digital operations per pass are saved by the time-shared analog mechanization. Clearly the latter requires 22 analog multipliers (see the analog multiply/divide column in Table 2.1), 2 trig function generators, 3 two-variable function generators, and 3 square-root generators (analog squarers in amplifier feedback loops). This is a reasonably small complement of analog equipment, although the 2-variable analog function generators might pose a problem. Actually, one of the three 2-variable functions (the computation of α_{TRANS}) can be mechanized algebraically, so that

only the 2-variable functions representing blade section lift and drag coefficients need be implemented.

Assuming all this is done, reference to Table 3.1 shows that for N = 6 (6 blades) and s = 5 (5 blade segments in the equivalent digital mechanization) there is still considerable digital computation remaining, namely, the operations dependent on N and independent of N. These represent perhaps 40% of the original digital load for doing all the equations, so that the digital task is still formidable. Thus we have to perform more of the task on the analog, e.g., integration of the blade equations of motion (Eqs. (9.5), (9.6), (12.1), and (12.2)), as well as a large number of coordinate conversions. In fact, if we are to make a major impact on the digital operations count, say reduce it by an order of magnitude, clearly most of the N dependent as well as all of the Ns dependent operations in Table 2.1 must be performed on the time-shared analog circuit. In addition to the components required above for the Ns dependent equations (22 analog multipliers, etc.,) reference to the summary at the end of Table 2.1 shows that up to 80 analog multipliers and 8 trig function generators would be required. Although this is still much less analog equipment than would be needed for the conventional hybrid mechanization of Section 4, it would require a total of at least two analog consoles if general-purpose equipment were utilized.

In the above time-shared hybrid mechanization the analog circuit inputs, coming from DAC's (digital-to-analog converters), would be digitally-generated components of shaft-axis velocity, angular velocity, acceleration,

and angular acceleration. The analog circuit outputs, applied to A to D channels interfaced to the digital computer, would be a discrete time series of force and moment components along shaft axes due to each blade. After the time-shared analog circuit completes a duty cycle for a given blade, the force and moment contributions due to that blade are converted to digital form through the interface. The analog computation then proceeds through next blade duty cycle, etc.

5.3 Dynamic Considerations

From the previous section it is clear that the time-shared analog circuit is required to solve the blade equations of motion, i.e., integrate Eqs. (9.5), (9.6), (12.1), and (12.2) in Appendix B. These integrations will proceed continuously over each individual blade duty cycle, but many of the terms on the right-hand side of the equations will be fixed over the duty cycle, e.g., the blade moments m_{pxj} and m_{pzj} in Eqs. (9.5) and (9.6). Thus the mechanization for each degree of freedom (lagging and flapping) becomes in principle a second-order loop with two continuous analog integrators but with a sample-data feedback loop. The dynamics of such loops have been studied extensively using z-transform theory[3]. In particular, the damping ratio and frequency errors due to the finite frame time T of the feedback loop, plus the additional delay of T needed to calculate the quantity fed back (aerodynamic moment) turn out to be the following:

$$\text{Damping ratio error} = -\frac{3}{4}\, a\, T \tag{5.1}$$

$$\text{Fractional freq. error} = -\,0.864\,(aT)^2,\quad a\,T \ll 1 \tag{5.2}$$

[3] Gilbert, op. cit.

Here T is the duty-cycle time for each blade computation (time to sweep from hinge to tip to calculate total blade moment components) and a is the frequency of the two-integrator loop. We will assume that this frequency turns out to be the order of the rotor spin frequency, i.e., 30 rad/sec.

Actually, the circuit should probably be mechanized with a separate pair of integrators for each degree of freedom for each blade, i.e. 4N integrators in all. Then the group of 4 integrators assigned to each blade will integrate only for 1/N of the overall duty cycle, and will be on hold for the remining time while the equations for the other N-1 blades are integrated. In effect this means that each analog integrator must be programmed to operate at N times real time, since it integrates over only 1/N of each total duty cycle (duration N times the individual duty cycle period, T). Thus the frequency a in Eqs. (5.1) and (5.2) is effectively N times 30 or 30N rad/sec.

If a damping ratio error of 0.01 is deemed an acceptable upper limit, then Eq. (5.1) shows that $aT = (4.3)(.01) = 0.0133$. This corresponds to 75 frames per radian. For 6 blades (N = 6) $a \cong 30(6) = 180$ radians, so that the frame rate = $1/T = 75(180) = 13,500$ frames per second. The corresponding duty cycle period $T = 75 \times 10^{-6}$, or 75 microseconds. This is probably unacceptedly short, since one would expect time-constants in the analog computing elements (especially the function generators) to be the order of one microsecond. Furthermore, mode control timing errors could be $\sim$ 1 microsecond. The result would be dynamic errors in the analog circuit of perhaps several percent.

Fortunately, the sampled-data feedback delay in each two-integrator loop is known (to first order it is 1.5T) so that rate compensation for this delay can be implemented. The resulting errors in damping ratio and frequency now depend on $(aT)^2$ and acceptable dynamic accuracy (better than 0.01 in damping, one percent in frequency) can be obtained with $aT = 0.1$.[3] For a = 30(6) = 180 rad/sec, this corresponds to 1800 frames per second, or $T = 556 \times 10^{-6}$ or 556 microseconds. This is a more reasonable duty cycle and should minimize the effect of analog component dynamic errors.

To summarize, the time shared hybrid approach seems feasible for solving the RSRA equations, but will require at least two analog consoles. Naturally, it suffers from all the programming and reliability problems associated with such a hybrid approach.

[3] Gilbert, op. ct.

6. SUMMARY RECOMMENDATIONS

As a result of this study the following recommendations are made:

1. The real-time simulation of the RSRA equations should be implemented on a specially-configured digital computer using floating point if the speed is sufficient. If fixed point computation is necessary, it is recommended that equations similar to those in Appendix B of this report be used.

2. It is recommended that NASA lead an effort to standardize the notation and sign conventions used in rotary-wing aircraft math models, and that this be as consistent as possible with conventional aircraft notation.

3. It is recommended that NASA conduct an ongoing research program in rotary-wing aircraft modeling for real-time simulation. This effort should involve coordination of past and present efforts of the rotary-wing aircraft manufacturers, implementation of 2. above, systematic consideration of competing modeling approaches, determination of possible equation simplifications, investigation of different integration algorithms, determination of required integration frame rates, and correlation of results with flight tests.

APPENDIX A

DEVELOPMENT OF HELICOPTER EQUATIONS OF MOTION AND ROTOR MODEL

A.1 INTRODUCTION

In this appendix we develop from first principles the helicopter equations of motion, including the rotor model. The purpose of this development is to verify the equations furnished by ARC,[1] understand certain simplifications made in those equations, and in some cases suggest alternate mechanization which may be more suitable for computer simulation. In Appendix B, the equations are rewritten in dimensionless form in order to facilitate the simulation if hybrid or fixed-point digital-computation is utilized.

A.1.0 NOTATION FOR VECTOR COMPONENTS

In our equations of motion we are working with components of vectors along a set of mutually orthogonal right-handed axes. The vectors represent velocities or accelerations of one axis system relative to another. For convenience we will designate the various axis systems with a single letter; thus the I-frame is an inertial reference system, B-frame is a set of body axes, etc. The individual axes will be designated with a lower case subscript; thus x_b, y_b, z_b are the x, y and z body axes. A vector velocity of one axis system relative to another usually will be designated with a double subscript; for example, $\bar{\Omega}_{pq}$ is the angular velocity of the P-frame relative to the Q-frame. This vector

[1] Mackie, D. Brian, and Thomas S. Alderete, "A Real-Time Dual Processor Simulation of the Rotor System Research Aircraft," NASA TN-D-8328, January 1977.

can, of course, be projected geometrically into a third reference frame, say the R-frame. This third reference frame will be designated with a lower case superscript, where necessary for clarity. For example, the x_r, y_r, z_r components of $\bar{\Omega}_{pq}$ will be written P^r_{pq}, Q^r_{pq}, R^r_{pq}, respectively.

We have used the convention that if the vector is relative to inertial space, the I-frame, then the second subscript may be omitted. Thus the R-frame components of $\bar{\Omega}_{pi}$, the angular velocity of the P-frame relative to the I-frame, may be written P^r_p, Q^r_p, R^r_p. If a single subscript is used, it always is implied that the second subscript is "i".

In many cases the vector is projected onto the axis system given by the first subscript. When this is the case, the superscript may be omitted. Thus P_{pq}, Q_{pq}, R_{pq} are the P-frame components of $\bar{\Omega}_{pq}$, and P_b, Q_b, R_b are body axis components of $\bar{\Omega}_{bi}$.

A.1.1 DEFINITION OF AXIS SYSTEMS USED

A.1.1.1 Inertial Axes, I-Frame

For this study it is assumed that the earth is flat and non-rotating so that a frame translating with a constant velocity (i.e., the horizontal wind velocity) with respect to the earth may be considered Newtonian. We designate this atmospheric frame as the I-frame.

A.1.1.2 Body Axes, B-Frame

These are conventional vehicle body axes. Origin of the B-frame is the vehicle center of mass. If there is a plane of symmetry (such as

most airplanes have) it is the $x_b z_b$ plane. In straight and level flight the positive x_b axis points approximately forward, the positive y_b axis points approximately to the pilot's right and the positive z_b axis points approximately downward. The B-frame usually is defined by the vehicle manufacturer.

A.1.1.3 Hub Axes, H-Frame

Origin of the rotor-hub axes is displaced from the vehicle center of mass by the vector $\bar{r}_H$, where

$$\bar{r}_H = (x_h, y_h, z_h)$$

Hub axes are parallel to body axes, as shown in Figure 1.1.

A.1.1.4 Shaft Axes, S-Frame

Origin of the S-frame is the same as hub axes. The S-frame is rotated from the hub frame through the fixed Euler angles i_θ and i_ϕ. The Euler angles result from positive rotation of i_θ about the y_h axis followed by i_ϕ about the resulting x_s axis.

A.1.1.5 Rotating Shaft Axes, R_j-Frame

Origin of the R_j-frame for the j^{th} blade is the same as the S-frame, namely the hub. As can be seen in Figure 1.1, the x_{rj}, y_{rj}, z_{rj}, R_j-frame axes are rotated with respect to the x_s, y_s, z_s S-frame axes by the azimuthal angle $\pi/2 - \Psi_j$ about the z_s axis. Thus the z_{rj} and z_s axes are coincident. The angular velocity of the R_j frame with respect to the S-frame is given by Ω_s and is directed along the z_s (i.e., z_{rj}) axis. Clearly $\dot{\Psi}_j = -\Omega_s$. There are separate R_j-frame axes for each

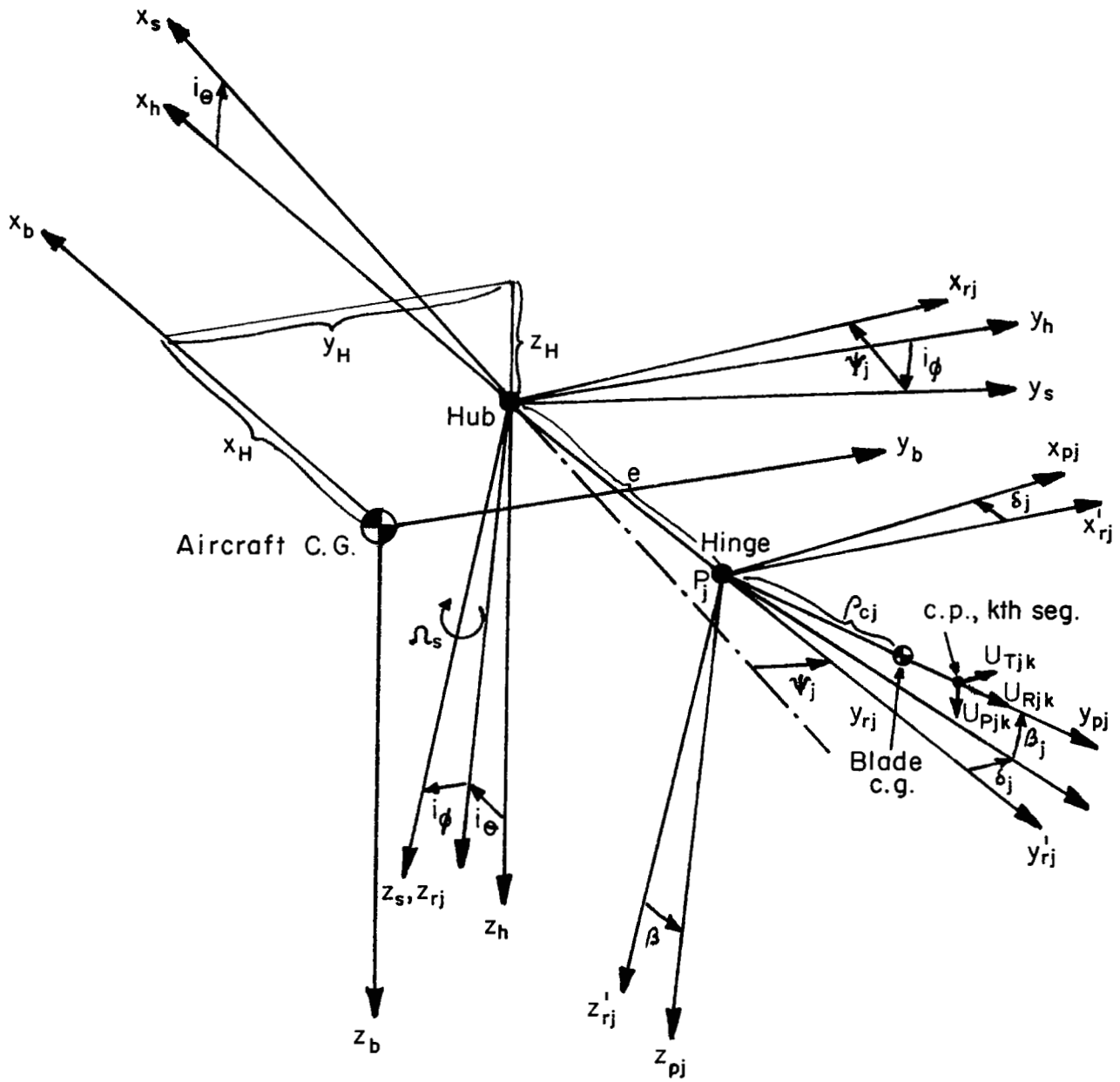

Figure 1.1 Relative orientation of body axes (x_b, y_b, z_b), hub axes (x_h, y_h, z_h), shaft axes (x_s, y_s, z_s), rotating shaft axes (x_{rj}, y_{rj}, z_{rj}) and blade-span axes (x_{pj}, y_{pj}, z_{pj}) for the j^{th} blade.

of N rotor blades, i.e., $j=1,2,\ldots,N$.

A.1.1.6 Blade Span Axes, P_j-Frame

Origin of the P_j-frame is at the blade-hinge point P_j shown in Figure 1.1. The hinge-point P_j is located a distance e along y_{rj} from the hub. In Figure 1.1 there is indicated an axis system x'_{rj}, y'_{rj}, z'_{rj} which is just the R_j-frame axes, x_{rj}, y_{rj}, z_{rj}, translated from the hub to the hinge-point P_j. The P_j-frame is rotated from the R_j-frame through the blade lag-angle δ_j (negative rotation about z'_{rj}) and the blade flapping-angle β_j (negative rotation about x_{pj}). The y_{pj} axis of the P_j-frame is along the spanwise direction of the blade. There are separate P_j-frame axes for each of N rotor blades.

A.2. HELICOPTER EQUATIONS OF MOTION

A.2.0 SUMMARY

A block diagram of the overall equations of motion in vector form is shown in Fig. 2.1. It will be used as a reference for the listing of the scalar equations in the following sections. The latter are the basis for establishing the computational requirements for simulation. The blocks in Figure 2.1 are numbered in the lower left or lower right corner. Block 1 represents the overall aircraft translational and rotational equations of motion as determined by summing forces and moments about the aircraft, e.g., Blocks 2 through 5 represent the equations for the accelerations and velocities of the rotor hub axes and rotating rotor shaft axes. Blocks 6 and 7 represent equations for the velocity and

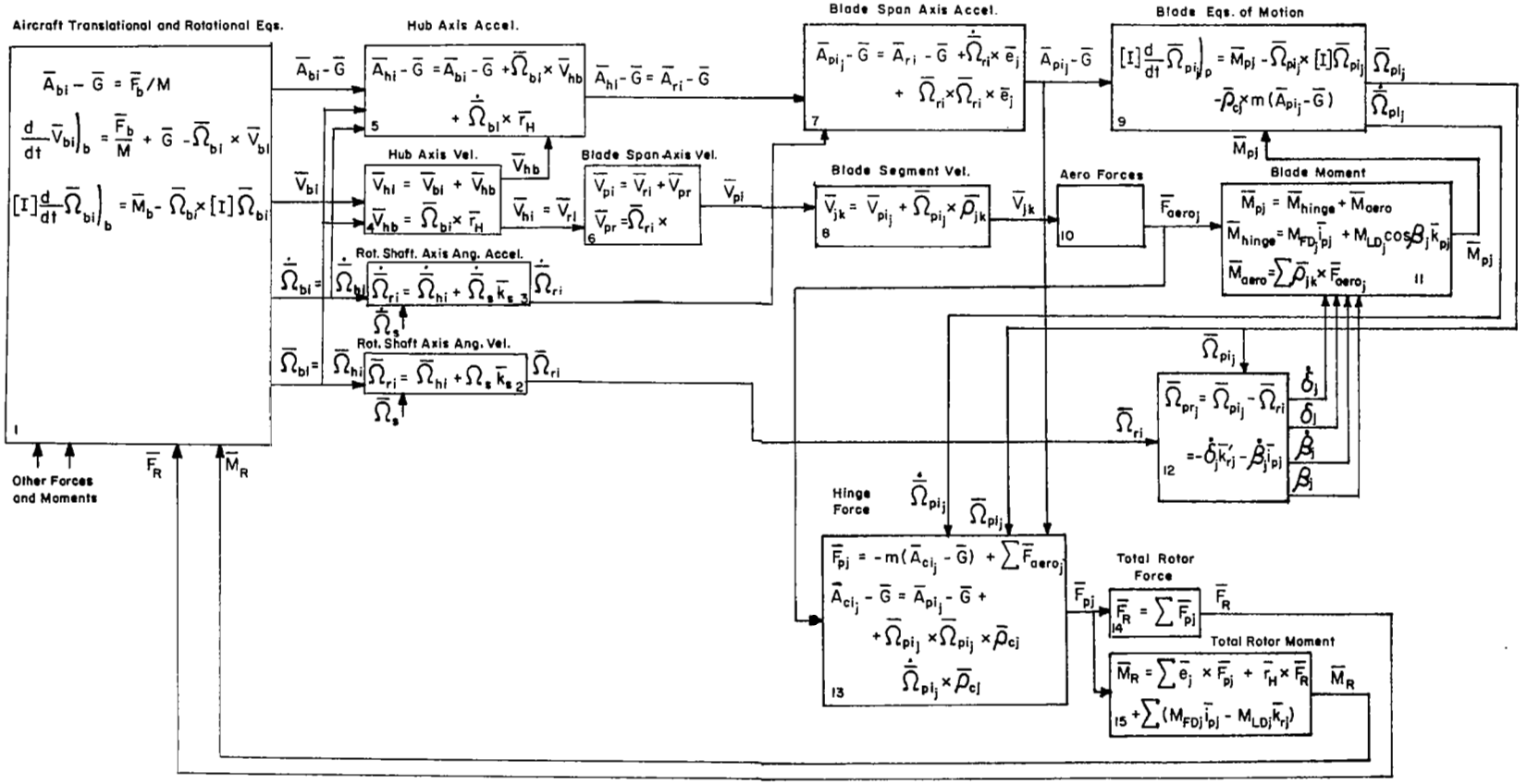

Figure 2.1 Block Diagram of Helicopter Equations in Vector Form

acceleration of the rotor blade-span axes. Block 8 shows the equations for the velocities of the individual blade segments. Block 9 represents the blade equations of motion, with two degrees of freedom (lagging and flapping) for each blade. Block 10 represents the equations for generating aerodynamic forces on the blade, while block 11 shows the equations for calculating the total external moment on the blade (except gravity). Block 12 represents the equations for relative velocity of blade span axes with respect to rotating shaft axes, which are used to establish equations for $\dot{\delta}$ and $\dot{\beta}$, where δ and β are blade lag and flap angles, respectively. Finally, blocks 13, 14, and 15 show the equations for computing the overall vehicle force and moment due to the rotor forces.

A.2.1 TRANSLATIONAL AND ROTATIONAL AIRCRAFT EQUATIONS

The translational equations for the aircraft are based on the vector equation

$$\bar{A}_{bi} - \bar{G} = \bar{F}_b/M \tag{1.1}$$

Here $\bar{A}_{bi}$ is the translational acceleration of the aircraft body axes (x_b, y_b, z_b, centered at aircraft c.g.) with respect to the inertial reference frame which is the atmosphere through which the aircraft flies. $\bar{G}$ is the gravity acceleration vector and $\bar{F}_b$ is the total of all other external forces acting on the aircraft. M is the aircraft mass (not including rotor blades). In scalar form, Eq. (1.1) becomes

$$A_{bx} - G_x = F_{bx}/M \tag{1.2}$$

$$A_{by} - G_y = F_{by}/M \tag{1.3}$$

$$A_{bz} - G_z = F_{bz}/M \tag{1.4}$$

Thus the external force components, F_{bx}, F_{by}, and F_{bz} are used to provide the three acceleration-less-gravity output components of block 1 in Figure 1.1. We note that

$$\bar{A}_{bi} \equiv \frac{d}{dt}\bar{V}_{bi})_i = \frac{d}{dt}\bar{V}_{bi})_b + \bar{\Omega}_{bi} \times \bar{V}_{bi} \tag{1.5}$$

Here $\bar{V}_{bi}$ is the body axis translational velocity vector with respect to the inertial reference frame and $\bar{\Omega}_{bi}$ is the body axis angular velocity vector with respect to the same frame. $\frac{d}{dt}\bar{V}_{bi})_i$ is the time-rate-of-change of $\bar{V}_{bi}$ as viewed from the inertial (I) frame, and $\frac{d}{dt}\bar{V}_{bi})_b$ is the time-rate-of-change of $\bar{V}_{bi}$ as viewed by an observer in the body axis (B)-frame. Thus

$$\bar{V}_{bi} = U_b \bar{i}_b + V_b \bar{j}_b + W_b \bar{k}_b \tag{1.6}$$

where $\bar{i}_b$, $\bar{j}_b$, and $\bar{k}_b$ are the unit vectors, respectively, along the x_b, y_b, z_b body axes. Hence U_b, V_b, W_b are the components of aircraft velocity $\bar{V}_{bi}$ along the three body axes, respectively. Also

$$\bar{\Omega}_{bi} = P_b \bar{i}_b + Q_b \bar{j}_b + R_b \bar{k}_b \tag{1.7}$$

where P_b, Q_b, R_b are, respectively, the components of aircraft angular velocity along the three body axes. Thus P_b represents conventional aircraft roll rate, Q_b the pitch rate, and R_b the yaw rate.

From Eq. (1.6) we obtain

$$\frac{d\bar{V}_{bi}}{dt})_b = \dot{U}_b \bar{i}_b + \dot{V}_b \bar{j}_b + \dot{W}_b \bar{k}_b \tag{1.8}$$

since it follows that for an observer in the body-axis frame, the body axis unit vectors $\bar{i}_b$, $\bar{j}_b$, $\bar{k}_b$ do not change. We also note that the gravity accelerations in Eqs. (1.2) through (1.4) are given by

$$G_x = - g_o \sin \theta_b \tag{1.9}$$

$$G_y = g_o \cos \theta_b \sin \phi_b \tag{1.10}$$

$$G_z = g_o \cos \theta_b \cos \phi_b \tag{1.11}$$

where θ_b and ϕ_b are the conventional aircraft pitch and bank angle, respectively, and where g_o is the sea level gravity acceleration. Substituting Eqs. (1.6), (1.7) and (1.8) into (1.5), and the scalar components of (1.5) into (1.2) through (1.4), we obtain the following three equations using (1.9) through (1.11):

$$\dot{U}_b = - W_b Q_b + V_b R_b - g_o \sin \theta_b + F_{bx}/M \tag{1.12}$$

$$\dot{V}_b = - U_b R_b + W_b P_b + g_o \cos \theta_b \sin \phi_b + F_{by}/M \tag{1.13}$$

$$\dot{W}_b = - V_b P_b + U_b Q_b + g_o \cos \theta_b \cos \phi_b + F_{bz}/M \tag{1.14}$$

These translational equations of motion are integrated to obtain the body-axis velocity components U_b, V_b, and W_b.

The rotational equations of motion are obtained from the following equation:

$$\left(\frac{d \bar{H}_b}{dt} \right)_i = \bar{M}_b \tag{1.15}$$

where $\bar{M}_b$ is the external moment acting on the aircraft c.g. and $\bar{H}_b$ is the angular momentum of the aircraft about the c.g. $\bar{H}_b$ is in turn given by

$$\bar{H}_b = [I]\bar{\Omega}_{bi} \tag{1.16}$$

Here [I] is the inertia matrix for the aircraft, not including the inertia of the rotor blades. This is because the angular momentum associated with the blades is considered separately in the blade equations of motion, and the resulting blade reaction moments on the hub are part of the total external moment $\bar{M}_b$ acting on the aircraft. Also in Eq. (1.16) we have not included the angular momentum of the turbine power-plant assembly, although this can easily be done.

If we neglect products of inertia in the inertia matrix [I], then Eq. (1.16) can be written as

$$\bar{H}_b = I_{xx} P_b \bar{i}_b + I_{yy} Q_b \bar{j}_b + I_{zz} R_b \bar{k}_b \tag{1.17}$$

where I_{xx}, I_{yy} and I_{zz} are the aircraft moments of inertia about the body axes, x_b, y_b, z_b, respectively and $\bar{i}_b$, $\bar{j}_b$ and $\bar{k}_b$ are the unit vectors along the respective body axes. Differentiating Eq. (1.16) with respect to time we have

$$\frac{d}{dt}\bar{H}_b)_i = [I]\frac{d}{dt}\bar{\Omega}_{bi})_b + \bar{\Omega}_{bi} \times [I]\bar{\Omega}_{bi} \tag{1.18}$$

In Eq. (1.18), $\frac{d}{dt}\bar{\Omega}_{bi})_b$, i.e., the time rate of change of body-axis angular velocity as viewed by an observer in the body axes, is given by

$$\frac{d}{dt}\bar{\Omega}_{bi})_b = \dot{P}_b \bar{i}_b + \dot{Q}_b \bar{j}_b + \dot{R}_b \bar{k}_b \tag{1.19}$$

ince we have neglected the products of inertia,

$$[I]\bar{\Omega}_{bi} = I_{xx} P_b \bar{i}_b + I_{yy} Q_b \bar{j}_b + I_{zz} R_b \bar{k}_b \tag{1.20}$$

and hence

$$\bar{\Omega}_{bi} \times [I]\bar{\Omega}_{bi} = (I_{zz}-I_{yy})Q_b R_b \bar{i}_b + (I_{xx}-I_{zz})R_b P_b \bar{j}_b + (I_{yy}-I_{xx})P_b Q_b \bar{k}_b \qquad (1.21)$$

Substituting Eqs. (1.19) and (1.21) into Eq. (1.18), and (1.18) into (1.15), we obtain the following thress scalar equations of motion of the aircraft:

$$\dot{P}_b = -\frac{I_{zz} - I_{yy}}{I_{xx}} Q_b R_b + \frac{M_{bx}}{I_{xx}} \qquad (1.22)$$

$$\dot{Q}_b = -\frac{I_{xx} - I_{zz}}{I_{yy}} R_b P_b + \frac{M_{by}}{I_{yy}} \qquad (1.23)$$

$$\dot{R}_b = -\frac{I_{yy} - I_{xx}}{I_{zz}} P_b Q_b + \frac{M_{bz}}{I_{zz}} \qquad (1.24)$$

In Eqs. (1.22) through (1.24) M_{bx}, M_{by}, and M_{bz} represent the external moments acting along the respective body axes.

In case the products of inertia are not negligible, it is straightforward to add the requisite terms to Eqs. (1.22) through (1.24). These equations are integrated to obtain the body-axis angular velocity components, P_b, Q_b, R_b, which in turn are used to compute the time-rates-of-change of the body axis Euler angles Ψ_b (heading), θ_b (pitch) and ϕ_b (bank angle). Thus we have the familiar formulas

$$\dot{\Psi}_b = (R_b \cos \phi_b + Q_b \sin \phi_b)/\cos \theta_b \qquad (1.25)$$

$$\dot{\theta}_b = Q_b \cos \phi_b - R_b \sin \phi_b \qquad (1.26)$$

$$\dot{\phi}_b = P_b + \dot{\Psi}_b \sin \theta_b \qquad (1.27)$$

These are integrated in turn to compute the Euler angles Ψ_b, θ_b, and ϕ_b.

If our simulation requires computation of the aircraft position, it is necessary to calculate aircraft velocity components along earth axes, e.g., north, east, and vertical. Denoting $\bar{V}^e_{bi}$ as the aircraft velocity vector expressed in components along the earth (e) axes and $\bar{V}^b_{bi} \equiv \bar{V}_{bi}$ as the aircraft velocity vector expressed in components along the body axes, we write

$$\bar{V}^e_{bi} = [T_{be}]\bar{V}^b_{bi} \tag{1.28}$$

where $[T_{be}]$ is the matrix used to transform body-axis components of a vector to earth-axis components. It is straightforward to show that

$[T_{be}] =$

$$\begin{bmatrix} \cos\theta_b\cos\Psi_b & -\cos\phi_b\sin\Psi_b+\sin\phi_b\sin\theta_b\cos\Psi_b & \sin\phi_b\sin\Psi_b+\cos\phi_b\sin\theta_b\cos\Psi_b \\ \cos\theta_b\sin\Psi_b & \cos\phi_b\cos\Psi_b+\sin\phi_b\sin\theta_b\sin\Psi_b & -\sin\phi_b\cos\Psi_b+\cos\phi_b\sin\theta_b\sin\Psi_b \\ -\sin\theta_b & \sin\phi_b\cos\theta_b & \cos\theta_b\cos\phi_b \end{bmatrix} \tag{1.29}$$

Letting $\dot{S}_x$, $\dot{S}_y$, and $\dot{S}_z$ (i.e., $-\dot{h}$) represent the velocity components north, east, and downward (h is altitude), we have from Eqs. (1.28) and (1.29)

$$\dot{S}_x = U_b\cos\theta_b\cos\Psi_b + V_b(-\cos\phi_b\sin\Psi_b + \sin\phi_b\sin\theta_b\cos\Psi_b) + W_b(\sin\phi_b\sin\Psi_b + \cos\phi_b\sin\theta_b\cos\Psi_b) \tag{1.30}$$

$$\dot{S}_y = U_b\cos\theta_b\sin\Psi_b + V_b(\cos\phi_b\cos\Psi_b + \sin\phi_b\sin\theta_b\sin\Psi_b) + W_b(-\sin\phi_b\cos\Psi_b + \cos\phi_b\sin\theta_b\sin\Psi_b) \tag{1.31}$$

$$\dot{S}_z = -\dot{h} = -U_b \sin\theta_b + V_b \sin\phi_b \cos\theta_b + W_b \cos\theta_b \cos\phi_b \quad (1.32)$$

We note in passing that the inverse of the matrix $[T_{be}]$ is its transpose. Thus

$$\bar{V}_{bi}^{b} = [T_{eb}]\bar{V}_{bi}^{e} \quad (1.33)$$

where

$$[T_{eb}] = [T_{be}]^T \quad (1.34)$$

and $[T_{be}]$ is given in Eq. (1.29).

In this section we have assumed as an inertial reference frame the atmosphere through which the aircraft is moving. If there are steady wind components they are easily added to Eqs. (1.30) through (1.32) to take care of wind drift.

In summary, we have in this section indicated the derivation of the six-degree-of-freedom equations of motion of the rigid aircraft. Three of the state variables are the translational velocity components U_b, V_b and W_b along the body axes. Equations (1.12), (1.13) and (1.14) are integrated to obtain these variables. Three more state variables are the rotational velocity components P_b, Q_b, R_b along the body axes. Equations (1.22), (1.23) and (1.24) are integrated to obtain these variables. The Euler angles Ψ_b, θ_b, ϕ_b constitute another three state variables, and Eqs. (1.25), (1.26) and (1.27) are integrated to compute them. Finally, distance north (S_x), distance east (S_y) and altitutde ($h = -S_z$) are the remaining state variables. Equations (1.32), (1.33) and (1.34) are integrated to compute them.

Although the equations derived in this section are well known and widely used, it was felt worthwhile to include the derivation because the

methodology carries through to the subsequent derivation of rotor blade equations of motion.

A.2.2 ROTATING SHAFT AXIS ANGULAR VELOCITY

Although the rotor hub is located at a position remote from the aircraft c.g., reference to Figure 1.1 shows that the hub axes x_h, y_h, z_h are aligned with the body axes x_b, y_b, z_b. Thus the angular velocity of the two axis systems is identical, and hence we write

$$\bar{\Omega}_{bi} = \bar{\Omega}_{hi} \tag{2.1}$$

Next we determine formulas for the components of $\bar{\Omega}_{hi}$ along the shaft axes x_s, y_s, z_s. From Figure 1.1 we see that the shaft axes differ from the hub axes by the pitch angle i_θ and roll angle i_ϕ. Denoting the transformation matrix from hub to shaft axes as $[T_{hs}]$, we have

$$\bar{\Omega}^s_{hi} = [T_{hs}]\bar{\Omega}^h_{hi} \tag{2.2}$$

where $\bar{\Omega}^s_{hi}$ indicates that $\bar{\Omega}_{hi}$ is expressed in terms of shaft-axis components and $\bar{\Omega}^h_{hi}$ indicates that $\bar{\Omega}_{hi}$ is expressed in terms of hub-axis components.

The matrix $[T_{hs}]$ is obtained easily by analogy with conventional Euler angles, for which we have already written the matrix $[T_{be}]$ in Eq. (1.29) for the transformation of vector components from body to earth axes. In Eq. (2.2) $[T_{hs}]$ is equivalent to a matrix for transforming vector components from earth to body axes where $\theta_b = i_\theta$, $\phi_b = i_\phi$, and $\Psi_b = 0$. Thus we set $\theta_b = i_\theta$, $\phi_b = i_\phi$, and $\Psi_b = 0$ in $[T_{eb}] = [T_{be}]^T$ to obtain $[T_{hs}]$. Making these substitutions in the transpose of $[T_{be}]$ in Eq. (1.29), we obtain

$$[T_{hs}] = \begin{bmatrix} \cos i_\theta & 0 & -\sin i_\theta \\ \sin i_\phi \sin i_\theta & \cos i_\phi & \sin i_\phi \cos i_\theta \\ \cos i_\phi \sin i_\theta & -\sin i_\phi & \cos i_\phi \cos i_\theta \end{bmatrix} \tag{2.3}$$

Since i_θ and i_ϕ are fixed angles, the angular velocity of the shaft axes x_s, y_s, z_s is equal to the angular velocity of the hub axes x_h, y_h, z_h. Hence, we can write

$$\bar{\Omega}_{si} = \bar{\Omega}_{hi} \tag{2.4}$$

Thus, Eqs. (2.2) and (2.3) can be used to compute the components of shaft-axis angular rate along the shaft axes.

Reference to Figure 1.1 shows that the rotating shaft axes x_{rj}, y_{rj}, z_{rj} for the j^{th} rotor blade differ from the shaft axes x_s, y_s, z_s by the azimuthal angle $\pi/2-\Psi_j$ in the x_s, y_s or x_{rj} y_{rj} plane, where

$$\dot{\Psi}_j = -\Omega_s \tag{2.5}$$

Note that Ψ_j and hence the rotating shaft axes are different for each of the N blades (j=1, 2, . . . , N). To obtain the angular velocity $\bar{\Omega}_{ri}$ of the rotating shaft axes for each blade, we note that

$$\bar{\Omega}_{ri} = \bar{\Omega}_{si} + \Omega_s \bar{k}_s \tag{2.6}$$

where $\bar{k}_s$ is the unit vector along the z_s axis and Ω_s is assumed to be the velocity of the rotating shaft axes with respect to the shaft axes (see block 2 in Fig. 2.1). Note that the angular velocity of the rotating shaft axes is the same for all blades. This is why we denote the angular velocity as $\bar{\Omega}_{ri}$ (angular velocity of R_j-frame with respect to the inertial frame) without an added subscript j for the j^{th} blade.

Using Eqs. (2.2), (2.3), (2.4) and (2.6), we obtain the following three scalar equations for the components P_r^s, Q_r^s, and R_r^s of rotating shaft axis angular velocity along shaft axes:

$$P_r^s = P_b \cos i_\theta - R_b \sin i_\theta \tag{2.7}$$

$$Q_r^s = P_b \sin i_\phi \sin i_\theta + Q_b \cos i_\phi + R_b \sin i_\phi \cos i_\theta \tag{2.8}$$

$$R_r^s = P_b \cos i_\phi \sin i_\theta - Q_b \sin i_\phi + R_b \cos i_\phi \cos i_\theta + \Omega_s \tag{2.9}$$

Note that P_r^s, Q_r^s, and R_r^s are the same for each blade. For this reason we don't add the subscript j for the j^{th} blade.

Next we determine the components of $\bar{\Omega}_{ri}$ along the rotating shaft axes x_r, y_r, z_r. Again, reference to Figure 1.1 shows that the rotating shaft axes x_{rj}, y_{rj}, z_{rj} for the j^{th} blade differ from the shaft axes x_s, y_s, z_s by the equivalent Euler angles $\theta_b = 0$, $\phi_b = 0$, $\Psi_b = \pi/2 - \Psi_j$. Making these substitutions into $[T_{eb}] = [T_{be}]^T$, where $[T_{be}]$ is given in Equation (1.29), and noting that $\cos(\pi/2 - \Psi_j) = \sin \Psi_j$, $\sin(\pi/2 - \Psi_j) = \cos \Psi_j$, we obtain the following transformation matrix:

$$[T_{sr_j}] = \begin{bmatrix} \sin \Psi_j & \cos \Psi_j & 0 \\ -\cos \Psi_j & \sin \Psi_j & 0 \\ 0 & 0 & 1 \end{bmatrix} \tag{2.10}$$

Thus

$$\bar{\Omega}^r_{ri_j} = [T_{sr_j}] \bar{\Omega}^s_{ri} \tag{2.11}$$

and from (2.10) and (2.11) we have

$$P^r_{rj} = P^s_r \sin \Psi_j + Q^s_r \cos \Psi_j \tag{2.12}$$

$$Q^r_{rj} = - P^s_r \cos \Psi_j + Q^s_r \sin \Psi_j \tag{2.13}$$

$$R^r_{rj} = R^s_r \tag{2.14}$$

as the components of rotating shaft axis angular velocity along the R_j-frame axes for the j^{th} blade. Since there is a rotating shaft axis system for each blade, Eqs. (2.12) through (2.14) are repeated N times for N blades, each blade having a different Ψ_j (j=1, 2, . . . , N).

Note that the N blades will be equally spaced in azimuth with a separation of $2\pi/N$ between each blade. Thus if Ψ_1 is the azimuthal angle for the first blade, then the angle Ψ_j for the j^{th} blade is given by

$$\Psi_j = \Psi_1 + 2\pi(j-1)/N, \quad j=1, 2, \ldots, N \tag{2.15}$$

It follows that

$$\sin \Psi_j = \sin[\Psi_1 + \frac{2\pi(j-1)}{N}] = \sin \Psi_1 \cos[\frac{2\pi(j-1)}{N}] + \cos \Psi_1 \sin[\frac{2\pi(j-1)}{N}] \tag{2.16}$$

and

$$\cos \Psi_j = \cos[\Psi_1 + \frac{2\pi(j-1)}{N}] = \cos \Psi_1 \cos[\frac{2\pi(j-1)}{N}] - \sin \Psi_1 \sin [\frac{2\pi(j-1)}{N}] \tag{2.17}$$

Thus once $\sin \Psi_1$ and $\cos \Psi_1$ are computed for the first blade, $\sin \Psi_j$ and $\cos \Psi_j$ for the j^{th} blade can be computed using Eqs. (2.16) and (2.17). Each equation only requires two multiplies and an add, which may save considerable time over computing $\sin \Psi_j$ and $\cos \Psi_j$ directly.

Finally, we develop the equations for obtaining the components of rotating shaft axis angular velocity along the blade span axes for the j^{th} blade. In Figure 1.1 we see that the blade span axes, x_{pj}, y_{pj}, z_{pj} are displaced from the rotating shaft axes x_{rj}, y_{rj}, and z_{rj} by the yaw angle δ_j (called the blade lag angle) and the roll angle β_j (called the blade flap angle). Again, using the Euler angle analogy, $\theta_b = 0$, $\phi_b = -\beta_j$, and $\Psi_b = -\delta_j$. Making these substitutions into $[T_{eb}] = [T_{be}]^T$, where $[T_{be}]$ is given in Eq. (1.29), we obtain the following formula for the transformation matrix from rotating shaft axes to the j^{th} blade span axes:

$$[T_{rp_j}] = \begin{bmatrix} \cos\delta_j & -\sin\delta_j & 0 \\ \sin\delta_j \cos\beta_j & \cos\delta_j \cos\beta_j & -\sin\beta_j \\ \sin\delta_j \sin\beta_j & \cos\delta_j \sin\beta_j & \cos\beta_j \end{bmatrix} \tag{2.18}$$

since

$$\bar{\Omega}^p_{ri_j} = [T_{rp_j}]\bar{\Omega}^r_{ri_j} \tag{2.19}$$

we have

$$P^p_{rj} = P^r_{rj}\cos\delta_j - Q^r_{rj}\sin\delta_j \tag{2.20}$$

$$Q^p_{rj} = P^r_{rj}\sin\delta_j\cos\beta_j + Q^r_{rj}\cos\delta_j\cos\beta_j - R^r_{rj}\sin\beta_j \tag{2.21}$$

$$R^p_{rj} = P^r_{rj}\sin\delta_j\sin\beta_j + Q^r_{rj}\cos\delta_j\sin\beta_j + R^r_{rj}\cos\beta_j \tag{2.22}$$

Actually, it turns out that Q^p_{rj} in Eq. (2.21) is not needed in the mechanization.

Thus block 2 in Figure 2.1, which involves the computation of rotating shaft angular velocity components, requires the use of Eqs.

(2.7), (2.8) and (2.9); Eqs. (2.12), (2.13) and (2.14) times N for N blades; and Eqs. (2.20) and (2.22) times N for N blades.

A.2.3 ROTATING SHAFT AXIS ANGULAR ACCELERATION

Next we consider the equations for $\dot{\bar{\Omega}}_{ri}$, the angular acceleration of the rotating shaft axes x_r, y_r, z_r. Consider first $\dot{\bar{\Omega}}_{si}$, the angular acceleration of the shaft axes x_s, y_s, z_s. Since the alignment of these axes is fixed with respect to the body axes (the angles i_θ and i_ϕ are constant in Figure 1.1), clearly

$$\dot{\bar{\Omega}}_{si} = \dot{\bar{\Omega}}_{bi} \tag{3.1}$$

where $\dot{\bar{\Omega}}_{bi}$ is the angular acceleration of the body axes. In section A.2.1 we noted from Eq. (1.7) that the body-axis angular velocity, $\bar{\Omega}_{bi}$, is by definition given by

$$\bar{\Omega}_{bi} = P_b \bar{i}_b + Q_b \bar{j}_b + R_b \bar{k}_b \tag{3.2}$$

Differentiating $\bar{\Omega}_{bi}$, we have

$$\frac{d}{dt}\bar{\Omega}_{bi})_i = \frac{d}{dt}\bar{\Omega}_{bi})_b + \bar{\Omega}_{bi} \times \bar{\Omega}_{bi} = \frac{d}{dt}\bar{\Omega}_{bi})_b \tag{3.3}$$

since $\bar{\Omega}_{bi} \times \bar{\Omega}_{bi} = 0$. Equation (3.3) shows that the time-rate-of-change of $\bar{\Omega}_{bi}$ as viewed from the inertial frame is the same as the time rate of change as viewed by an observer in the body axis frame. But from Eq. (3.2) this is simply

$$\dot{\bar{\Omega}}_{bi} = \dot{P}_b \bar{i}_b + \dot{Q}_b \bar{j}_b + \dot{R}_b \bar{k}_b \tag{3.4}$$

where $\dot{\bar{\Omega}}_{bi}$ is the time rate of change of $\bar{\Omega}_{bi}$ as viewed from the inertial

frame. Thus the body axis components of the $\dot{\bar{\Omega}}_{bi}$ output from block 1 in Figure 2.1 are simply $\dot{P}_b$, $\dot{Q}_b$, and $\dot{R}_b$, respectively, as given in Eqs. (1.22), (1.23) and (1.24).

The shaft axis components of $\dot{\bar{\Omega}}_{si}$ can be obtained from body axis components by using the transformation matrix $[T_{hs}] = [T_{bs}]$ as given in Eq. (2.3). Thus

$$\dot{\bar{\Omega}}^s_{si} = [T_{hs}]\dot{\bar{\Omega}}^h_{si} \tag{3.5}$$

and since from Eq. (3.1), $\dot{\bar{\Omega}}_{si} = \dot{\bar{\Omega}}_{bi}$, we have

$$\dot{P}^s_s = \dot{P}_b \cos i_\theta - \dot{R}_b \sin i_\theta \tag{3.6}$$

$$\dot{Q}^s_s = \dot{P}_b \sin i_\phi \sin i_\theta + \dot{Q}_b \cos i_\phi + \dot{R}_b \sin i_\phi \cos i_\theta \tag{3.7}$$

$$\dot{R}^s_s = \dot{P}_b \cos i_\phi \sin i_\theta - \dot{Q}_b \sin i_\phi + \dot{R}_b \cos i_\phi \cos i_\theta \tag{3.8}$$

as the formulas for shaft-axis angular acceleration components along shaft axes. Next we compute the components of $\bar{\Omega}_{si_j}$ along the rotating shaft axes of the j^{th} blade using the formula

$$\dot{\bar{\Omega}}^r_{si_j} = [T_{sr_j}]\dot{\bar{\Omega}}^s_{si} \tag{3.9}$$

where $[T_{sr_j}]$ is given in Eq. (2.10), Section A.2.2. Thus

$$\dot{P}^r_{sj} = \dot{P}^s_s \sin \Psi_j + \dot{Q}^s_s \cos \Psi_j \tag{3.10}$$

$$\dot{Q}^r_{sj} = -\dot{P}^s_s \cos \Psi_j + \dot{Q}^s_s \sin \Psi_j \tag{3.11}$$

$$\dot{R}^r_{sj} = \dot{R}^s_s \tag{3.12}$$

We have already seen in Eq. (2.6) of Section A.2.2 that $\bar{\Omega}_{ri}$, the angular velocity of the rotating shaft axes, is given by

$$\bar{\Omega}_{ri} = \bar{\Omega}_{si} + \Omega_s \bar{k}_s \tag{3.13}$$

Differentiating $\bar{\Omega}_{ri}$, we obtain

$$\dot{\bar{\Omega}}_{ri} = \frac{d}{dt}\bar{\Omega}_{ri})_i = \frac{d}{dt}\bar{\Omega}_{ri})_r + \bar{\Omega}_{ri} \times \bar{\Omega}_{ri} = \frac{d}{dt}\bar{\Omega}_{ri})_r \tag{3.14}$$

since $\bar{\Omega}_{ri} \times \bar{\Omega}_{ri} = 0$. Thus from (3.13) and (3.14)

$$\dot{\bar{\Omega}}_{ri} = \frac{d}{dt}(\bar{\Omega}_{si} + \Omega_s \bar{k}_r)_r \tag{3.15}$$

where $\bar{k}_r = \bar{k}_s$. Even though there are N rotating shaft axes (one for each of N blades) until now we have not designated either $\bar{\Omega}_{ri}$ or $\dot{\bar{\Omega}}_{ri}$ with an additional subscript j for the j^{th} blade because each rotating blade-axis differs from the other rotating blade axes by a fixed azimuthal angle. Hence $\bar{\Omega}_{ri}$ and $\dot{\bar{\Omega}}_{ri}$ are the same for all blades. But as soon as we write the formulas for the components of $\dot{\bar{\Omega}}_{ri}$ along the rotating shaft axes for the j^{th} blade, we must use the additional subscript j. Thus in Eq. (3.15) for the j^{th} blade

$$\bar{\Omega}^r_{si_j} = P^r_{sj} \bar{i}_r + Q^r_{sj} \bar{j}_r + R^r_{sj} \bar{k}_r \tag{3.16}$$

and from Eqs. (3.10) through (3.16) we have

$$\dot{P}^r_{rj} = \dot{P}^s_s \sin \Psi_j + \dot{Q}^s_s \cos \Psi_j \tag{3.17}$$

$$\dot{Q}^r_{rj} = -\dot{P}^s_s \cos \Psi_j + \dot{Q}^s_s \sin \Psi_j \tag{3.18}$$

$$\dot{R}^r_{rj} = \dot{R}^s_s + \dot{\Omega}_s \tag{3.19}$$

To summarize, the components of rotating shaft axis angular acceleration along rotating shaft axes for the j^{th} blade are first obtained from Eqs. (3.6), (3.7), and (3.8) followed by Eqs. (3.17), (3.18) and (3.19). Actually, $\dot{Q}^r_{rj}$ in Eq. (3.18) is not needed. Equations (3.17), (3.18)

and (3.19) must be repeated N times for the N blades.

A.2.4 HUB AXIS VELOCITY

The computation of hub-axis velocity, $\bar{V}_{hi}$, is indicated in block 4 of Figure 2.1. It is given by the formula

$$\bar{V}_{hi} = \bar{V}_{bi} + \bar{V}_{hb} \tag{4.1}$$

where $\bar{V}_{bi}$ is the velocity of the body axes (i.e., the aircraft c.g.) and $\bar{V}_{hb}$ is the velocity of the hub with respect to the aircraft c.g. (body-axis origin). $\bar{V}_{hb}$ is given by

$$\bar{V}_{hb} = \bar{\Omega}_{bi} \times \bar{r}_H \tag{4.2}$$

where $\bar{\Omega}_{bi}$ is the body-axis angular velocity and $\bar{r}_H$ is the position of the hub with respect to the aircraft c.g. From Figure 1.1 we see that

$$\bar{r}_H = x_H \bar{i}_b + y_H \bar{j}_b + z_H \bar{k}_b \tag{4.3}$$

where $\bar{i}_b$, $\bar{j}_b$, and $\bar{k}_b$ are the respective unit vectors along the body axes. Noting that $\bar{\Omega}_{bi} = P_b \bar{i}_b + Q_b \bar{j}_b + R_b \bar{k}_b$ we have from Eqs. (4.2) and (4.3) the following formulas for the body-axis (and hence hub-axis) components of $\bar{V}_{hb}$.

$$U^b_{hb} = Q_b z_H - R_b y_H \tag{4.4}$$

$$V^b_{hb} = R_b x_H - P_b z_H \tag{4.5}$$

$$W^b_{hb} = P_b y_H - Q_b x_H \tag{4.6}$$

To get the components of $\bar{V}_{hi}$ along shaft axes x_s, y_s, z_s, we need to use the transformation matrix $[T_{hs}]$ given in Eq. (2.3). Thus

$$\bar{V}^{s}_{hi} = [\mathbf{T}_{hs}]\bar{V}^{h}_{hi} = [T_{hs}](\bar{V}^{b}_{hi} + \bar{V}^{b}_{hb}) \tag{4.7}$$

Finally, we note that

$$\bar{V}_{ri} = \bar{V}_{hi}, \tag{4.8}$$

i.e., the translational velocity of the rotating shaft axes is the same as the hub axes, since they have a common origin. From Eqs. (2.3), (4.7) and (4.8), we obtain

$$U^{s}_{r} = (U_b + U^{b}_{hb})\cos i_\theta - (W_b + W^{b}_{hb})\sin i_\theta \tag{4.9}$$

$$V^{s}_{r} = (U_b + U^{b}_{hb})\sin i_\phi \sin i_\theta + (V_b + V^{b}_{hb})\cos i_\phi + (W_b + W^{b}_{hb})\sin i_\phi \cos i_\theta \tag{4.10}$$

$$W^{s}_{r} = (U_b + U^{b}_{hb})\cos i_\phi \sin i_\theta - (V_b + V^{b}_{hb})\sin i_\phi + (W_b + W^{b}_{hb})\cos i_\phi \cos i_\theta \tag{4.11}$$

Eqs. (4.4), (4.5) and (4.6), along with Eqs. (4.9), (4.10), and (4.11), are used to compute the velocity outputs of block 4 in Figure 2.1. As before, we note that i_θ and i_ϕ in Eqs. (4.9), (4.10) and (4.11) are constants, so that the coefficients in the equations can be precomputed as fixed parameters.

A.2.5 HUB AXIS ACCELERATION

The computation of hub-axis acceleration, $\bar{A}_{hi}$, is indicated in block 5 in Figure 2.1. It is given by the formula

$$\bar{A}_{hi} = \frac{d}{dt}\bar{V}_{hi})_i \tag{5.1}$$

But from Eq. (4.1) $\bar{V}_{hi} = \bar{V}_{bi} + \bar{V}_{hb}$. Substituting (4.1) into (5.1), and noting that $\frac{d}{dt}\bar{V}_{bi} \equiv \bar{A}_{bi}$, we have

$$\bar{A}_{hi} = \bar{A}_{bi} + \frac{d}{dt}\bar{V}_{hb})_i$$

or

$$\bar{A}_{hi} = \bar{A}_{bi} + \frac{d}{dt}\bar{V}_{hb})_b + \bar{\Omega}_{bi} \times \bar{V}_{hb} \qquad (5.2)$$

But from Eq. (4.2), $\bar{V}_{hb} = \bar{\Omega}_{bi} \times \bar{r}_H$ and since $\bar{r}_H$ is fixed in the body-axis frame,

$$\frac{d}{dt}\bar{V}_{hb})_b = \frac{d}{dt}(\bar{\Omega}_{bi} \times \bar{r}_H)_b = \frac{d}{dt}(\bar{\Omega}_{bi})_b \times \bar{r}_H = \dot{\bar{\Omega}}_{bi} \times \bar{r}_H \qquad (5.3)$$

where

$$\dot{\bar{\Omega}}_{bi} = \frac{d}{dt}\bar{\Omega}_{bi})_i = \frac{d}{dt}\bar{\Omega}_{bi})_b + \bar{\Omega}_{bi} \times \bar{\Omega}_{bi} = \frac{d}{dt}\bar{\Omega}_{bi})_b .$$

Substituting Eq. (5.3) into (5.2) and subtracting the gravity acceleration vector $\bar{G}$, we obtain

$$\bar{A}_{hi} - \bar{G} = \bar{A}_{bi} - \bar{G} + \dot{\bar{\Omega}}_{bi} \times \bar{r}_H + \bar{\Omega}_{bi} \times \bar{V}_{hb} \qquad (5.4)$$

which is just the equation shown in block 5 of Figure 2.1. Writing Eq. (5.4) as three scalar equations, we obtain

$$A_{hz} - G_x = A_{bx} - G_x + Q_b W^b_{hb} - R_b V^b_{hb} + \dot{Q}_b z_H - \dot{R}_b y_H \qquad (5.5)$$

$$A_{hy} - G_y = A_{by} - G_y + R_b U^b_{hb} - P_b W^b_{hb} + \dot{R}_b x_H - \dot{P}_b z_H \qquad (5.6)$$

$$A_{hz} - G_z = A_{bz} - G_z + P_b V^b_{hb} - Q_b U^b_{hb} + \dot{P}_b y_H - \dot{Q}_b x_H \qquad (5.7)$$

As before we can transform these body-axis (and hence hub-axis) components of $\bar{A}_{hi} - \bar{G}$ to shaft-axis components using the transformation matrix $[T_{hs}]$ in Eq. (2.3). Thus

$$(\bar{A}^s_{hi} - \bar{G}^s) = [T_{hs}](\bar{A}^h_{hi} - \bar{G}^h) \tag{5.8}$$

We also note that the hub axes x_h, y_h, z_h in Figure 1.1 have a common origin with the rotating shaft axes x_r, y_r, z_r. Hence

$$\bar{A}_{ri} - \bar{G} = \bar{A}_{hi} - \bar{G} \tag{5.9}$$

From Eqs. (2.3), (5.8), and (5.9), we can write the following three scalar equations:

$$A^s_{rx} - G^s_x = (A_{hx} - G_x)\cos i_\theta - (A_{hz} - G_z)\sin i_\theta \tag{5.10}$$

$$A^s_{ry} - G^s_y = (A_{hx} - G_x)\sin i_\phi \sin i_\theta + (A_{hy} - G_y)\cos i_\phi + (A_{hz} - G_z)\sin i_\phi \cos i_\theta \tag{5.11}$$

$$A^s_{rz} - G^s_z = (A_{hx} - G_x)\cos i_\phi \sin i_\theta - (A_{hy} - G_y)\sin i_\phi + (A_{hz} - G_z)\cos i_\phi \cos i_\theta \tag{5.12}$$

As before, the coefficients can be precomputed as fixed parameters since i_ϕ and i_θ are constants.

Equations (5.5) through (5.7) and (5.10) through (5.12) are used to compute the hub-axis and hence rotating-shaft-axis acceleration components along the shaft axes.

A.2.6 BLADE SPAN AXIS VELOCITY

In Section A.2.4 we determined the formulas for calculating the rotating-shaft-axis velocity components U^s_r, V^s_r, and W^s_r along the shaft axes. To obtain the components along the rotating shaft axes for the j^{th} blade we use the formula

$$\bar{V}^r_{ri_j} = [T_{sr_j}]\bar{V}^s_{ri} \tag{6.1}$$

where the transformation matrix $[T_{sr_j}]$ is given in Eq. (2.10). Thus from Eqs. (2.10) and (6.1) we obtain

$$U^r_{rj} = U^s_r \sin \Psi_j + V^s_r \cos \Psi_j \tag{6.2}$$

$$V^r_{rj} = - U^s_r \cos \Psi_j + V^s_r \sin \Psi_j \tag{6.3}$$

$$W^r_{rj} = W^s_r \tag{6.4}$$

We next determine the formula for the translational velocity, $\bar{V}_{pi_j}$, of the j^{th} blade hinge point P_j in Figure 1.1. This is given by

$$\bar{V}_{pi_j} = \bar{V}_{ri_j} + \bar{V}_{pr_j} \tag{6.5}$$

where $\bar{V}_{pr_j}$ is the velocity of the hinge point P_j relative to the hub (i.e., the origin of the rotating shaft axes). Thus

$$\bar{V}_{pr_j} = \bar{\Omega}_{ri} \times \bar{e}_j \tag{6.6}$$

Here $\bar{\Omega}_{ri}$ is the angular velocity of the rotating shaft axes (we recall that $\bar{\Omega}_{ri}$ is the same for all blades, i.e., is independent of j) and $\bar{e}_j$ is the position of the hinge point P_j with respect to the hub. Thus

$$\bar{e}_j = e\bar{j}_{rj} \tag{6.7}$$

where $\bar{j}_{rj}$ is the unit vector along the y_{rj} axis in Figure 1.1. Noting that $\bar{\Omega}_{ri} = P^r_{rj}\bar{i}_{rj} + Q^r_{rj}\bar{j}_{rj} + R^r_{rj}\bar{k}_{rj}$ and $\bar{V}_{ri_j} = U^r_{rj}\bar{i}_{rj} + V^r_{rj}\bar{j}_{rj} + W^r_{rj}\bar{k}_{rj}$, we have from Eqs. (6.5), (6.6) and (6.7)

$$U^r_{pj} = U^r_{rj} - R^r_{rj}e \tag{6.8}$$

$$V^r_{pj} = V^r_{rj} \tag{6.9}$$

$$W^r_{pj} = W^r_{rj} + P^r_{rj}e \tag{6.10}$$

Thus Eqs. (6.2) through (6.4) together with Eqs. (6.8) through (6.10) are used to compute the rotating shaft axis components of the hinge velocity for the j^{th} blade. All equations must be solved N times for N blades and provide the output of block 6 in Figure 2.1.

A.2.7 BLADE-SPAN AXIS ACCELERATION

The blade span axis acceleration $\bar{A}_{pi_j}$ is the acceleration of the hinge point P_j for the j^{th} blade with respect to the inertial reference (I-frame). It is computed using the same approach as in Section A.2.5 for the hub acceleration. Thus by direct analogy with Eq. (5.4)

$$\bar{A}_{pi_j} - \bar{G} = \bar{A}_{ri} - \bar{G} + \dot{\bar{\Omega}}_{ri} \times \bar{e}_j + \bar{\Omega}_{ri} \times \bar{\Omega}_{ri} \times \bar{e}_j \qquad (7.1)$$

Here $\bar{A}_{ri} = \bar{A}_{hi}$ (the rotating-shaft axes and hub axes have a common origin), $\bar{\Omega}_{ri}$ is the angular velocity of the rotating shaft axes, and $\bar{e}_j$ is the position of hinge-point P_j with respect to the hub. $\bar{\Omega}_{ri} \times \bar{e}_j = \bar{V}_{ph_j} = \bar{V}_{pr_j}$, the velocity of hinge-point P_j with respect to the hub.

Let us write Eq. (7.1) in terms of scalar components along the rotating shaft axes, x_{rj}, y_{rj}, z_{rj} for the j^{th} blade. To do this we first need to write the formulas for R-frame components of $\bar{A}_{ri} - G$ in terms of S-frame components using the transformation matrix $[T_{sr_j}]$ given in Eq. (2.10). Thus

$$A^r_{rxj} - G^r_{xj} = (A^s_{rx} - G^s_x)\sin\Psi_j + (A^s_{ry} - G^s_y)\cos\Psi_j \qquad (7.2)$$

$$A^r_{ryj} - G^r_{yj} = -(A^s_{rx} - G^s_x)\cos\Psi_j + (A^s_{ry} - G^s_y)\sin\Psi_j \qquad (7.3)$$

$$A^r_{rzj} - G^r_{zj} = A^s_{rx} - G^s_z \qquad (7.4)$$

where $(A^s_{rx} - G^s_x)$, $(A^s_{ry} - G^s_y)$, and $(A^s_{rz} - G^s_z)$ are given in Eqs. (5.10), (5.11) and (5.12).

The R-frame components of $\dot{\bar{\Omega}}_{ri}$ are given in Eqs. (3.17), (3.18) and (3.19); $\bar{e}_j$ is given in Eq. (6.7); the R-frame components of $\bar{\Omega}_{ri}$ are given in Eqs. (2.12), (2.13) and (2.14). These equations provide all the R-frame components necessary to express Eq. (7.1) as three scalar equations along the respective rotating shaft axes x_{rj}, y_{rj}, z_{rj}. Thus we obtain

$$A^r_{pxj} - G^r_{xj} = A^r_{rxj} - G^r_{xj} + (Q^r_{rj} P^r_{rj} - \dot{R}^r_{rj})e \tag{7.5}$$

$$A^r_{pyj} - G^r_{yj} = A^r_{ryj} - G^r_{yj} - [(R^r_{rj})^2 + (P^r_{rj})^2]e \tag{7.6}$$

$$A^r_{pzj} - G^r_{zj} = A^r_{rzj} - G^r_{zj} + (Q^r_{rj} R^r_{rj} + \dot{P}^r_r)e \tag{7.7}$$

Equations (7.2) through (7.7) must of course be repeated N times for each of N blades (j=1, 2, . . . , N).

A.2.8 BLADE SEGMENT VELOCITY

In order to compute the aerodynamic forces acting on each of the blade segments, it is necessary to compute the velocity vector $\bar{V}_{jk}$ at the center of pressure of the k^{th} segment of the j^{th} blade. This is simply given by the vector formula

$$\bar{V}_{jk} = \bar{V}_{pi_j} + \bar{\Omega}_{pi_j} \times \bar{\rho}_{jk} \tag{8.1}$$

where $\bar{V}_{pi_j}$ is the velocity of the blade hinge at point P_j in Figure 1.1, $\bar{\Omega}_{pi_j}$ is the angular velocity of the j^{th} blade-span axes, and $\bar{\rho}_{jk}$ is the position of the k^{th} segment center of pressure with respect to the hinge point P_j. Thus

$$\bar{\rho}_{jk} = y_{2k}\bar{j}_{pj} \tag{8.2}$$

where y_{2k} is the distance from P_j to the segment center of pressure and $\bar{j}_{pj}$ is the unit vector along the y_{pj} blade span axis in Figure 1.1. We denote the blade-span-axis angular velocity $\bar{\Omega}_{pij}$ for the j^{th} blade by

$$\bar{\Omega}_{pij} = P_{pj}\bar{i}_{pj} + Q_{pj}\bar{j}_{pj} + R_{pj}\bar{k}_{pj} \tag{8.3}$$

The components of blade-span-axis velocity $\bar{V}_{pi_j}$ have already been given in Eqs. (6.8), (6.9) and (6.10). To resolve them into components along the blade span axes x_{pj}, y_{pj}, z_{pj} requires the transformation matrix $[T_{rp_j}]$ given in Eq. (2.18). Thus

$$\bar{V}^{p}_{pi_j} = [T_{rp_j}]\bar{V}^{r}_{pi_j} \tag{8.4}$$

or from Eq. (2.18)

$$U^{p}_{pj} = U^{r}_{pj}\cos\delta_j - V^{r}_{pj}\sin\delta_j \tag{8.5}$$

$$V^{p}_{pj} = U^{r}_{pj}\sin\delta_j\cos\beta_j + V^{r}_{pj}\cos\delta_j\cos\beta_j - W^{r}_{pj}\sin\beta_j \tag{8.6}$$

$$W^{p}_{pj} = U^{r}_{pj}\sin\delta_j\sin\beta_j + V^{r}_{pj}\cos\delta_j\sin\beta_j + W^{r}_{pj}\cos\beta_j \tag{8.7}$$

Substituting Eqs. (8.2) and (8.3) into Eq. (8.1), we obtain the following

three scalar equations for U_{Tjk}, U_{Rjk}, and U_{Pjk} the tangential, radial, and perpendicular components of the k^{th} segment velocity, $\bar{V}_{jk}$, along the respective j^{th} blade span axes:

$$U_{Tjk} = U^{P}_{pj} - R_{pj}\, y_{2k} \tag{8.8}$$

$$U_{Pjk} = V^{P}_{pj} \tag{8.9}$$

$$U_{Pjk} = W^{P}_{pj} + P_{pj}\, y_{2k} \tag{8.10}$$

Equations (8.5) through (8.10) are mechanized in block 8 in Figure 2.1. Equations (8.8), (8.9) and (8.10) must be repeated Ns times for N blades (j=1, 2, . . . , N) and s segments per blade (k=1, 2, . . . , s).

A.2.9 ROTATIONAL EQUATIONS OF MOTION FOR THE BLADE

The rotational equations of motion of the blade are obtained by summing moments acting on the blade about the hinge point P_j in Figure 1.1. If we let $\bar{H}_{pi_j}$ be the j^{th} blade angular momentum (with respect to the inertial frame) about the point P_j, $\bar{M}_{Bj}$ be the total external moment about P_j acting on the blade, and $\bar{A}_{pi_j}$ be the acceleration (with respect to the inertial frame) of the point P_j, then we can write[2]

$$\frac{d}{dt}\bar{H}_{pi_j})_i = \bar{M}_{Bj} - \bar{\rho}_{cj} \times m\, \bar{A}_{pi_j} \tag{9.1}$$

Here $\bar{\rho}_{cj}$ is the position of the blade c.g. with respect to the hinge point P_j and m is the blade mass. Thus $-\bar{\rho}_{cj} \times m\, \bar{A}_{pi_j}$ is the additional inertial moment due to the acceleration $\bar{A}_{pi_j}$ of the point P_j.

[2] Greenwood, D. T., "Principles of Dynamics," Prentice-Hall, Inc., 1965, p. 146.

Now $\bar{H}_{pi_j} = [I_B]\bar{\Omega}_{pi_j}$, where $[I_B]$ is the blade inertia matrix and $\bar{\Omega}_{pi_j}$ is the angular velocity of the j^{th} blade. We will assume that

$$I_b = \begin{bmatrix} I_b & 0 & 0 \\ 0 & 0 & 0 \\ 0 & 0 & I_b \end{bmatrix} \tag{9.2}$$

i.e., the blade has equal moments of inertia, I_b, along the x_{pj} and z_{pj} blade-span axes, and negligible inertia along the blade-span direction, the y_{pj} axis. From Eq. (9.2), then

$$\bar{H}_{pi_j} = I_b P_{pj} \bar{i}_{pj} + I_b R_{pj} \bar{k}_{pj} \tag{9.3}$$

where P_{pj} and R_{pj} are the blade-span-axis (and hence blade) angular velocity components along x_{pj} and z_{pj}, respectively. Note that Q_{pj}, the blade-span-axis angular velocity component y_{pj}, is not equal to the blade angular velocity component along that axis, since in general the blade can be twisted (pitched) with respect to the blade-span-axes. But since the blade inertia about the y_{pj} axis is neglected, we don't need to consider the y_{pj} angular velocity component in representing the blade angular momentum $\bar{H}_{pi_j}$.

Next we note that

$$\frac{d}{dt}\bar{H}_{pi_j})_i = \frac{d}{dt}\bar{H}_{pi_j})_p + \bar{\Omega}_{pi_j} \times \bar{H}_{pi_j} \tag{9.4}$$

where

$$\bar{\Omega}_{pi_j} = P_{pj} \bar{i}_{pj} + Q_{pj} \bar{j}_{pj} + R_{pj} \bar{k}_{pj} \tag{9.5}$$

From Eq. (9.3) we see that $\frac{d}{dt}\bar{H}_{pi_j})_p$ is simply

$$\frac{d}{dt}\bar{H}_{pi_j})_p = I_b \dot{P}_{pj} \bar{i}_{pj} + I_b \dot{R}_{pj} \bar{k}_{pj} \tag{9.6}$$

Substituting Eqs. (9.3), (9.5) and (9.6) into ((.4), we obtain

$$\frac{d}{dt}\bar{H}_{pi_j})_i = I_b(\dot{P}_{pj} + Q_{pj}R_{pj})\bar{i}_{pj} + I_b(\dot{R}_{pj} - P_{pj}Q_{pj})\bar{k}_{pj} \tag{9.7}$$

Next we let $\bar{M}_{pj}$ represent the external moment exclusive of gravity acting on the j^{th} blade, e.g.,

$$\bar{M}_{Bj} = \bar{M}_{pj} + \bar{r}_{cj} \times m\bar{G} \tag{9.8}$$

Substituting Eq. (9.8) into Eq. (9.1), we obtain

$$\frac{d}{dt}\bar{H}_{pi_j})_i = \bar{M}_{pj} - \bar{\rho}_{cj} \times m(\bar{A}_{pi_j} - \bar{G}). \tag{9.9}$$

But we have already developed in Section A.2.7 the equations for $(\bar{A}_{pi_j} - \bar{G})$, except that in Eqs. (7.5), (7.6) and (7.7) the components are along the rotating shaft axes. To convert them to components along the blade-span axes the transformation matrix $[T_{rp_j}]$ in Eq. (2.18) is used. Thus

$$A^p_{pxj} - G^p_{xj} = (A^r_{pxj} - G^r_{xj})\cos\delta_j - (A^r_{pyj} - G^r_{yj})\sin\delta_j \tag{9.10}$$

$$A^p_{pyj} - G^p_{yj} = (A^r_{pxj} - G^r_{xj})\sin\delta_j \cos\beta_j + (A^r_{pyj} - G^r_{yj})\cos\delta_j \cos\beta_j - (A^r_{pzj} - G^r_{zj})\sin\beta_j \tag{9.11}$$

$$A^p_{pzj} - G^p_{zj} = (A^r_{pxj} - G^r_{xj})\sin\delta_j \sin\beta_j + (A^r_{pyj} - G^r_{yj})\cos\delta_j \sin\beta_j + (A^r_{pzj} - G^r_{zj})\cos\beta_j \tag{9.12}$$

Substituting Eq. (9.7) into (9.9), writing the result as two scalar

equations (note that $\bar{F}_{cj} = \rho_c \bar{j}_{pj}$), and solving for $\dot{P}_{pj}$ and $\dot{R}_{pj}$, we obtain

$$\dot{P}_{pj} = -Q_{pj} R_{pj} + \frac{1}{I_b}[M_{pxj} - \rho_c m(A^P_{pzj} - G^P_{zj})] \tag{9.13}$$

$$\dot{R}_{pj} = P_{pj} Q_{pj} + \frac{1}{I_b}[M_{pzj} - \rho_c m(A^P_{pxj} - G^P_{xj}] \tag{9.14}$$

where M_{pxj} and M_{pzj} are the x_{pj} and z_{pj} components of external moment $\bar{M}_{pj}$ on the j^{th} blade, not including gravity.

There is no equation for $\dot{Q}_{pj}$ because we have neglected the blade inertia about the y_{pj} axis. Q_{pj}, the angular velocity of the blade-span axes along y_{pj}, depends explicitly on the blade pitch control input and is not a state variable. It may very well be negligible.

Equations (9.13) and (9.14) are integrated to obtain P_{pj} and R_{pj}, respectively, for the j^{th} blade. They must be repeated N times for the N blades (j=1, 2, . . . , N).

A.2.10 AERODYNAMIC FORCES ON BLADE SEGMENTS

In Section A.2.8 we developed the equations for determining the tangential (U_{Tjk}), radial (U_{Rjk}), and perpendicular (U_{Pjk}) components of velocity $\bar{V}_{jk}$ of the k^{th} segment of the j^{th} blade. These components are taken, respectively, along the blade span axes x_{pj}, y_{pj} and z_{pj}, as shown in Figure 10.1. The total velocity of the k^{th} blade element with respect to the inertial reference frame is V_{jk}, which is given by

$$V_{jk} = (U^2_{Tjk} + U^2_{Rjk} + U^2_{Pjk})^{1/2} = |\bar{V}_{jk}| \tag{10.1}$$

The yawed angle of attack between the segment velocity vector $\bar{V}_{jk}$ and

its projection on the x_{pj}, y_{pj} blade-span-axis plane is denoted by ϕ_{Yjk} in Figure 10.1. Clearly

$$\sin \phi_{Y_{jk}} = \frac{U_{Pjk}}{|\vec{V}_{jk}|} = \frac{U_{Pjk}}{V_{jk}} \tag{10.2}$$

and

$$\cos \phi_{Y_{jk}} = \frac{(U^2_{Tjk} + U^2_{Rjk})^{1/2}}{V_{jk}} \tag{10.2}$$

Also, from Figure 10.1, γ_{jk}, the angle-of-attack yaw angle in the x_{pj}, y_{pj} plane, is given by

$$\sin \gamma_{jk} = \frac{U_{rjk}}{(U^2_{Tjk} + U^2_{Rjk})^{1/2}} \tag{10.3}$$

or

$$\cos \gamma_{jk} = \frac{U_{Tjk}}{(U^2_{Tjk} + U^2_{Rjk})^{1/2}} \tag{10.4}$$

Now in general at the k^{th} segment, the blade itself has a pitch angle θ_{Ajk} with respect to the blade-span axes, measured in the x_{pj}, z_{pj} plane, as shown in Figure 10.1. From the Figure it is clear that

$$\tan \theta_{Ajk} = \frac{(AB)}{(BC)} = \frac{(AB)}{(B'C)\cos \gamma_{jk}} \tag{10.5}$$

We now resolve θ_{Ajk} into the plane containing the yawed angle of attack $\theta_{Y_{jk}}$. This resolved angle $\theta_{Y_{jk}}$ can be computed by noting that the distance (A'B') = (AB) and

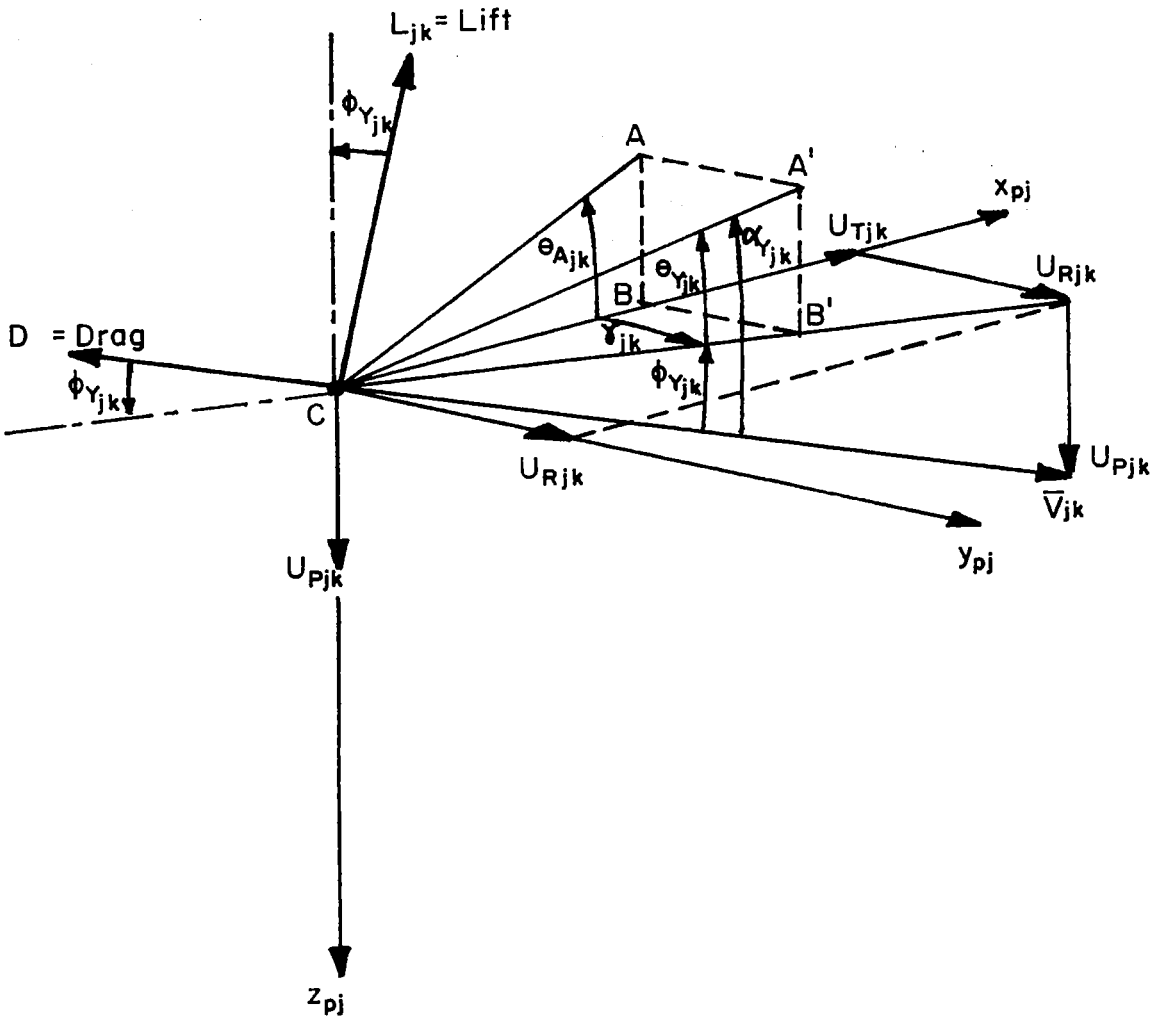

Figure 10.1 Segment Geometry for Aerodynamic Force Calculation

$$\tan \theta_{Y_{jk}} = \frac{(A'B')}{(B'C)} = \frac{(AB)}{(B'C)} \tag{10.6}$$

But from Eq. (10.5), $(AB) = (B'C) \tan \theta_{Ajk} \cos \gamma_{jk}$. Substituting this into Eq. (10.6), we have

$$\tan \theta_{Y_{jk}} = \tan \theta_{Ajk} \cos \gamma_{jk} \tag{10.7}$$

The total yawed angle of attack, $\alpha_{Y_{jk}}$, is simply

$$\alpha_{Y_{jk}} = \phi_{Y_{jk}} + \theta_{Y_{jk}} \tag{10.8}$$

or

$$\tan \alpha_{Y_{jk}} = \frac{\tan \phi_{Y_{jk}} + \tan \theta_{Y_{jk}}}{1 - \tan \phi_{Y_{jk}} \tan \theta_{Y_{jk}}} \tag{10.9}$$

where

$$\tan \phi_{Y_{jk}} = \frac{U_{Pjk}}{(U_{Tjk}^2 + U_{Rjk}^2)^{1/2}} \tag{10.10}$$

or from Eq. (10.4)

$$\tan \phi_{Y_{jk}} = \frac{U_{Pjk}}{U_{Tjk}} \cos \gamma_{jk} \tag{10.11}$$

Substituting Eqs. (10.7) and (10.11) into (10.9) and solving for $\alpha_{Y_{jk}}$, we obtain

$$\alpha_{Y_{jk}} = \tan^{-1} \frac{(U_{Tjk} \tan \theta_{Ajk} + U_{Pjk}) |\cos \gamma_{jk}|}{U_{Tjk} - U_{Pjk} \tan \theta_{Ajk} \cos^2 \gamma_{jk}} \tag{10.12}$$

where the absolute value signs are added around $\cos \gamma_i$ in accordance

with the NASA Ames model.[1] Also, the magnitude of the projection of $\alpha_{Y_{jk}}$ into the x_{pj}, z_{pj} plane is given by

$$\alpha_{TRANS_{jk}} = |\alpha_{Y_{jk}} \cos \gamma_{jk}| \tag{10.13}$$

This x_{pj}, y_{pj} projection of angle of attack, namely $\alpha_{TRANS_{jk}}$, is used as the angle of attack variable in the calculation of blade-section lift and drag coefficients for small angles of attack.[1] For larger angles a variation of Eq. (10.13) is used, so that in general we write[1]

$$\alpha_{TRANS_{jk}} = f_1(\alpha_{Y_{jk}} \cos \gamma_{jk}) \tag{10.14}$$

The lift and drag coefficients also depend on the Mach number, M_{jk}, for the k^{th} segment of the j^{th} blade, which is given by

$$M_{jk} = \frac{(U_{Rjk}^2 + U_{Pjk}^2)^{1/2}}{a} \tag{10.15}$$

where a is the speed of sound. Note that the Mach number is based on the velocity component in the x_{pj}, z_{pj} plane and not the total velocity.

The segment lift and drag coefficients are given, respectively, by[1]

$$C_{\ell jk} = f_2(\alpha_{TRANS_{jk}}, M_{jk}) \tag{10.16}$$

and

$$C_{djk} = \text{sgn } \alpha_{Yjk} f_3(\alpha_{TRANS_{jk}}, M_{jk}) \tag{10.17}$$

with a correction factor in $C_{\ell jk}$ for tip loss in the last blade segment.

It is assumed that the aerodynamic drag force D_{jk} acts in the direction opposite to the segment velocity $\bar{V}_{jk}$, as shown in Figure 10.1, and that the lift force L_{jk} is perpendicular to D_{jk} and lies in the

[1] Mackie and Alderete, op. cit.

plane of the yawed angle of attack $\alpha_{Y_{jk}}$. In general

$$L_{jk} = \frac{1}{2} \rho A_k V_{jk}^2 C_{\ell jk} \tag{10.18}$$

and

$$D_{jk} = \frac{1}{2} \rho A_k V_{jk}^2 C_{djk} \tag{10.19}$$

where ρ is the air density and A_k the area of the k^{th} blade segment. We can resolve L_{jk} and D_{jk} into force components F_{Tjk}, F_{Rjk} and F_{Pjk} along the respective blade-span-axes x_{pj}, y_{pj} and z_{pj}. From Figure 10.1, we see that

$$F_{Tjk} = (L_{jk} \sin \phi_{Y_{jk}} - D_{jk} \cos \phi_{Y_{jk}}) \cos \gamma_{jk} \tag{10.20}$$

$$F_{Rjk} = (L_{jk} \sin \phi_{Y_{jk}} - D_{jk} \cos \phi_{Y_{jk}}) \sin \gamma_{jk} \tag{10.21}$$

$$F_{Pjk} = -(L_{jk} \cos \phi_{Y_{jk}} + D_{jk} \sin \phi_{Y_{jk}}) \tag{10.22}$$

Finally, we need to write the formula for the geometric pitch angle, θ_{Ajk} of the k^{th} blade segment. This is given by[1]

$$\theta_{Ajk} = \theta_{CUFF} - A_{1S} \cos(\Psi_j + \Delta_{SP}) - B_{1S} \sin(\Psi_j + \Delta_{SP}) + \theta_1[y_{2k} - e'] - \beta_j \tan \delta_3 + K_{\alpha_1} \alpha_j + K_{\alpha_2} \delta_j^2 \tag{10.23}$$

where Δ_{SP}, the swash plate rotation, is a control input and Ψ_j, β_j, and δ_j are problem state variables. The remainder of the parameters in Eq. (10.23) are constants, where only the y_{2k} is dependent on the segment index k.

Equations (10.1) through (10.4), (10.12) and (10.14) through (10.23) are used to compute the blade segment forces. They must be repeated

[1] Mackie and Alderete, op. cit.

Ns times for N blades with s segments per blade (k=1, 2, . . . , s).

From Eqs. (10.2) through (10.4) we can rewrite Eqs. (10.18) through (10.22) in the following form:

$$F_{Tjk} = \frac{1}{2} \rho A_k V_{jk} [C_{\ell jk} U_{Pjk} \cos \gamma_{jk} - C_{djk} U_{Tjk}] \qquad (10.24)$$

$$F_{Rjk} = \frac{1}{2} \rho A_k V_{jk} [C_{\ell jk} U_{Pjk} \sin \gamma_{jk} - C_{djk} U_{Rjk}] \qquad (10.25)$$

$$F_{Pjk} = \frac{1}{2} \rho A_k V_{jk} [C_{\ell jk} (U_{Tjk}^2 + U_{Rjk}^2)^{1/2} + C_{djk} U_{Pjk}] \qquad (10.26)$$

These equations may be preferable to Eqs. (10.18) through (10.22) for computer mechanization.

Note that we have not included downwash corrections in the segment velocity components U_{Tjk}, U_{Rjk}, and U_{Pjk} with respect to the air flow because of uncertainty on just how to incorporate the corrections. It appears that downwash effects, which certainly must be included, will not add a major computational load.

A.2.11 BLADE MOMENT EQUATIONS

In the blade equations of motion in Section A.2.9 given by Eqs. (9.13) and (9.14) we see that the external moment components (not including gravity), M_{pxj} and M_{pzj} along the x_{pj} and z_{pj} blade span axes, must be calculated. In general the external moment vector $\bar{M}_{pj}$ consists of aerodynamic and hinge moments, as expressed in the following equation:

$$\bar{M}_{pj} = \bar{M}_{aero} + \bar{M}_{hinge} \qquad (11.1)$$

where all moments are taken about the hinge point P_j in Figure 1.1. The aerodynamic moment due to the k^{th} blade segment is simply the cross product of the position vector, $y_{2k}\bar{j}_{pj}$ from P_j to segment c.p. times the aerodynamic force at the k^{th} segment. The force components are given in Eqs. (10.20) through (10.22) or (10.24) through (10.26). The total moment is the sum of the segment moments. Thus

$$\bar{M}_{aero} = \sum_{j=1}^{s} y_{2k}\bar{j}_{pj} \times (F_{Tjk}\bar{i}_{pj} + F_{Rjk}\bar{j}_{pj} + F_{Pjk}\bar{k}_{pj})$$

or

$$\bar{M}_{aero} = \left[\sum_{j=1}^{s} y_{2k}F_{Pjk}\bar{i}_{pj} - \sum_{j=1}^{s} y_{2k}F_{Tjk}\right]\bar{k}_{pj} \qquad (11.2)$$

The hinge moments are due to the spring-damper constraints for the lagging and flapping degrees of freedom of the blade. Thus M_{LDj}, the hinge lagging moment for the j^{th} blade, is given by[1]

$$M_{LDj} = L_L[f(\delta_j) + \text{sgn}\,\dot{\delta}_j F'_\delta] \qquad (11.3)$$

Reference to Figure 1.1 shows that for positive δ_j the opposing moment due to spring restraint will act in the direction of z'_{rj} and hence has a component $M_{LDj}\cos\beta_j$ along z_{pj}.

M_{FDj}, the hinge flapping moment, is given by[1]

$$M_{FDj} = -[K_\beta\beta_j + K_{\dot{\beta}}\dot{\beta}_j] \qquad (11.4)$$

Reference to Figure 1.1 shows that for positive β_j, the opposing moment lies along the x_{pj} axis. Thus

$$\bar{M}_{hinge} = [K_\beta\beta_j + K_{\dot{\beta}}\dot{\beta}_j]\bar{i}_{pj} + L_L[f(\delta_j) + \text{sgn}\,\dot{\delta}_j F'_\delta]\cos\beta_j\bar{k}_{pj} \qquad (11.5)$$

---

[1] Mackie and Alderete, op. cit.

Combining Eqs. (11.2) and (11.5), we obtain the following equations for the respective components of $\overline{M}_{p_j}$ along x_{pj} and z_{pj}:

$$M_{pxj} = \sum_{j=1}^{s} y_{2k} F_{Pjk} - M_{FDj} \tag{11.6}$$

$$M_{pzj} = - \sum_{j=1}^{s} y_{2k} F_{Tjk} + M_{LDj} \cos \beta_j \tag{11.7}$$

where M_{FDj} and M_{LDj} are given in Eqs. (11.3) and (11.4). Equations (11.6) and (11.7) are repeated N times for N blades (j=1, 2, . . . , N).

A.2.12 EQUATIONS FOR COMPUTING $\dot{\delta}_j$ AND $\dot{\beta}_j$

In Section A.2.2 we developed the equations for computing the components of $\overline{\Omega}_{ri}$, the angular velocity of the rotating shaft axes, x_{rj}, y_{rj}, z_{rj}, and hence the axes x'_{rj}, y'_{rj}, z'_{rj} in Figure 1.1. Because $\overline{\Omega}_{ri}$ is the same for all N blades, the subscript j denoting the j^{th} blade is not included in $\overline{\Omega}_{ri}$. Equations (9.13) and (9.14) in Section A.2.9, when integrated, give components of $\overline{\Omega}_{pi_j}$, the angular velocity of the j^{th} blade-span axes. The angular rates $\dot{\delta}_j$ and $\dot{\beta}_j$ for the j^{th}-blade lagging and flapping angles are related to the difference between $\overline{\Omega}_{pi_j}$ and $\overline{\Omega}_{ri}$, i.e.,

$$\overline{\Omega}_{pr_j} = \overline{\Omega}_{pi_j} - \overline{\Omega}_{ri} \tag{12.1}$$

where $\overline{\Omega}_{pr_j}$ is the angular velocity of the j^{th} blade-span axes, x_{pj}, y_{pj}, z_{pj}, with respect to the j^{th} rotating shaft axes, x_{rj}, y_{rj}, z_{rj}, or equivalently, x'_{rj}, y'_{rj}, z'_{rj}. From Figure 1.1 we see that

$$\bar{\Omega}_{pr_j} = -\dot{\delta}_j \bar{k}'_{rj} - \dot{\beta}_j \bar{i}_{pj} \tag{12.2}$$

where $\bar{k}'_{rj}$ is the unit vector along the z'_{rj} axis and $\bar{i}_{pj}$ is the unit vector along the x_{pj} axis.

Also, from Figure 1.1 it is apparent that

$$\bar{k}'_{rj} = \cos\beta_j \bar{k}_{pj} - \sin\beta_j \bar{j}_{pj} \tag{12.3}$$

Substituting Eq. (12.3) into (12.2), we obtain

$$\bar{\Omega}_{pr_j} = -\dot{\beta}_j \bar{i}_{pj} + \dot{\delta}_j \sin\beta_j \bar{j}_{pj} - \dot{\delta}_j \cos\beta_j \bar{k}_{pj} \tag{12.4}$$

Also, from Eq. (12.1) we can write

$$\bar{\Omega}_{pr_j} = (P_{pj} - P^p_{rj})\bar{i}_{pj} + (Q_{pj} - Q^p_{rj})\bar{j}_{pj} + (R_{pj} - R^p_{rj})\bar{k}_{pj} \tag{12.5}$$

where P_{pj}, Q_{pj}, R_{pj} are the j^{th} blade-span axis (P-frame) components of $\bar{\Omega}_{pi}$, and P^p_{rj}, Q^p_{rj}, R^p_{rj} are the j^{th} blade-span axis components of $\bar{\Omega}_{ri}$. Equating coefficients of $\bar{i}_{pj}$ and $\bar{k}_{pj}$ in Eqs. (12.4) and (12.5) and solving for $\dot{\delta}_j$ and $\dot{\beta}_j$, we obtain

$$\dot{\delta}_j = \frac{1}{\cos\beta_j}(R^p_{rj} - R_{pj}) \tag{12.6}$$

and

$$\dot{\beta}_j = P^p_{rj} - P_{pj} \tag{12.7}$$

Equations (12.6) and (12.7) are integrated to obtain β_j and δ_j, respectively.

A.2.13 COMPUTATION OF HINGE SHEAR FORCE

Each blade has acting on it the sum of the gravity force, $m\bar{G}$, the aerodynamic force, $\bar{F}_{aero}$, and the hinge shear force at point P_j, $-\bar{F}_{p_j}$. The sum of these forces must equal the blade mass m times the

acceleration of the j^{th} blade c.g., $\bar{A}_{ci_j}$. Thus,

$$m\bar{A}_{ci_j} = m\bar{g} + \bar{F}_{aero} - \bar{F}_{P_j} \tag{13.1}$$

where we have written the hinge force acting on the blades as $-\bar{F}_{P_j}$ since the opposite force, $\bar{F}_{P_j}$, will be the blade force acting on the hinge. Solving for $\bar{F}_{P_j}$ in Eq. (13.1) we have

$$\bar{F}_{P_j} = -m(\bar{A}_{ci_j} - \bar{G}) + \bar{F}_{aero} \tag{13.2}$$

In Section A.2.7 we have developed the equations for $\bar{A}_{pi_j} - \bar{G}$, the acceleration less gravity of the hinge point P_j. From this we must now determine the acceleration less gravity of the blade c.g. By direct analogy with Eq. (5.4) in Section A.2.5

$$\bar{A}_{ci_j} - \bar{G} = \bar{A}_{pi_j} - \bar{G} + \dot{\bar{\Omega}}_{pi_j} \times \bar{\rho}_{cj} + \bar{\Omega}_{pi_j} \times \bar{\Omega}_{pi_j} \times \bar{\rho}_{cj} \tag{13.3}$$

where $\bar{\rho}_{cj} = \rho_c \bar{j}_{pj}$, the position of the blade c.g. with respect to the hinge point P_j. Noting that $\bar{\Omega}_{pi_j} = P^p_{pj}\bar{i}_{pj} + Q^p_{pj}\bar{j}_{pj} + R^p_{pj}\bar{k}_{pj}$ and $\dot{\bar{\Omega}}_{pi_j} = \dot{P}^p_{pj}\bar{i}_{pj} + \dot{Q}^p_{pj}\bar{i}_{pj} + \dot{R}^p_{pj}\bar{k}_{pj}$, we obtain from Eq. (13.3), the following three scalar equations:

$$A^p_{cxj} - G^p_{xj} = A^p_{pxj} - G^p_{xj} + \rho_c(Q_{pj}P_{pj} - \dot{R}_{pj}) \tag{13.4}$$

$$A^p_{cyj} - G^p_{yj} = A^p_{pyj} - G^p_{yj} - \rho_c(R^2_{pj} + P^2_{pj}) \tag{13.5}$$

$$A^p_{czj} - G^p_{zj} = A^p_{pzj} - G^p_{zj} + \rho_c(Q_{pj}R_{pj} + \dot{P}_{pj}) \tag{13.6}$$

where $A^p_{pxj} - G^p_{xj}$, $A^p_{pyj} - G^p_{yj}$, and $A^p_{pzj} - G^p_{zj}$ are already given in Eqs. (9.10) through (9.12).

$\bar{F}_{aero}$ is, of course, just the sum of the aerodynamic forces on each blade segment, as given in Eqs. (10.20) through (10.22) as components F_{Tjk}, F_{Rjk}, F_{Pjk} along x_{pj}, y_{pj}, z_{pj} for the k^{th} segment. Thus the hinge shear force components F_{Pxj}, F_{Pyj}, F_{Pzj} along x_p, y_p, z_p become, from Eq. (13.2)

$$F^p_{Pxj} = -m(A^p_{cxj} - G^p_{xj}) + \sum_{k=1}^{s} F_{Tjk} \tag{13.7}$$

$$F^p_{Pyj} = -m(A^p_{cyj} - G^p_{yj}) + \sum_{k=1}^{s} F_{Rjk} \tag{13.8}$$

$$F^p_{Pzj} = -m(A^p_{czj} - G^p_{zj}) + \sum_{k=1}^{s} F_{Pjk} \tag{13.9}$$

These force components form the output of block 13 in Figure 2.1.

A.2.14 TOTAL ROTOR FORCE

The hinge shear force components, F^p_{Pxj}, F^p_{Pyj}, and F^p_{Pzj}, for the j^{th} blade, as given in Eqs. (13.7) through (13.9) in the previous section, must be summed for all N blades to compute the total rotor force acting on the aircraft. But first the individual blade forces must be resolved into rotating shaft axes, i.e.,

$$\bar{F}^r_{P_j} = [T_{pr_j}]\bar{F}^p_{P_j} = [T_{rp_j}]^T \bar{F}^p_{P_j} \tag{14.1}$$

where $[T_{rp_j}]$ is given in Eq. (2.18). Thus

$$F^r_{Pxj} = F^p_{Pxj}\cos\delta_j + F^p_{Pyj}\sin\delta_j\cos\beta_j + F^p_{Pzj}\sin\delta_j\sin\beta_j \tag{14.2}$$

$$F^r_{yj} = -F^p_{xj}\sin\delta_j + F^p_{Pyj}\cos\delta_j\cos\beta_j + F^p_{Pzj}\cos\delta_j\sin\beta_j \tag{14.3}$$

$$F^r_{Pzj} = - F^p_{Pyj} \sin \beta_j + F^p_{Pzj} \cos \beta_j \tag{14.4}$$

Next the components must be resolved into shaft axes, which are common for all blades, i.e.,

$$\bar{F}^s_{P_j} = [T_{rs_j}]\bar{F}^r_{P_j} = [T_{sr_j}]^T \bar{F}^r_{P_j} \tag{14.5}$$

where $[T_{sr_j}]$ is given in Eq. (2.10). Thus

$$F^s_{Pxj} = F^r_{Pxj} \sin \Psi_j - F^r_{Pyj} \cos \Psi_j \tag{14.6}$$

$$F^s_{Pyj} = F^r_{Pxj} \cos \Psi_j + F^r_{Pyj} \sin \Psi_j \tag{14.7}$$

$$F^s_{Pzj} = F^r_{Pzj} \tag{14.8}$$

Summation over the N blades produces the total rotor force components along shaft axes. Thus

$$F^s_{Rx} = \sum_{j=1}^{N} F^s_{Pxj} \tag{14.9}$$

$$F^s_{Ry} = \sum_{j=1}^{N} F^s_{Pyj} \tag{14.10}$$

$$F^s_{Rz} = \sum_{j=1}^{N} F^s_{Pzj} \tag{14.11}$$

To obtain the body axis force components, we use the transformation

$$\bar{F}^b_R = [T_{sb}]\bar{F}^s_R = [T_{sh}]\bar{F}^s_R = [T_{hs}]^T \bar{F}^s_R \tag{14.12}$$

where $[T_{sb}] = [T_{sh}]$ because hinge and body axes have the same direction. Using Eq. (2.3) for $[T_{hs}]$, we obtain

$$F^b_{Rx} = F^s_{Rx} \cos i_\theta + F^s_{Ry} \sin i_\phi \sin i_\theta + F^s_{Rz} \cos i_\phi \sin i_\theta \quad (14.13)$$

$$F^b_{Ry} = F^s_{Ry} \cos i_\phi - F^s_{Rz} \sin i_\phi \quad (14.14)$$

$$F^b_{Rx} = - F^s_{Rx} \sin i_\theta + F^s_{Ry} \sin i_\phi \cos i_\theta + F^s_{Rz} \cos i_\phi \cos i_\theta \quad (14.15)$$

Equations (14.2) through (14.4) and (14.6) through (14.8) must be repeated N times for N blades. Equations (14.9) through (14.11) and (14.13) through (14.15) complete the rotor force computation.

A.2.15 TOTAL ROTOR MOMENT

The moment transmitted through the j^{th} hinge for each blade consists of hinge spring damper components $- M_{LDj}$ along z'_{rj} and M_{FDj} along x_{pj} in Figure 1.1, where M_{LDj} and M_{FDj} are given in Equations (11.3) and (11.4). These moments are transmitted through to the hub along with the moment resulting from the hinge shear force $\bar{F}_{Pj}$ calculated in Section 13. Thus the total moment $\bar{M}_{hj}$ acting at the hub for the j^{th} blade is given by

$$\bar{M}_{hj} = - M_{LDj} \bar{k}_{rj} + M_{FDj} \bar{i}_{pj} + \bar{e}_j \times \bar{F}_{P_j} \quad (15.1)$$

where $\bar{e}_j = e\bar{j}_{rj}$ and is the vector position of hinge point P_j with respect to the hub. We continue to neglect any monents along y'_{rj} and hence y_{rj}. The component of $M_{FDj} \bar{i}_{pj}$ along x'_{rj} and hence x_{rj} is simply $M_{FDj} \cos \delta_j$. Equating scalar components along $\bar{i}_{rj}$, $\bar{j}_{rj}$ and $\bar{k}_{rj}$ in Equation (15.1), we obtain

$$M^r_{hxj} = M_{FDj} \cos \delta_j + e F^r_{Pzj} \quad (15.2)$$

$$M^r_{hzj} = - M_{LDj} - e F^r_{Pxj} \quad (15.3)$$

We resolve these components to shaft axes with the formula

$$\bar{M}^s_{h_j} = [T_{rs}]\bar{M}^r_{h_j} = [T_{sr}]^T \bar{M}^r_{h_j} \tag{15.4}$$

where $[T_{sr}]$ is given in Eq. (2.10). Thus, since we assume $M^r_{hyj} = 0$,

$$M^s_{hxj} = M^r_{hxj} \sin \Psi_j \tag{15.5}$$

$$M^s_{hyj} = M^r_{hxj} \cos \Psi_j \tag{15.6}$$

$$M^s_{hzj} = M^r_{hzj} \tag{15.7}$$

Since the shaft axes are common for all blades, the moment components in Eqs. (15.5) through (15.7) due to an individual blade can be summed over the N blades. Thus we have for the total rotor moment components at the hub the following equations:

$$M^s_{hx} = \sum_{j=1}^{N} M^s_{hxj} \tag{15.8}$$

$$M^s_{hy} = \sum_{j=1}^{N} M^s_{hyj} \tag{15.9}$$

$$M^s_{hz} = \sum_{j=1}^{N} M^s_{hzj} \tag{15.10}$$

These are resolved into hub and hence body axes using the formula

$$\bar{M}^b_h = [T_{sb}]\bar{M}^s_h = [T_{sh}]\bar{M}^s_h = [T_{hs}]^T \bar{M}^s_h \tag{15.11}$$

where $[T_{hs}]$ is given in Eq. (2.3). Thus

$$M^b_{hx} = M^s_{hx} \cos i_\theta + M^s_{hy} \sin i_\phi \sin i_\theta + M^s_{hz} \cos i_\phi \sin i_\theta \tag{15.12}$$

$$M^b_{hy} = M^s_{hy} \cos i_\phi - M^s_{hz} \sin i_\phi \tag{15.13}$$

$$M^b_{hz} = -M^s_{hx} \sin i_\theta + M^s_{hy} \sin i_\phi \cos i_\theta + M^s_{hz} \cos i_\phi \cos i_\theta \tag{15.14}$$

These hub moments are transmitted to the aircraft c.g. Also transmitted to the aircraft c.g. is the moment $\bar{r}_H \times \bar{F}_R$, where $\bar{F}_R$ is the rotor force acting at the hub and computed in Section A.2.14, and $\bar{r}_H$ is the moment arm from aircraft c.g. to hub. Thus the total rotor moment $\bar{M}_R$ acting about the aircraft c.g. is given by

$$\bar{M}_R = \bar{M}_h + \bar{r}_H \times \bar{F}_R \tag{15.15}$$

where Eqs. (15.12) through (15.14) give the components of hub moment $\bar{M}_h$ along body axes, $\bar{r}_H = x_H \bar{i}_b + y_H \bar{j}_b + z_H \bar{k}_b$, and $\bar{F}_R = F^b_{Rx} \bar{i}_b + F^b_{Ry} \bar{j}_b + F^b_{Rz} \bar{k}_b$. Making these substitutions into Eq. (15.15), we obtain

$$M^b_{Rx} = M^b_{hx} + y_H F^b_{Rz} - z_H F^b_{Ry} \tag{15.16}$$

$$M^b_{Ry} = M^b_{hy} + z_H F^b_{Rx} - x_H F^b_{Rz} \tag{15.17}$$

$$M^b_{Rz} = M^b_{hz} + x_H F^b_{Ry} - y_H F^b_{Rx} \tag{15.18}$$

These are the rotor moment inputs to the rotational equations of motion in Section A.2.1.

APPENDIX B

SCALING CONSIDERATIONS IN SOLVING THE HELICOPTER FLIGHT EQUATIONS

B.1. BLOCK 1

In solving the helicopter flight equations using either a hybrid computer or a fixed-point digital computer, the scaling relationships between problem variables and computing-machine variables must be considered. Fortunately the maximum range of each problem variable in the equations of motion is either known or easily estimated. Under these conditions one can define new dimensionless problem variables given by the original variable divided by the maximum magnitude of the variable. Then by letting one computing machine unit equal one dimensionless problem unit, one can easily mechanize the equations. In the following sections we will discuss the application of this approach to each of the 15 computational blocks in Figure 2.1 in Appendix A containing the equations given in Sections A.2.2 through A.2.15.

First consider the 3 translational equations given in Section A.2.1, Eqs. (1.12), (1.13), and (1.14). First we divide the equations by the gravity acceleration g_o, so that every term in the equations is a dimensionless acceleration in units of g_o. Thus

$$\frac{\dot{U}_b}{g_o} = -\frac{W_b Q_b}{g_o} + \frac{V_b R_b}{g_o} - \sin\theta_b + \frac{F_{bx}}{Mg_o} \tag{1.1}$$

$$\frac{\dot{V}_b}{g_o} = -\frac{U_b R_b}{g_o} + \frac{W_b P_b}{g_o} + \cos\theta_b \sin\phi_b + \frac{F_{by}}{Mg_o} \tag{1.2}$$

$$\frac{\dot{W}_b}{g_o} = -\frac{V_b P_b}{g_o} + \frac{U_b Q_b}{g_o} + \cos\theta_b \cos\phi_b + \frac{F_{bz}}{Mg_o} \qquad (1.3)$$

Rather than use a separate maximum range for each variable, it would appear simpler to use a single maximum range for each group of three variables representing scalar components of a single vector. For example, if V_{max} is the maximum expected magnitude of the vehicle velocity vector, then we define dimensionless body-axis velocity components (using lower case letters) by the following formulas:

$$u_b = \frac{U_b}{V_{max}}, \quad v_b = \frac{V_b}{V_{max}}, \quad w_b = \frac{W_b}{V_{max}} \qquad (1.4)$$

Similarly, for Ω_{max} assumed as the maximum magnitude of the body-axis angular velocity vector, we obtain the following formulas for dimensionless angular velocity components:

$$p_b = \frac{P_b}{\Omega_{max}}, \quad q_b = \frac{Q_b}{\Omega_{max}}, \quad r_b = \frac{R_b}{\Omega_{max}} \qquad (1.5)$$

Although this scheme is not quite as efficient as introducing a separate maximum value for each individual component, it is simple and should easily provide sufficient accuracy when a 16 bit digital word is employed for each dimensionless variable.

Let us also define dimensionless external body-axis force components as follows:

$$f_{bx} = \frac{F_{bx}}{Mg_o} \Big/ \left(\frac{F_b}{Mg_o}\right)_{max}, \quad f_{by} = \frac{F_{by}}{Mg_o} \Big/ \left(\frac{F_b}{Mg_o}\right)_{max}, \quad f_{bz} = \frac{F_{bz}}{Mg_o} \Big/ \left(\frac{F_b}{Mg_o}\right)_{max} \qquad (1.6)$$

Using Eqs. (1.4) - (1.6), Eqs. (1.1) - (1.3) become

$$\dot{u}_b/\Omega_{max} = [\, -w_b q_b + v_b r_b - k_g \sin\theta_b + k_f f_{bx}] \tag{1.7}$$

$$\dot{v}_b/\Omega_{max} = [\, -u_b r_b + w_b p_b + k_g \cos\theta_b \sin\phi_b + k_f f_{by}] \tag{1.8}$$

$$\dot{w}_b/\Omega_{max} = [\, -v_b p_b + u_b q_b + k_g \cos\theta_b \cos\phi_b) + k_f f_{bz}] \tag{1.9}$$

where the constants k_f and k_g are given by

$$k_g = \frac{g_o}{V_{max}\Omega_{max}}, \quad k_f = k_g \left(\frac{F_b}{Mg_o}\right)_{max} \tag{1.10}$$

and will both be less than unity for any practical case.

All the variables on the right side of Eqs. (1.7) thru (1.10) are dimensionless and easily interpreted. To retrive the scaled variables (e.g., for display purposes) one need only multiply by the maximum value used to make each variable dimensionless. The common factor Ω_{max} in Eqs. (1.7) - (1.9) is simply the integrator gain in an analog mechanization. In digital integration Ω_{max} is multiplied by the numerical interval of integration T, where clearly the product $\Omega_{max} T < 1$ in any practical case. It also seems clear that the sum of the bracketed terms on the right side of Eqs. (1.7) - (1.9) is quite unlikely to exceed unity. This is because terms such as $u_b q_b$ in Eqs. (1.9) have a maximum possible value of unity, which represents an actual acceleration equal to $V_{max}\Omega_{max}$. Typically, we might have V_{max} = 300 ft/sec, Ω_{max} = 1 rad/sec in a helicopter simulation. Then $V_{max}\Omega_{max}$ = 300 ft/sec^2 or almost 10 g's. Even if both u_b and q_b reached maximum values simultaneously, i.e., corresponding to an actual acceleration magnitude of 10 g's, the

the remaining terms within the brackets in Eqs. (1.7) - (1.9) would have much smaller equivalent accelerations in any allowable flight maneuver.

Next, we consider the rotational equations of motion given by (1.22), (1.23), and (1.24) in Section A.2.1. We define dimensionless external moment components by

$$m_{bx} = \frac{M_{bx}}{I_{xx}} \Big/ \left(\frac{M_b}{I}\right)_{max}, \quad m_{by} = \frac{M_{by}}{I_{yy}} \Big/ \left(\frac{M_b}{I}\right)_{max}, \quad m_{bz} = \frac{M_{bz}}{I_{zz}} \Big/ \left(\frac{M_b}{I}\right)_{max} \tag{1.11}$$

Using Eqs. (1.5) and (1.11) above the rotational equations (1.22), (1.23), and (1.24) in Section A.2.1 become

$$\frac{\dot{p}_b}{\Omega_{max}} = -\left(\frac{I_{zz}-I_{yy}}{I_{xx}}\right) q_b r_b + k_m m_{bx} \tag{1.12}$$

$$\frac{\dot{q}_b}{\Omega_{max}} = -\left(\frac{I_{xx}-I_{zz}}{I_{yy}}\right) r_b p_b + k_m m_{by} \tag{1.13}$$

$$\frac{\dot{r}_b}{\Omega_{max}} = -\left(\frac{I_{yy}-I_{xx}}{I_{zz}}\right) p_b q_b + k_m m_{bz} \tag{1.14}$$

where

$$k_m = \left(\frac{M_b}{I}\right)_{max} \frac{1}{\Omega^2_{max}} \tag{1.15}$$

All terms in Eqs. (1.12, (1.13), (1.14) are dimensionless and will remain less than unity, with the $k_m m_{bx}$, $k_m m_{by}$, and $k_m m_{bz}$ terms predominating (the effect of external moments). p_b, q_b, and r_b are obtained by integration of the respective equations using an integration gain of Ω_{max}.

In terms of dimensionless angular rates the Euler angle equations (1.25), (1.26), and (1.27) in Section A.2.1 become

$$\frac{\dot{\psi}_b}{\Omega_{max}} = (r_b \cos\phi_b + q_b \sin\phi_b)/\cos\theta_b \tag{1.16}$$

$$\frac{\dot{\theta}_b}{\Omega_{max}} = q_b \cos\phi_b - r_b \sin\phi_b \tag{1.17}$$

$$\frac{\dot{\phi}_b}{\Omega_{max}} = p_b + \frac{\dot{\psi}_b}{\Omega_{max}} \sin\theta_b \tag{1.18}$$

Again, integration with gain Ω_{max} yields ψ_b, θ_b, ϕ_b. Actually, the gain will be Ω_{max}/π so that the resulting angles range over $\pm$ 1, corresponding to $\pm$ π radians.

Finally, the equations for earth-axis velocities, (1.30), (1.31), and (1.32) in Section A.2.1, become

$$\frac{\dot{S}_x}{V_{max}} = u_b\cos\theta_b\cos\psi_b + v_b(-\cos\phi_b\sin\psi_b + \sin\phi_b\sin\theta_b\cos\psi_b) + w_b(\sin\phi_b\sin\psi_b + \cos\phi_b\sin\theta_b\cos\psi_b) \tag{1.19}$$

$$\frac{\dot{S}_y}{V_{max}} = u_b\cos\theta_b\sin\psi_b + v_b(\cos\phi_b\cos\psi_b + \sin\phi_b\sin\theta_b\sin\psi_b) + w_b(-\sin\phi_b\cos\psi_b + \cos\phi_b\sin\theta_b\sin\psi_b) \tag{1.20}$$

$$\frac{\dot{S}_z}{V_{max}} = \frac{-\dot{h}}{V_{max}} = -u_b\sin\theta_b + v_b\sin\phi_b\cos\theta_b + w_b\cos\theta_b\cos\phi_b \tag{1.21}$$

Here the integrator gains will depend on the desired range in distance north (S_x), distance east (S_y) and altitude ($h = -S_z$).

B.2 Block 2

Here we compute the angular velocity components of the rotating shaft axes. As before we use lower case letters to denote dimensionless components. Thus

$$p_r^s = \frac{P_r^s}{\Omega_{max}} , \quad q_r^s = \frac{Q_r^s}{\Omega_{max}} , \quad r_r^s = \frac{R_r^s}{\Omega_{max}} \tag{2.1}$$

Then Eqs. (2.7), (2.8), and (2.9) in Section A.2.2 become

$$p_r^s = p_b \cos i_\theta - r_b \sin i_\theta \tag{2.2}$$

$$q_r^s = p_b \sin i_\phi \sin i_\theta + q_b \cos i_\phi + r_b \sin i_\phi \cos i_\theta \tag{2.3}$$

$$r_r^s - \frac{\Omega_s}{\Omega_{max}} = p_b \cos i_\phi \sin i_\theta - q_b \sin i_\phi + r_b \cos i_\phi \cos i_\theta \tag{2.4}$$

Note that $r_r^s - \Omega_s/\Omega_{max}$ is computed rather than r_r^s. Thus we compute the dimensionless difference between the z_s axis components of rotating shaft axis angular velocity and angular velocity of rotating shaft axes with respect to shaft (non-rotating) axes. In this way $r_r^s - \Omega_s/\Omega_{max}$ does not exceed unity, whereas r_r^s would, since $(\Omega_s)_{max} >> \Omega_{max}$.

Eqs. (2.12), (2.13), and (2.14) in Section A.2.2 are simply rewritten in dimensionless form, i.e., with lower-case letters. Thus for the jth blade

$$p_{rj}^r = p_r^s \sin\psi_j + q_r^s \cos\psi_j \tag{2.5}$$

$$q_{rj}^r = -p_r^s \cos\psi_j + q_r^s \sin\psi_j \tag{2.6}$$

$$r_{rj}^r - \frac{\Omega_s}{\Omega_{max}} = r_{rj}^s - \frac{\Omega_s}{\Omega_{max}} \tag{2.7}$$

Finally, from Eqs. (2.20) and (2.22) in Section A.2.2 we have the following expressions for dimensionless blade-span axis components of rotating shaft-axis angular velocity:

$$p^{p}_{rj} = p^{r}_{rj} \cos\delta_j - q^{r}_{rj} \sin\delta_j \tag{2.8}$$

$$r^{p}_{rj} - \frac{\Omega_s}{\Omega_{max}} \cos\beta_j = p^{r}_{rj} \sin\delta_j \sin\beta_j + q^{r}_{rj} \cos\delta_j \sin\beta_j + (r^{r}_{rj} - \frac{\Omega_s}{\Omega_{max}}) \cos\beta_j \tag{2.9}$$

where we have not included the formula for q^{p}_{rj} since it is not needed.

B.3. Block 3

In this block the angular acceleration components of the rotating shaft axes are computed. In terms of the dimensionless angular acceleration components given in Eqs. (1.12), (1.13), and (1.14) in Section B.1 Eqs. (3.6), (3.7), and (3.8) in Section A.2.3 become

$$\frac{\dot{p}^{s}_{s}}{\Omega_{max}} = \frac{\dot{p}_b}{\Omega_{max}} \cos i_\theta - \frac{\dot{r}_b}{\Omega_{max}} \sin i_\theta \tag{3.1}$$

$$\frac{\dot{q}^{s}_{s}}{\Omega_{max}} = \frac{\dot{p}_b}{\Omega_{max}} \sin i_\phi \sin i_\theta + \frac{\dot{q}_b}{\Omega_{max}} \cos i_\phi + \frac{\dot{r}_b}{\Omega_{max}} \sin i_\phi \cos i_\theta \tag{3.2}$$

$$\frac{\dot{r}^{s}_{s}}{\Omega_{max}} = \frac{\dot{p}_b}{\Omega_{max}} \cos i_\phi \sin i_\theta - \frac{\dot{q}_b}{\Omega_{max}} \sin i_\phi + \frac{\dot{r}_b}{\Omega_{max}} \cos i_\phi \cos i_\theta \tag{3.3}$$

Eqs. (3.17) and (3.19) in Section A.2.3 for the jth blade become

$$\frac{\dot{p}^{r}_{rj}}{\Omega_{max}} = \frac{\dot{p}^{s}_{s}}{\Omega_{max}} \sin\psi_j + \frac{\dot{q}^{s}_{s}}{\Omega_{max}} \cos\psi_j \tag{3.4}$$

$$\frac{\dot{r}^{r}_{rj} - \dot{\Omega}_{s}/\Omega_{max}}{\Omega_{max}} = \frac{\dot{r}^{s}_{s}}{\Omega_{max}} \tag{3.5}$$

Note that $\dot{r}^{r}_{rj} - \dot{\Omega}_{s}/\Omega_{max}$ is computed rather than $\dot{r}^{r}_{rj}$. This is because in general $(\dot{\Omega}_{s})_{max} >> \Omega_{max}$, i.e., the angular acceleration of the rotating shaft axes with respect to the shaft axes (non-rotating) can be much larger that the overall aircraft angular accelerations. Thus $\dot{r}^{r}_{rj} - \dot{\Omega}_{s}/\Omega_{max}$ will remain reasonable in magnitude, whereas $\dot{r}^{r}_{rj}$ by itself will not.

B.4. Block 4

In Block 4 of Figure 2.1, Section A.2.2, the hub-axis velocity is computed by adding the velocity of the hub relative to the body axis to the body axis velocity. The relative velocity components are normalized by dividing the actual components by V_{rmax}, the maximum value of the hub-to-body relative velocity. Thus

$$u^{b}_{hb} = \frac{U^{b}_{hb}}{V_{rmax}}, \quad v^{b}_{hb} = \frac{V^{b}_{hb}}{V_{rmax}}, \quad w^{b}_{hb} = \frac{W^{b}_{hb}}{V_{rmax}} \tag{4.1}$$

If d_{max} is the largest of hub relative position components x_H, y_H, z_H, then clearly

$$V_{rmax} = \Omega_{max} d_{max} \tag{4.2}$$

In general V_{rmax} will be small compared with V_{max}, the maximum aircraft velocity. From Eqs. (4.1) and (4.2) along with Eqs. (1.4) and (1.5) in Section B.1, Eqs. (4.4), (4.5), and (4.6) in Section A.2.4 for the hub-to-body axis relative velocity components become

$$u_{hb}^{b} = \frac{z_H}{d_{max}} q_b - \frac{y_H}{d_{max}} r_b \tag{4.3}$$

$$v_{hb}^{b} = \frac{x_H}{d_{max}} r_b - \frac{z_H}{d_{max}} p_b \tag{4.4}$$

$$w_{hb}^{b} = \frac{y_H}{d_{max}} p_b - \frac{x_H}{d_{max}} q_b \tag{4.5}$$

Then Eqs. (4.9), (4.10), and (4.11) in Section A.2.4 become the following for the dimensionless hub-axis velocities along the shaft axes:

$$u_r^s = (u_b + \hat{k}_r u_{hb}^b) \cos i_\theta - (w_b + k_r w_{hb}^b) \sin i_\theta \tag{4.6}$$

$$v_r^s = (u_b + \hat{k}_r u_{hb}^b) \sin i_\phi \sin i_\theta + (v_b + k_r u_{hb}^b) \cos i_\phi + (w_b + k_r w_{hb}^b) \sin i_\phi \cos i_\theta \tag{4.7}$$

$$w_r^s = (u_b + \hat{k}_r u_{hb}^b) \cos i_\phi \sin i_\theta - (v_b + k_r v_{hb}^b) \sin i_\phi + (w_b + k_r w_{hb}^b) \cos i_\phi \cos i_\theta \tag{4.8}$$

where

$$\hat{k}_r = \frac{V_{rmax}}{V_{max}} = \frac{\Omega_{max} d_{max}}{V_{max}} \tag{4.9}$$

In Eqs. (4.6)-(4.8) we have used V_{max} to make u_r^s, v_r^s, and w_r^s dimensionless, i.e.,

$$u_r^s = \frac{U_r^s}{V_{max}}, \quad v_r^s = \frac{V_r^s}{V_{max}}, \quad w_r^s = \frac{W_r^s}{V_{max}} \tag{4.10}$$

Note that the constant $\hat{k}_r$ will generally be small compared with unity.

B.5 Block 5

In this block the hub-axis accelerations are computed from the

body-axis accelerations less gravity. The latter are simply the external forces acting on the aircraft divided by the aircraft mass. Thus the maximum magnitude of body-axis acceleration less gravity is simply $(F_b/M)_{max}$. This is then used to define dimensionless components of body-axis acceleration less gravity, i.e.

$$a_{bx}-g_x = \frac{A_{bx}-G_x}{(F_b/M)_{max}}, \quad a_{by}-g_y = \frac{A_{by}-G_y}{(F_b/M)_{max}}, \quad a_{bz}-g_z = \frac{A_{bz}-G_z}{(F_b/M)_{max}} \tag{5.1}$$

We also use $(F_b/M)_{max}$ to define dimensionless components of hub-axis acceleration less gravity. Thus

$$a_{hx}-g_x = \frac{A_{hx}-G_x}{(F_b/M)_{max}}, \quad a_{hy}-g_y = \frac{A_{hy}-G_y}{(F_b/M)_{max}}, \quad a_{hz}-g_z = \frac{A_{hz}-G_z}{(F_b/M)_{max}} \tag{5.2}$$

From Eqs. (1.5) in Section B.1, Eqs. (5.1) and (5.2) above, and Eqs. (4.3), (4.4), and (4.5) in Section B.4, Eqs. (5.5), (5.6), and (5.7) in Section A.2.5 become

$$a_{hx}-g_x = a_{bx}-g_x + \hat{k}_a\left(q_b w^b_{hb} - r_b v^b_{hb} + \frac{z_H}{d_{max}}\frac{\dot{q}_b}{\Omega_{max}} - \frac{y_H}{d_{max}}\frac{\dot{r}_b}{\Omega_{max}}\right) \tag{5.3}$$

$$a_{hy}-g_y = a_{by}-g_y + \hat{k}_a\left(r_b u^b_{hb} - p_b w^b_{hb} + \frac{x_H}{d_{max}}\frac{\dot{r}_b}{\Omega_{max}} - \frac{z_H}{d_{max}}\frac{\dot{p}_b}{\Omega_{max}}\right) \tag{5.4}$$

$$a_{hz}-g_z = a_{bz}-g_z + \hat{k}_a\left(p_b v^b_{hb} - q_b u^b_{hb} + \frac{y_H}{d_{max}}\frac{\dot{p}_b}{\Omega_{max}} - \frac{x_H}{d_{max}}\frac{\dot{q}_b}{\Omega_{max}}\right) \tag{5.5}$$

where

$$\hat{k}_a = \frac{\Omega^2_{max}\, d_{max}}{(F_b/M)_{max}} \tag{5.6}$$

For the dimensionless components of rotating shaft-axis acceleration less gravity we have from Eqs. (5.10), (5.11), and (5.12) in Section

A.2.5

$$a^s_{rx} - g^s_x = (a_{hx} - g_x)\cos i_\theta - (a_{hz} - g_z)\sin i_\theta \tag{5.7}$$

$$a^s_{ry} - g^s_y = (a_{hx} - g_x)\sin i_\phi \sin i_\theta + (a_{hy} - g_y)\cos i_\phi + (a_{hz} - g_z)\sin i_\phi \cos i_\theta \tag{5.8}$$

$$a^s_{rz} - g^s_z = (a_{hx} - g_x)\cos i_\phi \sin i_\theta - (a_{hy} - g_y)\sin i_\phi + (a_{hz} - g_z)\cos i_\phi \cos i_\theta \tag{5.9}$$

B.6. Block 6

In block 6 the velocity of the blade-span axes, i.e., the hinge point P_j for the jth blade, is computed for each of N blades (j = 1, 2, . . . , N). Again we use V_{max} (the maximum body-axis velocity) to normalize the velocity components, which in dimensionless form are given as lower-case letters. Also, we recall that Ω_{max} (the maximum body-axis angular velocity) is used to normalize the angular velocity components. Thus from Eqs. (6.2), (6.3), (6.4), (6.8), (6.9), and (6.10) in Section A.2.6 we obtain for the jth blade

$$u^r_{pj} = u^s_r \sin\psi_j + v^s_r \cos\psi_j - \left(r^r_{rj} - \frac{\Omega_s}{\Omega_{max}}\right)\frac{e\Omega_{max}}{V_{max}} - \frac{e\Omega_{s_{max}}}{V_{max}}\,\omega_s \tag{6.1}$$

$$v^r_{pj} = -u^s_r \cos\psi_j + v^s_r \sin\psi_j \tag{6.2}$$

$$w^r_{pj} = w^s_r + \frac{e\Omega_{max}}{V_{max}}\, p^r_{rj} \tag{6.3}$$

where the dimensionless angular velocity ω_s of the rotating shaft axes relative to the non-rotating shaft axes is given by

$$\omega_s = \frac{\Omega_s}{\Omega_{s_{max}}} \tag{6.4}$$

Note that $r^r_{rj}-\Omega_s/\Omega_{max}$, as computed in Eq. (2.7) of Section B.2, is used in Eq. (6.1) rather than r^r_{rj} itself to preserve good scaling. For e, the distance from hub to hinge, equal to perhaps one or two feet and $\Omega_{s_{max}}$ equal to perhaps 30 rad/sec, clearly $e\,\Omega_{s_{max}}/V_{max}$ will generally be small compared with unity. Since $\Omega_{max} << \Omega_{s_{max}}$, clearly $e\,\Omega_{max}/V_{max}$ is quite small compared with unity. Thus good scaling of Eqs. (6.1), (6.2), and (6.3) is assured.

B.7 Block 7

Here we compute the dimensionless components of acceleration less gravity for the hinge point P_j of each blade. First we write the dimensionless components of rotating shaft axis acceleration less gravity. In Eqs. (5.7), (5.8), and (5.9) these are given as components along the shaft axes. Using the transformation matrix $[T_{sr}]$ in Eq. (2.10), Section A.2.2, these become the following components along the rotating shaft axes for the jth blade:

$$a^r_{rxj}-g^r_{xj} = (a^s_{rx}-g^s_x)\sin\psi_j+(a^s_{ry}-g^s_y)\cos\psi_j \qquad (7.1)$$

$$a^r_{ryj}-g^r_{yj} = -(a^s_{rx}-g^s_y)\cos\psi_j+(a^s_{ry}-g^s_y)\sin\psi_j \qquad (7.2)$$

$$a^r_{rzj}-g^r_{zj} = a^s_{rz}-g^s_z \qquad (7.3)$$

Next Eqs. (7.5), (7.6), and (7.7) in Section A.2.7 are used as the basis for computing the dimensionless components of blade-span-axis acceleration less gravity. We recall that $(F_b/M)_{max}$ is the normalizing factor for acceleration components and Ω_{max} for angular acceleration and velocity components. Also, Eq. (2.7) in Section B.2 shows that

$r^r_{rj}-\Omega_s/\Omega_{max}$ is computed rather than r^r_{rj} directly. Similarly, Eqs. (3.5) shows that $(\dot{r}^r_{rj}-\dot{\Omega}_s/\Omega_{max})/\Omega_{max}$ is computed rather than $\dot{r}^r_{rj}/\Omega_{max}$. We also note that $\omega_s = \Omega_s/\Omega_{s_{max}}$ in Eq. (6.4), Section B.6. With these considerations we obtain the following equations as the dimensionless equivalents to Eqs. (7.5), (7.6), and (7.7) in Section A.2.7:

$$a^r_{pxj}-g^r_{xj} = a^r_{rxj}-g^r_{xj}+k_q\left[\, q^r_{rj}p^r_{rj} - \frac{\dot{r}^r_{rj}-\dot{\Omega}_s/\Omega_{max}}{\Omega_{max}}\,\right] -k_qk_r\frac{\dot{\omega}_s}{\Omega_{max}} \qquad (7.4)$$

$$a^r_{pyj}-g^r_{yj}+k_qk_r^2\omega_s^2 = a^r_{ryj}-g^r_{yj}-k_q\left[\,(r^r_{rj}-\Omega_s/\Omega_{max})^2+(p^r_{rj})^2\right] -2k_qk_r(r^r_{rj}-\Omega_s/\Omega_{max})\omega_s \qquad (7.5)$$

$$a^r_{pzj}-g^r_{zj} = a^r_{zxj}-g^r_{zj}+k_q\left[\, q^r_{rj}(r^r_{rj}-\Omega_s/\Omega_{max})+\frac{\dot{p}^r_{rj}}{\Omega_{max}}\,\right] +k_qk_rq^r_{rj}\omega_s \qquad (7.6)$$

where

$$k_q = \frac{(\Omega_{max})^2 e}{(F_b/M)_{max}}\,, \quad k_r = \frac{\Omega_{s_{max}}}{\Omega_{max}} \qquad (7.7)$$

Typical parameter values might be Ω_{max} = 1 rad/sec, e = 2 feet, $(F_b/M)_{max}$ = 100 ft/sec^2 ($\sim$ 3g), $\Omega_{s_{max}}$ = 30 rad/sec. Then k_q = 0.02, k_r = 30. Thus the term $k_qk_r^2\omega_s^2$ in Eq. (7.5) can range up to 18, so that subtraction of this centrifugal acceleration from the y_{r_j} component of hinge acceleration-less-gravity improves the scaling considerably.

B.8. Block 8

In block 8 Eqs. (8.5),(8.6), and (8.7) in Section A.2.8 are implemented to transform the blade-span axis velocity components from rotating shaft axes (R-frame) to blade-span axes (P frame). In dimensionless form the equations become

$$u^p_{pj} = u^r_{pj} \cos\delta_j - v^r_{pj} \sin\delta_j \tag{8.1}$$

$$v^p_{pj} = u^r_{pj} \sin\delta_j \cos\beta_j + v^r_{pj} \cos\delta_j \cos\beta_j - w^r_{pj} \sin\beta_j \tag{8.2}$$

$$w^p_{pj} = u^r_{pj} \sin\delta_j \sin\beta_j + v^r_{pj} \cos\delta_j \sin\beta_j + w^r_{pj} \cos\beta_j \tag{8.3}$$

Eqs. (8.8), (8.9), and (8.10) in Section A.2.8 give the tangential, radial, and perpendicular components of the center of pressure of the kth segment of the jth blade. U_{Tjk}, the tangential component, will in general be the largest, with a maximum value well in excess of V_{max}, the maximum aircraft velocity. Thus we use V_{bmax} as a normalizing factor for the blade-segment velocity components, where $V_{bmax} \tilde{=} 1000$ ft/sec. Then the dimensionless components for the kth segment of the jth blade become

$$u_{Tjk} = \frac{U_{Tjk}}{V_{bmax}} \quad , \quad u_{Rjk} = \frac{U_{Rjk}}{V_{bmax}} \quad , \quad u_{pjk} = \frac{U_{Pjk}}{V_{bmax}} \tag{8.4}$$

where these components are, respectively, along the x_{pj}, y_{pj}, z_{pj} blade-span axes.

Let Ω_{pmax} be the maximum value of the components P_{pj}, Q_{pj}, and $R_{pj} - \Omega_s$ of blade-span axis (P-frame) angular velocity. We use Ω_{pmax} as the normalizing factor for the dimensionless blade-span axis angular velocity components. Thus for the jth blade

$$p_{pj} = \frac{P_{pj}}{\Omega_{pmax}} \quad , \quad q_{pj} = \frac{Q_{pj}}{\Omega_{pmax}} \quad , \quad r_{pj} - k_s \omega_s = \frac{R_{pj} - \Omega_s}{\Omega_{pmax}} \quad , \quad k_s = \frac{\Omega_{smax}}{\Omega_{pmax}} \tag{8.5}$$

where $\omega_s = \Omega_s / \Omega_{smax}$ as defined in Eqs. (6.4), Section B.6.

Noting that V_{max} is the normalizing factor for the velocity components in Eqs. (8.1), (8.2), and (8.3), we have from Eqs. (8.4) and

(8.5) the following formulas equivalent to Eqs. (8.8), (8.9), and (8.10) in Section A.2.8:

$$u_{Tjk} = \frac{V_{max}}{V_{bmax}} u^p_{pj} - \frac{\Omega_{pmax} y_{2k}}{V_{bmax}}(r_{pj} - k_s \omega_s) - \frac{\Omega_{smax} y_{2k}}{V_{bmax}} \omega_s \qquad (8.6)$$

$$u_{Rjk} = \frac{V_{max}}{V_{bmax}} v^p_{pj} \qquad (8.7)$$

$$u_{Pjk} = \frac{V_{max}}{V_{bmax}} w^p_{pj} + \frac{\Omega_{smax}}{V_{bmax}} p_{pj} \qquad (8.8)$$

Here the coefficient V_{max}/V_{bmax} will be less than unity whereas $\Omega_{smax} y_{2k}/V_{bmax}$ will be near unity for the blade tip segments.

B.9. Block 9

In this block the blade equations of motion are represented. Eqs. (9.10), (9.11), and (9.12) in Section A.2.9 simply transform the components of blade-span axis acceleration less gravity from rotating shaft axes to blade-span axes. Rewriting the equations in dimensionless form using Eqs. (7.4), (7.5), and (7.6) in Section B.7, we obtain

$$a^p_{pxj} - g^p_{xj} = (a^r_{pxj} - g^r_{xj})\cos\delta_j - (a^r_{pyj} - g^r_{yj} + k_q k_r^2 \omega_s^2)\sin\delta_j + k_q k_r^2 \omega_s^2 \sin\delta_j \qquad (9.1)$$

$$a^p_{pyj} - g^p_{yj} + k_q k_r^2 \omega_s^2 \cos\delta_j \cos\beta_j = (a^r_{pxj} - g^r_{xj})\sin\delta_j \cos\beta_j + (a^r_{pyj} - g^r_{yj} + k_q k_r^2 \omega_s^2)\cos\delta_j \cos\beta_j$$
$$- (a^r_{pzj} - g^r_{zj})\sin\beta_j \qquad (9.2)$$

$$a^p_{pzj} - g^p_{zj} = (a^r_{pxj} - g^r_{xj})\sin\delta_j \sin\beta_j + (a^r_{pyj} - g^r_{yj} + k_q k_r^2 \omega_s^2)\cos\delta_j \sin\beta_j$$
$$+ (a^r_{pzj} - g^r_{zj})\cos\beta_j - k_q k_r^2 \omega_s^2 \cos\delta_j \sin\beta_j \qquad (9.3)$$

where $\omega_s = \Omega_s / \Omega_{smax}$, as given in Eq. (6.4), Section B.6.

M_{pxj} and M_{pzj} in Section A.9 represent the x_{pj} and z_{pj} components of external moment less gravity acting on the jth blade, respectively. We make them dimensionless by dividing by $(M_p/I_b)_{max}$. Thus

$$m_{pxj} = \frac{M_{pxj}/I_b}{(M_p/I_b)_{max}} \quad , \quad m_{pzj} = \frac{M_{pzj}/I_b}{(M_p/I_b)_{max}} \tag{9.4}$$

Then the dimensionless counterpart of the equations of motion for the jth blade given in (9.13) and (9.14) of Section A.2.9 become, with the help of Eqs. (8.5) in Section B.2, the following:

$$\frac{\dot{p}_{pj}}{\Omega_{smax}} = -\frac{1}{k_s} q_{pj}(r_{pj}-k_s\omega_s) - q_{pj}\omega_s + \hat{k}_m m_{pxj} - \hat{k}_f(a^p_{pzj} - g^p_{zj}) \tag{9.5}$$

$$\frac{\dot{r}_{pj}-k_s\dot{\omega}_s}{\Omega_{smax}} = \frac{1}{k_s} p_{pj}q_{pj} + \hat{k}_m m_{pzj} + \hat{k}_f(a^p_{pxj} - g^p_{xj}) - \frac{\dot{\omega}_s}{\Omega_{pmax}} \tag{9.6}$$

where

$$\hat{k}_m = \frac{(M_p/I_b)_{max}}{\Omega_{pmax}\Omega_{smax}} \quad , \quad \hat{k}_f = \frac{\rho_c m(F_b/M)_{max}}{\Omega_{pmax}\Omega_{smax} I_b} \tag{9.7}$$

Eqs. (9.5) and (9.6) are integrated with gain Ω_{smax} to obtain p_{pj} and $r_{pj}-k_s\omega_s$. They are repeated N times for N blades (j=1,2,...,N).

B.10. Block 10

In block 10 in Figure 2.1 in Section A.2.0 the aerodynamic forces acting on the individual blade segments are computed using Eqs. (10.18) thru (10.22) in Section A.2.10. First we define dimensionless tangential, radial, and perpendicular velocity components for the kth segment of the jth blade using the following formulas:

$$f_{Tjk} = \frac{F_{Tjk}}{\frac{1}{2}\rho A_{max} V_{bmax}^2} \quad , f_{Rjk} = \frac{F_{Rjk}}{\frac{1}{2}\rho A_{max} V_{bmax}^2} \quad , f_{Pjk} = \frac{F_{Pjk}}{\frac{1}{2}\rho A_{max} V_{bmax}^2} \tag{10.1}$$

Assuming $|C_{\ell jk}|_{max} \tilde{=} 1$, Eq. (10.1) will define dimensionless force components with a maximum value of unity. The normalizing factor can easily be adjusted to accommodate the actual maximum C_ℓ and C_d range. From Eq. (10.1) above the dimensionless force equations can be written from Eqs. (10.18) thru (10.22) in Section A.2.10. Thus

$$f_{Tjk} = \frac{A_k}{A_{max}} v_{jk}^2 [C_{\ell jk} \sin\phi_{Y_{jk}} - C_{djk} \cos\phi_{Y_{jk}}] \cos\gamma_{jk} \tag{10.2}$$

$$f_{Rjk} = \frac{A_k}{A_{max}} v_{jk}^2 [C_{\ell jk} \sin\phi_{Y_{jk}} - C_{djk} \cos\phi_{Y_{jk}}] \sin\gamma_{jk} \tag{10.3}$$

$$f_{Pjk} = \frac{A_k}{A_{max}} v_{jk}^2 [C_{\ell jk} \cos\phi_{Y_{jk}} + C_{djk} \sin\phi_{Y_{jk}}] \tag{10.4}$$

where

$$v_{jk} = (u_{Tjk}^2 + u_{Rjk}^2 + u_{Pjk}^2)^{1/2} \tag{10.5}$$

The formulas for $\cos\gamma_{jk}$, $\sin\gamma_{jk}$, $\cos\phi_{Y_{jk}}$, $\sin\phi_{Y_{jk}}$ remain as before except for the substitution of dimensionless velocity components u_{Tjk}, u_{Rjk}, u_{Pjk} for U_{Tjk}, U_{Rjk}, U_{Pjk}.

The formula for θ_{Ajk} is reasonably scaled as is, with all angles in radians. The $\alpha_{Y_{jk}}$ equation is rewritten using dimensionless velocities u_{Tjk}, u_{Rjk}, u_{Pjk}, as is the formula for Mach number at the kth segment. Thus

$$M_j = \frac{V_{b\,max}}{a} \left(u_{Tjk}^2 + u_{Pjk}^2\right)^{1/2} \tag{10.6}$$

An alternative mechanization to Eqs. (10.2), (10.3), and (10.4) is based on Eqs. (10.24), (10.25), and (10.26) in Section A.2.10. Thus

$$f_{Tjk} = \frac{A_k}{A_{max}} v_{jk} \left[C_{\ell\,jk} u_{Pjk} \cos\gamma_{jk} - C_{djk} u_{Tjk} \right] \tag{10.7}$$

$$f_{Rjk} = \frac{A_k}{A_{max}} v_{jk} \left[C_{\ell\,jk} u_{Pjk} \sin\gamma_{jk} - C_{djk} u_{Rjk} \right] \tag{10.8}$$

$$f_{Pjk} = \frac{A_k}{A_{max}} v_{jk} \left[C_{\ell\,jk} \left(u_{Tjk}^2 + u_{Rjk}^2\right)^{1/2} + C_{djk} u_{Pjk} \right] \tag{10.9}$$

Slight variations in the scaling suggested above may be needed to obtain near optimal scaling, but the basic approach would be identical.

B.11. Block 11

Using Eqs. (9.4) and (10.1) we can rewrite Eqs. (11.3), (11.4), (11.6), and (11.7) in Section A.2.11 as the following two equations:

$$m_{pxj} = k_y \sum_{k=1}^{s} \left(\frac{y_{2k}}{y_{2\,max}}\right) f_{Pjk} + \frac{K_\beta}{M_{p\,max}} \beta_j + \frac{K_{\dot\beta}\, \Omega_{s\,max}}{M_{p\,max}} \frac{\dot\beta_j}{\Omega_{s\,max}} \tag{11.1}$$

and

$$m_{pzj} = -k_y \sum_{k=1}^{s} \left(\frac{y_{2k}}{y_{2\,max}}\right) f_{Tjk} + \frac{L_L}{M_{p\,max}} \left[f(\delta_j) + \operatorname{sgn}\dot\delta_j F'_j \right] \tag{11.2}$$

where

$$k_y = \frac{\frac{1}{2} \rho A_{max} V_{b\,max}^2 y_{2\,max}}{(M_b/I_b)_{max} I_b} \tag{11.3}$$

B.12. Block 12

Next we consider the dimensionless form of Eqs. (12.6) and (12.7) in Section A.2.12 for $\dot{\delta}_j$ and $\dot{\beta}_j$. From Eq. (8.5) in Section B.8 we note that $\Omega_{p\,max}$ is the normalizing factor for P_{pj} and $R_{pj}-\Omega_s$, and from Eqs. (2.1) and (2.9) in Section B.2 Ω_{max} is the normalizing factor for P^p_{rj} and $R^p_{rj}-\Omega_s\cos\beta_j$. Thus Eqs. (12.6) and (12.7) in Section A.2.12 become

$$\frac{\dot{\delta}_j}{\Omega_{p\,max}} = \frac{1}{\cos\beta_j}\left[\frac{k_s}{k_r}\left(r^p_{r_j}-\frac{\Omega_s}{\Omega_{max}}\cos\beta_j\right)-(r_{pj}-k_s\omega_s)-k_s\omega_s(1-\cos\beta_j)\right] \quad (12.1)$$

and

$$\frac{\dot{\beta}_j}{\Omega_{p\,max}} = \frac{k_s}{k_r}\,p^p_{rj} - p_{pj} \quad (12.2)$$

Here $\omega_s = \Omega_s/\Omega_{s\,max}$ (Eq. 6.4 in Section B.6), $k_r = \Omega_{s\,max}/\Omega_{max}$ (Eq. 7.7 in Section B.7) and $k_s = \Omega_{s\,max}/\Omega_{p\,max}$ (Eq. 8.5 in Section B.8). We recall in Eq. (12.2) that the two z_{pj}-axis dimensionless angular rates, $r^p_{rj}-(\Omega_s/\Omega_{max})\cos\beta_j$ for the rotating shaft axes (R-frame) and $r_{pj}-k_s\omega_s$ for the blade span axes (P-frame), do not include the component due to rotor-shaft spin rate $\Omega_s=\omega_s\Omega_{s\,max}$. I.e., it is subtracted off of each component as computed respectively in Eqs. (2.9) in Section B.2 and (9.6) in Section B.9. This avoids computing the small difference of large quantities to obtain $\dot{\delta}_j$. Equations (12.1) and (12.2) are integrated with gain $\Omega_{p\,max}$ to obtain β_j and δ_j.

B.13. Block 13

To compute the dimensionless form of the acceleration compo-

nents of the c.g. of the jth blade, we use $2\rho_c \Omega_{s\,max} \Omega_{p\,max}$ as a normalizing factor. Recalling that $(F_b/M)_{max}$ is the normalizing factor for acceleration components of the hinge point P_j (see Eqs. 9.1, 9.2, and 9.3, Section B.9), $\Omega_{p\,max}$ is the normalizing factor for blade angular velocity components (Eq. 8.5, Section B.8), and $\Omega_{s\,max}$ is the normalizing factor for blade angular acceleration components (Eqs. 9.5 and 9.6, Section B.9), we can rewrite Eqs. (13.4), (13.5) and (13.6) in Section A.2.13 as follows:

$$a^p_{cxj} - g^p_{xj} = k_c(a^p_{pxj} - g^p_{xj}) + \frac{1}{2}\left[\frac{1}{k_s} q_{pj} p_{pj} - \frac{\dot{r}_{pj} - k_s \dot{\omega}_s}{\Omega_{s\,max}}\right] - \frac{1}{2}\frac{\dot{\omega}_s}{\Omega_{p\,max}} \tag{13.1}$$

$$a^p_{cyj} - g^p_{yj} + \frac{k_s}{2}\left(1 + \frac{e}{\rho_c}\right)\omega_s^2 = k_c\left[a^p_{pyj} - g^p_{yj} + k_q k_r^2 \omega_s^2 \cos\delta_j \cos\beta_j\right]$$

$$-\frac{1}{2k_s}\left[p^2_{pj} + (r_{pj} - k_s\omega_s)^2\right] - \omega_s(r_{pj} - k_s\omega_s) + \frac{k_s\omega_s^2}{2}\left(\frac{e}{\rho_c}\right)(1 - \cos\delta_j \cos\beta_j) \tag{13.2}$$

$$a^p_{czj} - g^p_{zj} = k_c(a^p_{pzj} - g^p_{zj}) + \frac{1}{2}\left[\frac{1}{k_s} q_{pj}(r_{pj} - k_s\omega_s) + q_{pj}\omega_s + \frac{\dot{p}_{pj}}{\Omega_{s\,max}}\right] \tag{13.3}$$

where

$$k_c = \frac{(F_b/M)_{max}}{2\rho_c \Omega_{s\,max} \Omega_{p\,max}} \tag{13.4}$$

In Eq. (13.2) the term $\frac{k_s}{2}\left(1 + \frac{e}{\rho_c}\right)\omega_s^2$ represents the negative of the centrifugal acceleration of the blade c.g. By substracting it from the total y_{pj} axis acceleration component we improve the scaling by a very sizeable factor.

For the normalizing factor for the components of hinge shear force let us use $2m\rho_c \Omega_{s\,max} \Omega_{p\,max}$. Thus

$$f^p_{Pxj} = \frac{F_{pxj}}{2m\rho_c \Omega_{s\,max} \Omega_{p\,max}} \quad , f^p_{Pyj} = \frac{F_{pyj}}{2m\rho_c \Omega_{s\,max} \Omega_{p\,max}}$$

$$f^p_{Pzj} = \frac{F^p_{pzj}}{2m\rho_c \Omega_{s\,max} \Omega_{p\,max}} \tag{13.5}$$

Using Eqs. (13.1) thru (13.5) above, Eqs. (13.7), (13.8), and (13.9) in Section A.13 become the following:

$$f^p_{Pxj} = -(a^p_{cxj} - g^p_{xj}) + \sum_{k=1}^{s} k_a f_{Tjk} \tag{13.6}$$

$$f^p_{Pyj} - k'_s \omega^2_s = -(a^p_{cyj} - g^p_{yj} + k'_s \omega^2_s) + \sum_{k=1}^{s} k_a f_{Rjk} \tag{13.7}$$

$$f_{Pzj} = -(a^p_{czj} - g^p_{zj}) + \sum_{k=1}^{s} k_a f_{Pjk} \tag{13.8}$$

where

$$k_a = \frac{\frac{1}{2}\rho A_{max} V^2_{b\,max}}{2m\rho_c \Omega_{s\,max} \Omega_{p\,max}}, \qquad k'_s = \frac{1}{2}\left(1 + \frac{e}{\rho_c}\right) \tag{13.9}$$

Again note in Eq. (13.7) that the y_{pj} hinge force component has the centrifugal force term $k'_s \omega^2_s$ subtracted off.

B.14. Block 14

The dimensionless hinge force components for the jth blade, as given in Eqs. (13.6), (13.7), and (13.8) in Section B.13 must be resolved from blade-span axes (P-frame) to rotating shaft axis (R-frame) components using the matrix $[T_{rp_j}]^T$, where $[T_{rp_j}]$ is given in Eq. (2.18), Section A.2.2. Thus we obtain

$$f^r_{Pxj} = f^p_{Pxj}\cos\delta_j + (f^p_{Pyj} - k'_s\omega^2_s)\sin\delta_j\cos\beta_j + f^p_{Pzj}\sin\delta_j\sin\beta_j + k'_s\omega^2_s\sin\delta_j\cos\beta_j \tag{14.1}$$

$$f^r_{Pyj} - k'_s \omega_s^2 \cos\delta_j \cos\beta_j = -f^p_{Pxj} \sin\delta_j + (f^p_{Pyj} - k'_s \omega_s^2)\cos\delta_j \cos\beta_j + f^p_{Pzj} \cos\delta_j \sin\beta_j \tag{14.2}$$

$$f^r_{Pzj} = -(f^p_{Pyj} - k'_s \omega_s^2)\sin\beta_j + f^p_{Pzj} \cos\beta_j - k'_s \omega_s^2 \sin\beta_j \tag{14.3}$$

We note that k'_s as defined in Eq. (13.9) of Section B.13 is equal approximately to $k_s/2$ which from Eq. (8.5) in Section B.8 is equal to $\Omega_{s\,max}/2\Omega_{p\,max}$. We recall that $\Omega_{s\,max}$ is the maximum rotor spin velocity and $\Omega_{p\,max}$ is the maximum angular velocity of the rotor-blade components after Ω_s has been subtracted. Thus $\Omega_{s\,max}/2\Omega_{p\,max}$ (i.e., k'_s) will be likely to exceed unity by an appreciable amount. On the other hand k'_s only enters Eqs. (14.1) and (14.3) when multiplied by $\sin\delta_j$ or $\sin\beta_j$, so that the product should remain less than unity. Of course the $k'_s \omega_s^2 \cos\delta_j \cos\beta_j$ on the left side of Eq. (14.2) will be much larger than unity. This is exactly why we compute directly the small difference $f_{pyj} - k'_s \omega_s^2 \cos\delta_j \cos\beta_j$.

The dimensionless force components given in Eqs. (14.1), (14.2), and (14.3) are resolved from rotating shaft axes (R-frame) to shaft axes (S-frame) using the transformation matrix $[T_{sr_j}]^T$, where $[T_{sr_j}]$ is given in Eq. (2.10), Section A.2.10. Thus we have

$$f^s_{Pxj} + k'_s \omega_s^2 \cos\psi_j = f^r_{Pxj} \sin\psi_j - (f^r_{Pyj} - k'_s \omega_s^2 \cos\delta_j \cos\beta_j)\cos\psi_j + k'_s \omega_s^2 (1 - \cos\delta_j \cos\beta_j)\cos\psi_j \tag{14.4}$$

$$f^s_{Pyj} - k'_s \omega_s^2 \sin\psi_j = f^r_{Pxj} \cos\psi_j + (f^r_{Pyj} - k'_s \omega_s^2 \cos\delta_j \cos\beta_j)\sin\psi_j - k'_s \omega_s^2 (1 - \cos\delta_j \cos\beta_j)\sin\psi_j \tag{14.5}$$

$$f^s_{Pzj} = f^r_{Pzj} \tag{14.6}$$

Note in Eqs. (14.4) and (14.5) that the large $k_s' \omega_s^2$ terms have been subtracted from the left side of each equation and that the remaining $k_s' \omega_s^2$ terms on the right side are each multiplied by $(1-\cos\delta_j \cos\beta_j)$, which is small compared with unity.

Next we sum the dimensionless force components due to the jth blade, as given in Eqs. (14.4), (14.5), and (14.6), over the N blades. We continue to use $2\rho_c m \Omega_{s\,max} \Omega_{p\,max}$ as the normalizing factor. Thus let

$$f_{Rx}^s = \frac{F_{Rx}^s}{2\rho_c m \Omega_{s\,max} \Omega_{p\,max}}, \quad f_{Ry}^s = \frac{F_{Ry}^s}{2\rho_c m \Omega_{s\,max} \Omega_{p\,max}},$$

$$f_{Rz}^s = \frac{F_{Rz}^s}{2\rho_c m \Omega_{s\,max} \Omega_{p\,max}} \tag{14.7}$$

Then we have

$$\frac{f_{Rx}^s}{N} = \frac{1}{N} \sum_{j=1}^{N} (f_{Pxj}^s + k_s' \omega_s^2 \cos\psi_j) - \frac{k_s' \omega_s^2}{N} \sum_{j=1}^{N} \cos\psi_j \tag{14.8}$$

$$\approx 0$$

$$\frac{f_{Ry}^s}{N} = \frac{1}{N} \sum_{j=1}^{N} (f_{Pyj}^s - k_s' \omega_s^2 \sin\psi_j) + \frac{k_s' \omega_s^2}{N} \sum_{j=1}^{N} \sin\psi_j \tag{14.9}$$

$$\approx 0$$

$$\frac{f_{Rz}^s}{N} = \frac{1}{N} \sum_{j=1}^{N} f_{Pzj}^s \tag{14.10}$$

But because the N blades are equally spaced in azimuth along 2π radians, $\sum_{j=1}^{N} \cos\psi_j = 0$ and $\sum_{j=1}^{N} \sin\psi_j = 0$. I.e., the principle centrifugal force terms

acting on each blade cancel out. Only if a blade is lost do these terms need to be included in Eqs. (14.8) and (14.9). Thus optimal scaling is preserved.

Finally, the S-frame dimensionless force components in Eqs. (14.8), (14.9), and (14.10) above are transformed to hub and hence body-axis components using the matrix $[\ T_{hs}]^{T}$, where $[\ T_{hs}]$ is given in Eq. (2.3). Thus

$$\frac{1}{N} f^{b}_{Rx} = \frac{1}{N} f^{s}_{Rx} \cos i_{\theta} + \frac{1}{N} f^{s}_{Ry} \sin i_{\phi} \sin i_{\theta} + \frac{1}{N} f^{s}_{Rz} \cos i_{\phi} \sin i_{\theta} \qquad (14.11)$$

$$\frac{1}{N} f^{b}_{Ry} = \frac{1}{N} f^{s}_{Ry} \cos i_{\phi} - \frac{1}{N} f^{s}_{Rz} \sin i_{\phi} \qquad (14.12)$$

$$\frac{1}{N} f^{b}_{Rz} = -\frac{1}{N} f^{s}_{Rx} \sin i_{\theta} + \frac{1}{N} f^{s}_{Ry} \sin i_{\phi} \cos i_{\theta} + \frac{1}{N} f^{s}_{Rz} \cos i_{\phi} \cos i_{\theta} \qquad (14.13)$$

B.15. Block 15

The hinge force components F^{r}_{Pxj} and F^{r}_{Pzj} along the x_{rj} and z_{rj} R-frame axes for the jth blade were normalized in Section B.14 by dividing by $2\rho_{c} m \Omega_{s\,max} \Omega_{p\,max}$. This suggests that we normalize the jth blade hinge moment components M^{r}_{hxj} and M^{r}_{hzj} by dividing by $2e\rho_{c} m \Omega_{s\,max} \Omega_{p\,max}$. Thus let

$$m^{r}_{hxj} = \frac{M^{r}_{hxj}}{2e\rho_{c} m \Omega_{s\,max} \Omega_{p\,max}}, \quad m^{r}_{hzj} = \frac{M_{hzj}}{2e\rho_{c} m \Omega_{s\,max} \Omega_{p\,max}} \qquad (15.1)$$

Then from Eqs. (15.2) and (15.3) in Section A.2.15 the equations for dimensionless moment components at the jth blade hinge become

$$m^{r}_{hxj} = k_{h} \left[\frac{K_{\beta}}{M_{p\,max}} \beta_{j} + \frac{K_{\beta} \Omega_{s\,max}}{M_{p\,max}} \frac{\dot{\beta}_{j}}{\Omega_{s\,max}} \right] \cos\delta_{j} + f^{r}_{Pzj} \qquad (15.2)$$

$$m^r_{hzj} = - \frac{k_h}{M_{p\,max}} \left[f(\delta_j) + \operatorname{sgn} \dot{\delta}_j F'_{\dot{\delta}} \right] - f_{Pxj} \tag{15.3}$$

where

$$k_h = \frac{M_{p\,max}}{2e\rho_c\, m\, \Omega_{s\,max}\, \Omega_{p\,max}} \tag{15.4}$$

Here the terms inside the square brackets on the right side of Eqs. (15.2) and (15.3) have already been computed in Eqs. (11.1) and (11.2), Section 13.11.

The dimensionless moment components in Eqs. (15.2) and (15.3) are resolved into S-frame axes using $[T_{sr}]^T$, where $[T_{sr}]$ is given in Eqs. (2.10). Thus, since $m^r_{hyj} = 0$, we have

$$m^s_{hxj} = m^r_{hxj} \sin\psi_j \tag{15.5}$$

$$m^s_{hyj} = m^r_{hxj} \cos\psi_j \tag{15.6}$$

$$m^s_{hzj} = m^r_{hzj} \tag{15.7}$$

Next we sum the hub-moment components of Eqs. (15.5), (15.6), and (15.7) over all N blades to obtain the total dimensionless hub moment components. Thus

$$\frac{m^s_{hx}}{N} = \frac{1}{N} \sum_{j=1}^{N} m^s_{hxj} \tag{15.8}$$

$$\frac{m^s_{hy}}{N} = \frac{1}{N} \sum_{j=1}^{N} m^s_{hyj} \tag{15.9}$$

$$\frac{m^s_{hz}}{N} = \frac{1}{N} \sum_{j=1}^{N} m^s_{hzj} \tag{15.10}$$

where as before $2e\rho_c\, m\, \Omega_{s\,max}\, \Omega_{p\,max}$ is still used as the normalizer

for the dimensionless moment components m^s_{hx}, m^s_{hy}, m^s_{hz}. These are resolved into hub and hence body axis components using the matrix $[T_{hs}]^T$, where $[T_{sh}]$ is given in Eqs. (2.3). Thus

$$\frac{m^b_{hx}}{N} = \frac{m^s_{hx}}{N}\cos i_\theta + \frac{m^s_{hy}}{N}\sin i_\phi \sin i_\theta + \frac{m^s_{hz}}{N}\cos i_\phi \sin i_\theta \qquad (15.11)$$

$$\frac{m^b_{hy}}{N} = \frac{m^s_{hy}}{N}\cos i_\phi - \frac{m^s_{hz}}{N}\sin i_\phi \qquad (15.12)$$

$$\frac{m^b_{hz}}{N} = -\frac{m^s_{hx}}{N}\sin i_\theta + \frac{m^s_{hy}}{N}\sin i_\phi \cos i_\theta + \frac{m^s_{hz}}{N}\cos i_\phi \cos i_\theta \qquad (15.13)$$

The total rotor moment about the aircraft c.g. is the sum of the hub moment plus the moment due to the rotor force acting at the hub, i.e., as given in dimensional form in Eqs. (15.16), (15.17), (15.18), Section A.2.15.

To normalize the total rotor moment components about the aircraft c.g. we use $2Nd_{max}\rho_c m \Omega_{s\,max} \Omega_{p\,max}$, where in Section B.4 we defined d_{max} as the largest of the relative hub to c.g. position-vector components, x_H, y_H, z_H. Hence we let

$$m^b_{Rx} = \frac{M^b_{Rx}}{2Nd_{max}\rho_c m\Omega_{s\,max}\Omega_{p\,max}},$$

$$m^b_{Ry} = \frac{M^b_{Ry}}{2Nd_{max}\rho_c m\Omega_{s\,max}\Omega_{p\,max}},$$

$$m^b_{Rz} = \frac{M^b_{Rz}}{2Nd_{max}\rho_c m\Omega_{s\,max}\Omega_{p\,max}} \qquad (15.14)$$

Then Eqs. (15.16), (15.17), and (15.18) in Section A.2.15 become

$$m^b_{Rx} = \left(\frac{e}{d_{max}}\right)\frac{m^b_{hx}}{N} + \left(\frac{y_H}{d_{max}}\right)\frac{f^b_{Rz}}{N} - \left(\frac{z_H}{d_{max}}\right)\frac{f^b_{Ry}}{N} \tag{15.15}$$

$$m^b_{Ry} = \left(\frac{e}{d_{max}}\right)\frac{m^b_{hy}}{N} + \left(\frac{z_H}{d_{max}}\right)\frac{f^b_{Rx}}{N} - \left(\frac{x_H}{d_{max}}\right)\frac{f^b_{Rz}}{N} \tag{15.16}$$

$$m^b_{Rz} = \left(\frac{e}{d_{max}}\right)\frac{m^b_{hz}}{N} + \left(\frac{x_H}{d_{max}}\right)\frac{f^b_{Ry}}{N} - \left(\frac{y_H}{d_{max}}\right)\frac{f^b_{Rx}}{N} \tag{15.17}$$

LIST OF SYMBOLS

$\bar{A}_{bi}$	Acceleration of B-frame w.r.t. I-frame
A_{bx}, A_{by}, A_{bz}	Components of $\bar{A}_{bi}$ along x_b, y_b, z_b body axes.
$\bar{A}_{hi}$	Acceleration of H-frame w.r.t. I-frame.
A_{hx}, A_{hy}, A_{hz}	Components of $\bar{A}_{hi}$ along x_h, y_h, z_h axes.
$\bar{A}_{ri}$	Acceleration of R-frame w.r.t. I-frame.
$A^s_{rx}, A^s_{ry}, A^s_{rz}$	Components of $\bar{A}_{ri}$ along x_s, y_s, z_s axes.
$A^r_{rxj}, A^r_{ryj}, A^r_{rzj}$	Components of $\bar{A}_{ri}$ along x_{rj}, y_{rj}, z_{rj} axes.
$\bar{A}_{pi_j}$	Acceleration of P_j-frame w.r.t. I-frame.
$A^r_{pxj}, A^r_{pyj}, A^r_{pzj}$	Components of $\bar{A}_{pi_j}$ along x_{rj}, y_{rj}, z_{rj} axes.
$A^p_{pxj}, A^p_{pyj}, A^p_{pzj}$	Components of $\bar{A}_{pi_j}$ along x_{pj}, y_{pj}, z_{pj} axes.
$\bar{A}_{ci_j}$	Acceleration of the c.g. of the jth blade w.r.t. I-frame.
$A^p_{cxj}, A^p_{cyj}, A^p_{czj}$	Components of $\bar{A}_{ci_j}$ along x_{pj}, y_{pj}, z_{pj} axes.
A_{1S}	Constant in the blade geometric pitch equation.
a_{bx}, a_{by}, a_{bz}	Dimensionless components of $\bar{A}_{bj}$ along x, y, z axes.
a_{hx}, a_{hy}, a_{hz}	Dimensionless components of $\bar{A}_{hi}$ along x_h, y_h, z_h axes.
$a^s_{rx}, a^s_{ry}, a^s_{rz}$	Dimensionless components of $\bar{A}_{ri}$ along x_s, y_s, z_s axes.
$a^r_{rxj}, a^r_{ryj}, a^r_{rzj}$	Dimensionless components of $\bar{A}_{ri}$ along x_{rj}, y_{rj}, z_{rj} axes.
$a^r_{pxj}, a^r_{pyj}, a^r_{pzj}$	Dimensionless components of $\bar{A}_{pi_j}$ along x_{rj}, y_{rj}, z_{rj} axes.
$a^p_{pxj}, a^p_{pyj}, a^p_{pzj}$	Dimensionless components of $\bar{A}_{pi_j}$ along x_{pj}, y_{pj}, z_{pj} axes.
$a^p_{cxj}, a^p_{cyj}, a^p_{czj}$	Dimensionless components of $\bar{A}_{ci_j}$ along x_{pj}, y_{pj}, z_{pj} axes.
B-frame	The aircraft body-axis frame (x_b, y_b, z_b).
B_{1S}	Constant in the blade geometric pitch equation.

C_{djk}	Drag coefficient for kth segment of jth blade.
$C_{\ell jk}$	Lift coefficient for kth segment of jth blade.
D_{jk}	Drag of the kth segment of jth blade.
d_{max}	Largest of x_H, y_H, z_H (hub displacement from c.g.).
$\bar{e}_j$	Position of hinge point for jth blade w.r.t. the hub.
e	Magnitude of $\bar{e}_j$.
$\bar{F}_b$	Total external force acting on aircraft, less gravity.
F_{bx}, F_{by}, F_{bz}	Components of $\bar{F}_b$ along x_b, y_b, z_b body axes.
$\bar{F}_R$	Total force on aircraft due to rotor system.
$F^b_{Rx}, F^b_{Ry}, F^b_{Rz}$	Components of $\bar{F}_R$ along x_b, y_b, z_b body axes.
$F^s_{Rx}, F^s_{Ry}, F^s_{Rz}$	Components of $\bar{F}_R$ along x_s, y_s, z_s axes.
$F_{Tjk}, F_{Rjk}, F_{Pjk}$	Aerodynamic forces for j blade, kth segment along x_{pj}, y_{pj}, z_{pj} axes.
$\bar{F}_{Pj}$	Hinge shear force.
$F_{Pxj}, F_{Pyj}, F_{Pzj}$	Components of $\bar{F}_{P_j}$ along x_{pj}, y_{pj}, z_{pj} axes.
$F^r_{Pxj}, F^r_{Pyj}, F^r_{Pzj}$	Components of $\bar{F}_{P_j}$ along x_{rj}, y_{rj}, z_{rj} axes.
$F^s_{Pxj}, F^s_{Pyj}, F^s_{Pzj}$	Components of $\bar{F}_{P_j}$ along x_s, y_s, z_s axes.
f_{bx}, f_{by}, f_{bz}	Dimensionless components of $\bar{F}_b$ along x_b, y_b, z_b axes.
$f^b_{Rx}, f^b_{Ry}, f^b_{Rz}$	Dimensionless components of $\bar{F}_R$ along x_b, y_b, z_b axes.
$f^s_{Rx}, f^s_{Ry}, f^s_{Rz}$	Dimensionless components of $\bar{F}_R$ along $x_s, y_x z_s$ axes.
$f_{Tjk}, f_{Rjk}, f_{Pjk}$	Dimensionless components of aerodynamic force for jth blade, kth segment, along x_p, y_p, z_p axes.
$f_{Pxj}, f_{Pyj}, f_{Pzj}$	Dimensionless components of $\bar{F}_{P_j}$ along x_{pj}, y_{pj}, z_{pj} axes.
$f^r_{Pxj}, f^r_{Pyj}, f^r_{Pzj}$	Dimensionless components of $\bar{F}_{P_j}$ along x_{rj}, y_{rj}, z_{rj} axes.

$f^s_{Pxj}, f^s_{Pyj}, f^s_{Pzj}$	Dimensionless components of $\bar{F}_{P_j}$ along x_s, y_s, z_s axes.
F'_δ	Constant in equation for hinge lagging moment.
$f(\delta_j)$	Function in equation for hinge lagging moment.
$\bar{G}$	Gravity acceleration vector.
G_x, G_y, G_z	Components of $\bar{G}$ along x_b, y_b, z_b axes.
G^s_x, G^s_y, G^s_z	Components of $\bar{G}$ along x_s, y_s, z_s axes.
$G^r_{xj}, G^r_{yj}, G^r_{zj}$	Components of $\bar{G}$ along x_{rj}, y_{rj}, z_{rj} axes.
$G^p_{xj}, G^p_{yj}, G^p_{zj}$	Components of $\bar{G}$ along x_{pj}, y_{pj}, z_{pj} axes.
g_o	Sea level gravity acceleration magnitude.
g_x, g_y, g_z	Dimensionless components of $\bar{G}$ along x_b, y_b, z_b axes.
g^s_x, g^s_y, g^s_z	Dimensionless components of $\bar{G}$ along x_x, y_s, z_s axes.
$g^r_{xj}, g^r_{yj}, g^r_{zj}$	Dimensionless components of $\bar{G}$ along x_{rj}, y_{rj}, z_{rj} axes.
$g^p_{xj}, g^p_{yj}, g^p_{zj}$	Dimensionless components of $\bar{G}$ along x_{pj}, y_{pj}, z_{pj} axes.
$\bar{H}_b$	Angular momentum of aircraft about c.g. (not including the rotor blades).
$\bar{H}_{pi_j}$	Angular momentum of jth blade about hinge point P_j
H-frame	The hub-axis frame, x_h, y_h, z_h.
h	Altitude
I-frame	The inertial reference frame (non accelerating atmosphere).
[I]	Aircraft inertia matrix about c.g. (not including the rotor blades).
I_{xx}, I_{yy}, I_{zz}	Principle moment of inertia components of [I] along x_b, y_b, z_b.
$[I_B]$	Blade inertia matrix about hinge.
I_b	Components of $[I_B]$ along x_p, z_p axes.

$\bar{i}_b, \bar{i}_s, \bar{i}_{rj}, \bar{i}_{pj}$	Unit vectors along x_b, x_s, x_{rj}, x_{pj} axes.
i_θ, i_ϕ	Pitch and roll angles of shaft axes w.r.t. hub (and hence body) axes.
j	Index denoting blade number.
$\bar{j}_b, \bar{j}_s, \bar{j}_{rj}, \bar{j}_{pj}$	Unit vectors along y_b, y_s, y_{rj}, y_{pj} axes.
$K_{\alpha_1}, K_{\alpha_2}$	Constants in the blade geometric pitch equation.
$K_\beta, K_{\dot{\beta}}$	Constants in equation for hinge flapping moment.
$\bar{k}_b, \bar{k}_s, \bar{k}_{rj}, \bar{k}_{pj}$	Unit vectors along z_b, z_s, z_{rj}, z_{pj} axes.
k_a	Scaling constant, Eq. (13.9), Ap. B.
$\hat{k}_a$	Scaling constant, Eq. (5.6), Ap. B.
k_c	Scaling constant, Eq. (13.4), Ap. B.
k_f	Scaling constant, Eq. (1.10), Ap. B.
$\hat{k}_f$	Scaling constant, Eq. (9.7), Ap. B.
k_g	Scaling constant, Eq. (1.10), Ap. B.
k_h	Scaling constant, Eq. (15.4), Ap. B.
k_m	Scaling constant, Eq. (1.15), Ap. B.
$\hat{k}_m$	Scaling constant, Eq. (9.7), Ap. B.
k_q	Scaling constant, Eq. (7.7), Ap. B.
k_r	Scaling constant, Eq. (7.7), Ap. B.
$\hat{k}_r$	Scaling constant, Eq. (4.9), Ap. B.
k_s	Scaling constant, Eq. (8.5), Ap. B.
k_s'	Scaling constant, Eq. (13.9), Ap. B.
k_y	Scaling constant, Eq. (11.3), Ap. B.
M	Aircraft mass, not including rotor blades.

$\bar{M}_b$	Total external moment acting about aircraft c. g.
M_{bx}, M_{by}, M_{bz}	Components of $\bar{M}_b$ along x_b, y_b, z_b axes.
$\bar{M}_R$	Moment about aircraft c. g. due to rotor system.
$M^b_{Rx}, M^b_{Ry}, M^b_{Rz}$	Components of $\bar{M}_R$ along x_b, y_b, z_b axes.
$\bar{M}_h$	Moment about hub due to rotor system.
$M^b_{hx}, M^b_{hy}, M^b_{hz}$	Components of $\bar{M}_h$ along x_b, y_b, z_b axes.
$M^s_{hx}, M^s_{hy}, M^s_{hz}$	Components of $\bar{M}_h$ along x_s, y_s, z_s axes.
$\bar{M}_{h_j}$	Moment about hub due to jth blade.
$M^s_{hxj}, M^s_{hyj}, M^s_{hzj}$	Components of $\bar{M}_{h_j}$ along x_s, y_s, z_s axes.
$M^r_{hxj}, M^r_{hyj}, M^r_{hzj}$	Components of $\bar{M}_{h_j}$ along x_{rj}, y_{rj}, z_{rj} axes.
M_{FDj}	Flapping hinge moment for jth blade.
M_{LDj}	Lagging hinge moment for jth blade.
M_{jk}	Mach number of jth blade, kth segment.
$\bar{M}_{aero}$	Blade moment about hinge due to aerodynamic forces.
$\bar{M}_{hinge}$	Blade moment about hinge due to hinge moments.
$\bar{M}_{Bj}$	Total moment acting about hinge on jth blade.
$\bar{M}_{pj}$	Total moment (excluding gravity) acting about hinge on jth blade.
M_{pxj}, M_{pzj}	Components of $\bar{M}_P$ along x_{pj}, z_{pj} axes.
m	Blade mass
m_{bx}, m_{by}, m_{bz}	Dimensionless components of $\bar{M}_b$ along x_b, y_b, z_b axes.
$m^b_{Rx}, m^b_{Ry}, m^b_{R_z}$	Dimensionless components of $\bar{M}_R$ along x_b, y_b, z_b axes.
$m^b_{hx}, m^b_{hy}, m^b_{hz}$	Dimensionless components of $\bar{M}_h$ along x_b, y_b, z_b axes.
$m^s_{hx}, m^s_{hy}, m^s_{hz}$	Dimensionless components of $\bar{M}_h$ along x_s, y_s, z_s axes.

$m^s_{hxj}, m^s_{hyj}, m^s_{hzj}$	Dimensionless components of $\bar{M}_{h_j}$ along x_s, y_s, z_s axes.
$m^r_{hxj}, m^r_{hyj}, m^r_{hzj}$	Dimensionless components of $\bar{M}_{h_j}$ along x_{rj}, y_{rj}, z_{rj} axes.
m_{pxj}, m_{pzj}	Dimensionless components of M_{pj} along x_{pj}, z_{pj} axes.
N	Total number of blades in rotor system.
P_j-frame	The jth blade span axis frame, x_{pj}, y_{pj}, z_{pj}.
P_b, Q_b, R_b	Components of $\bar{\Omega}_{bi}$ along x_b, y_b, z_b axes.
P^s_r, Q^s_r, R^s_r	Components of $\bar{\Omega}_{ri}$ along x_s, y_s, z_s axes.
$P^r_{rj}, Q^r_{rj}, R^r_{rj}$	Components of $\bar{\Omega}_{ri}$ along x_{rj}, y_{rj}, z_{rj} axes.
$P^p_{rj}, Q^p_{rj}, R^p_{rj}$	Components of $\bar{\Omega}_{ri}$ along x_{pj}, y_{pj}, z_{pj} axes.
P_{pj}, Q_{pj}, R_{pj}	Components of $\bar{\Omega}_{pi_j}$ along x_{pj}, y_{pj}, z_{pj} axes.
p_b, q_b, r_b	Dimensionless components of $\bar{\Omega}_{bi}$ along x_b, y_b, z_b axes.
p^s_r, q^s_r, r^s_r	Dimensionless components of $\bar{\Omega}_{ri}$ along x_s, y_s, z_s axes.
$p^r_{rj}, q^r_{rj}, r^r_{rj}$	Dimensionless components of $\bar{\Omega}_{ri}$ along x_{rj}, y_{rj}, z_{rj} axes.
$p^p_{rj}, q^p_{rj}, r^p_{rj}$	Dimensionless components of $\bar{\Omega}_{ri}$ along x_{pj}, y_{pj}, z_{pj} axes.
p_{pj}, q_{pj}, r_{pj}	Dimensionless components of $\bar{\Omega}_{pi_j}$ along x_{pj}, y_{pj}, z_{pj} axes.
R_j-frame	The jth rotating shaft-axis frame, x_{rj}, y_{rj}, z_{rj}.
$\bar{r}_H$	Position of hub w.r.t. aircraft c.g.
S-frame	The shaft axis frame, x_s, y_s, z_s.
S_x, S_y, S_z	Distance north, east, and downward.
s	Number of segments per blade.
$[T_{be}]$	Matrix for transformation from body to earth axis components.
$[T_{eb}]$	Matrix for transformation from earth to body axis components.
$[T_{hs}]$	Matrix for transformation from H to S-frame axis components.

$[T_{sh}]$	Matrix for transformation from S to H-frame axis components.
$[T_{sr_j}]$	Matrix for transformation from S to R_j-frame axis components.
$[T_{rs_j}]$	Matrix for transformation from R_j to S-frame axis components.
$[T_{rp_j}]$	Matrix for transformation from R_j to P_j-frame axis components.
$[T_{pr_j}]$	Matrix for transformation from P_j to R_j-frame axis components.
U_b, V_b, W_b	Components of $\overline{V}_{bi}$ along x_b, y_b, z_b axes.
$U^b_{hb}, V^b_{hb}, W^b_{hb}$	Components of $\overline{V}_{hb}$ along x_b, y_b, z_b axes.
U^s_r, V^s_r, W^s_r	Components of $\overline{V}_{ri}$ along x_s, y_s, z_s axes.
$U^r_{rj}, V^r_{rj}, W^r_{rj}$	Components of $\overline{V}_{ri}$ along x_{rj}, y_{rj}, z_{rj} axes.
$U^r_{pj}, V^r_{pj}, W^r_{pj}$	Components of $\overline{V}_{pi_j}$ along x_{rj}, y_{rj}, z_{rj} axes.
$U^p_{pj}, V^p_{pj}, W^p_{pj}$	Components of $\overline{V}_{pi_j}$ along x_{pj}, y_{pj}, z_{pj} axes.
$U_{Tjk}, U_{Pjk}, U_{Rjk}$	Components of $\overline{V}_{jk}$ along x_{pj}, y_{pj}, z_{pj} axes.
u_b, v_b, w_b	Dimensionless components of $\overline{V}_{bi}$ along x_b, y_b, z_b axes.
$u^b_{hb}, v^b_{hb}, w^b_{hb}$	Dimensionless components of $\overline{V}_{hb}$ along x_b, y_b, z_b axes.
$u^s_{rs}, v^s_{rs}, w^s_{rs}$	Dimensionless components of $\overline{V}_{ri}$ along x_s, y_s, z_s axes.
$u^r_{pj}, v^r_{pj}, w^r_{pj}$	Dimensionless components of $\overline{V}_{pi_j}$ along x_{rj}, y_{rj}, z_{rj} axes.
$u^p_{pj}, v^p_{pj}, w^p_{pj}$	Dimensionless components of $\overline{V}_{pi_j}$ along x_{pj}, y_{pj}, z_{pj} axes.
$u_{Tjk}, u_{Rjk}, u_{Pjk}$	Dimensionless components of $\overline{V}_{jk}$ along x_{pj}, y_{pj}, z_{pj} axes.
$\overline{V}_{bi}$	Velocity of B-frame, x_b, y_b, z_b axes.
$\overline{V}_{hb}$	Velocity of H-frame w.r.t. B-frame.
$\overline{V}_{hi}$	Velocity of H-frame, x_h, y_h, z_h axes.

$\bar{V}_{ri}$	Velocity of R-frame, x_{rj}, y_{rj}, z_{rj} axes.
$\bar{V}_{pi_j}$	Velocity of P_j-frame, x_{pj}, y_{pj}, z_{pj} axes.
$\bar{V}_{jk}$	Velocity of c.p. of kth segment, jth blade.
V_{jk}	Magnitude of $\bar{V}_{jk}$
v_{jk}	Dimensionless V_{jk}
x_b, y_b, z_b	Body axes (B-frame)
x_h, y_h, z_h	Hub axes (H-frame)
x_s, y_s, z_s	Shaft axes (S-frame)
x_{rj}, y_{rj}, z_{rj}	Rotating shaft axes, jth blade (R_j frame).
$x'_{rj}, y'_{rj}, z'_{rj}$	Rotating shaft axes with origin translated to P_j.
x_{pj}, y_{pj}, z_{pj}	Blade-span axes for jth blade (P_j frame).
y_{2k}	Displacement from jth blade hinge to kth segment c.p.
$\alpha_{Y_{jk}}$	Angle of attack, jth blade, kth segment.
$\alpha_{TRANS_{jk}}$	Angle ofattack for drag and lift coef. computation.
β_j	Flapping angle, jth blade.
γ_{jk}	Angle of attack yaw angle, jth blade, kth segment.
Δ_{SP}	Swash plate rotation angle.
δ_j	Lagging angle, jth blade.
θ_b	Body axis pitch angle.
θ_{Ajk}	Blade twist angle, jth blade, kth segment.
θ_{Yjk}	Yawedblade twist angle, jth blade, kth segment.
$\bar{\rho}_{jk}$	Displacement of jth blade, kth segment c.p. w.r.t. hinge.
$\bar{\rho}_{cj}$	Displacement of jth blade c.g. w.r.t. hinge.

ϕ_b	Body-axis bank angle.
$\phi_{Y_{jk}}$	Aerodynamic angle of attack, jth blade, kth segment.
ψ_b	Body-axis heading angle.
ψ_j	Azimuthal angle for jth blade-span axes.
$\bar{\Omega}_{bi}$	Angular velocity of B-frame.
$\bar{\Omega}_{hi}$	Angular velocity of H-frame (same as B-frame).
$\bar{\Omega}_{si}$	Angular velocity of S-frame (same as B-frame).
$\bar{\Omega}_{ri}$	Angular velocity of R_j-frame.
$\bar{\Omega}_{pi_j}$	Angular velocity of P_j-frame.
Ω_s	Angular velocity of R_j-frame w.r.t. S-frame.
$\Omega_{p\,max}$	Normalizing factor for dimensionless blade-span axis angular velocity components.
ω_s	Dimensionless Ω_s.